4D HIGH RESOLUTION SEISMOLOGY: REPEATING EVENTS AND LARGE SCALE RELOCATION

A DISSERTATION
SUBMITTED TO THE DEPARTMENT OF GEOPHYSICS
AND THE COMMITTEE ON GRADUATE STUDIES
OF STANFORD UNIVERSITY
IN PARTIAL FULFILLMENT OF THE REQUIREMENTS
FOR THE DEGREE OF
DOCTOR OF PHILOSOPHY

David Schaff Candidate
April 2001

I certify that I have read this dissertation and that in my opinion it is fully adequate, in scope and quality, as a dissertation for the degree of Doctor of Philosophy.

Greg Beroza
(Principal Adviser)

I certify that I have read this dissertation and that in my opinion it is fully adequate, in scope and quality, as a dissertation for the degree of Doctor of Philosophy.

Amos Nur

I certify that I have read this dissertation and that in my opinion it is fully adequate, in scope and quality, as a dissertation for the degree of Doctor of Philosophy.

Paul Segall

Approved for the University Committee on Graduate Studies:

Abstract

Two common limitations frequently arise when working with geophysical data. First, the measurements are often too sparse both in time and space. Second, the signals sometimes contain significant noise. In earthquake seismology, it could be argued that the noise largely represents our ignorance about earth structure which can be quite complicated. Some other fields have it easier. In astronomy, the light rays, although they travel great distances, are contaminated little by the medium because most of their journey is through a vacuum. In making a CAT scan image of the brain, the medical community has complete control over their distribution of sources and receivers in a controlled setting.

The intial motivation and primary focus of this thesis was to make an analogous "CAT" scan image of the 1989 Loma Prieta earthquake to see if we could measure any perturbations of the earth's crust in the form of a change in seismic velocity through the source region. Since we don't know where or when the next large earthquake is likely to occur, it is challenging to set-up a controlled experiment (e.g. the Parkfield Earthquake Prediction Experiment). After the earthquake occurs, however, it is possible to go out and measure any postseismic signal. We have chosen to use natural sources from the microseismicity — large clusters of repeating events. Although we don't have control over the distribution of sources, both temporal and spatial resolution are improved because of the abundance of seismicity in California.

Two principal sources of noise affect our analysis of seismograms both to measure velocity changes and to locate earthquakes precisely. The first manifests as velocity model error due to unknown earth structure. To eliminate path effects for studying temporal velocity variations, we identify repeating events that occur in the same spot so that while the earth structure is still unknown, it is common for all events. For the earthquake location problem, much of the velocity model error is removed by using a relative event location approach.

The other main source of error is measurement error on the seismograms, themselves, due to mispicks or poor alignment of phases. To address this issue we've developed some robust waveform cross-correlation techniques to improve the relative timing accuracy. The net effect of all these combined methods is to greatly increase the resolution obtained from existing seismological data. We were successful in our original purpose and measured

a large coseismic decrease in velocity (~ 3.5 %) associated with the 1989 Loma Prieta mainshock. This signal subsequently heals postseismically with logarithmic decay similar to fault healing relationships obtained in the lab. The change in S-wave velocity is greater than the change in P-wave velocity suggesting that pore fluids are present and possibly high pore pressures. Consistent and reproducible results are also obtained for the 1984 Morgan Hill earthquake.

Upon isolation of repeating event clusters, an interesting phenomenon was noticed that they are actually repeating aftershocks which follow Omori type $1/t$ decay in recurrence. The clusters in some sense act as a creep meter at depth. This time signature indicates a plastic rheology as opposed to a viscous relaxation mechanism. At the other end of the spectrum from identifying repeating events would be applying correlation data for large scale relocation. On the Calaveras fault we realize a one to two order magnitude reduction in hypocentral errors. This reveals the seismically active fault zone is narrow (average 75 m width), linear streak features, and holes in the background seismicity that complement high slip patches from the 1984 Morgan Hill mainshock. Resolved nearby off-fault structures permit a stress inversion that constrains the maximum compressive stress to be oriented at a high angle to the fault implying that it is weak. While many of the benefits of correlation measurements have been previously known, we present striking results for many different applications due to an increased resolution on both small and large scales.

Acknowledgements

First I want to thank my advisor, Greg Beroza, who has been understanding, patient, and easy-going these six short years. Who has offered good direction and clever ideas as well as encouragement when progress was slow and seemingly fruitless at times. Who took away the cares of funding by successfully writing proposals to the National Science Foundation. (Thanks to NSF for providing support.) Who has a good sense of humor. Who taught me what research is all about and made time for me whenever I desired to talk to him. Who took a strong interest in this work. Without his guidance and input none of this would have been accomplished. Who laughed at my acrobats when he dragged me down a black diamond for the first time on a real mountain.

Thanks to Götz Bokelmann whose enthusiasm for seismology is contagious. He provided many new insights and is a great resource. He was very supportive, both in work and in play. Bill Ellsworth is a storehouse of good ideas and gave useful comments on so many aspects of this research. Thanks to my committee, Amos Nur, David Pollard, Paul Segall, and Mark Zoback, who have come from their specialties and offered their own unique points of view. It has helped me to see the big picture better. Amos, especially, for his visionary ponderings. Thanks to Norm Sleep for being my first advisor and George Thompson for always being excited at how similar repeating event waveforms actually are. Thanks to Bruce Shaw for helping me to publish my first paper. Nick Beeler provided many enlightening email conversations about laboratory experiments with rate and state friction. Thanks to Andy Michael for his friendship, wisdom, and the opportunity to play cello with a trombone, soprano, and the P- and S-wave ba-boom of an earthquake at Parkfield.

Thanks to all my colleagues who shared with me their ideas. Doug Dodge, I believe, shaved off two years of work from my thesis with all his programming experience and many

conversations at the beginning of my PhD. Felix Waldhauser shaved off another two years at the end of my PhD by writing the relocation code that I could not write. If it weren't for the relocation gang which organised in 1999, much of the second half of the thesis would still be work in progress. Thanks to James Packwood and Thomas Finkbiener who were good role models as older graduate students. For Stefan Baisch with similar research interests but whose visits from Germany were too short after I discovered his generosity of heart. I had much fun with the seismo group. Thanks to the ladies, Eva, Patti, and Xyoli, for letting me join them for pasta dinners, mexican dances, and squash. Thanks to Martin and Tanja for becoming great friends and sharing with me one of the highlights of my Stanford experience. Thanks to Baby Laila for teaching me what matters most.

Thanks to all my good friends who gave me life outside of research. Rachelle and Dwight for their compassion, Alton and Alyssa for the good laughs, Traci for inspiration, Mike for the gourmet food and the jet skiing. Thanks to my landlady Mrs. Steeples who mercifully kept the rent low for five years!

Thanks to my family, for always being there for me and helping me to where I am now. To my mom for giving me life, music, and love, to my dad for being proud of me, to my grandpa who is a **great** grandpa, to my uncle John — the professor, my aunt Joanne. To Elva, my stepmom, who has treated me as her own. To Tom and Tammy Slone who have been like a second family to me. To my aunt Jeanette for her love and speaking her mind. For my sister, Sharon, who is in many ways like me and many ways not, but still my best friend.

Finally, I thank the Man upstairs who has blessed me with these people in my life, enabled me to do well, and who has been with me always on those occasional dark and cold lonely, nights when they could not be near.

To Mom and Dad.

Contents

List of Tables

List of Figures

Chapter 1

Introduction

The motivation for this body of work came from attending Amos Nur's Crustal fluids course and hearing about the discovery of some repeating events that appeared to show evidence of velocity changes associated with the 1989 Loma Prieta earthquake. That combined with his paper, "Aftershocks Caused by Pore Fluid Flow?" [*Nur and Booker,* 1972] led to an interest to see if these velocity variations could be ascribed to some pore fluid mechanism in the earth through rock physics. It was decided to build on the study of *Ellsworth et al.* [1992] to try to map more of these changes using advanced techniques in waveform cross-correlation. As is typical in research, trying to answer one questions raises ten more. After chasing several rabbit trails we began to shed light on our original purpose and obtained intriguing results in other related endeavors, largely based on the power of the cross-correlation technique to improve measurements on existing data.

When studying past large earthquakes, it is important to be able to use the available existing data. This highlights the value of a permanent network. As of yet great earthquakes are not routinely predicted, so it is helpful to have a network of stations already in place to capture any coseismic, postseismic, and that elusive preseismic signal. To measure velocity changes, we have isolated several large sequences of repeating events (earthquakes that rupture approximately the same fault patch) each with one event that occurred before the mainshock. These enabled us to document the first sizeable coseismic decrease in velocity with subsequent healing associated with the 1989 Loma Prieta and 1984 Morgan Hill earthquakes. We have also applied correlation methods to part of the existing waveform

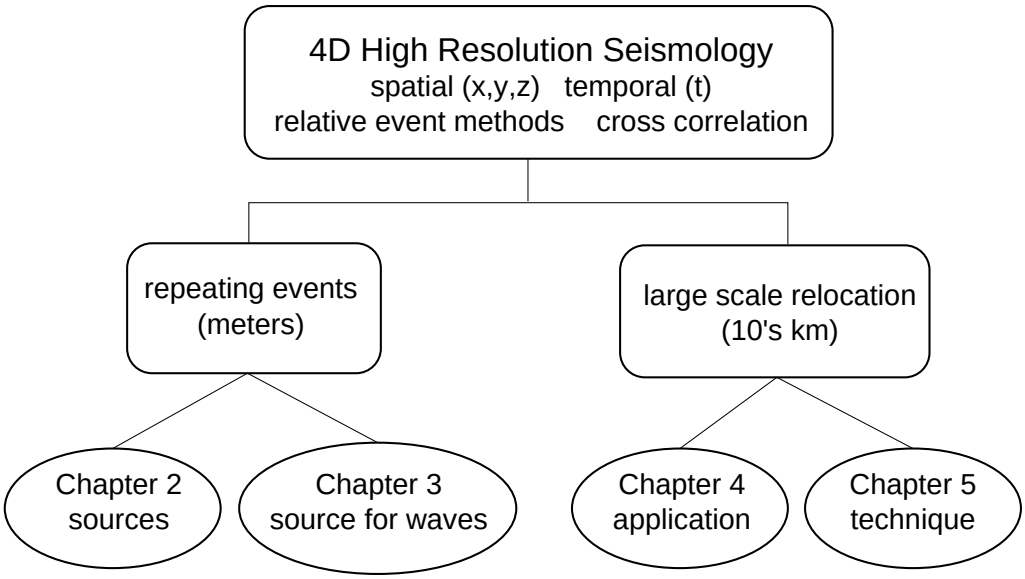

Figure 1.1: Organizational structure of thesis.

data base for Northern California in order to improve the relative arrival time accuracy between similar events. In combination with the double difference relative relocation scheme [*Waldhauser and Ellsworth*, 2000], we were then able to reduce errors in hypocentral coordinates by one to two orders of magnitude for the Calaveras fault. My advisor, Greg Beroza, has likened this to the application of the corrective lens for the Hubble telescope — a means of extracting from our present instrumentation a picture, once blurry, brought into sharp focus. This space metaphor can be extended where we reduce the contribution of unmodeled velocity structure by a relative relocation method. The reason for launching the Hubble telescope into orbit is to avoid contaminating effects from propagation through the unmodeled structure of the earth's atmosphere.

Figure 1 depicts the structure of the thesis. The increased resolution provided by correlation measurements has manifested both spatially and temporally, and over a range of length scales. The first half of the thesis (Chapters 2 & 3) analyzes in detail clusters of repeating events located to meter precision. The second half of the thesis (Chapters 4 & 5) examines how correlation methods can be tailored for large scale relocation of the Calaveras Fault on the order of 10's of kilometers. Many intermediate features such as streaks and holes in the seismicity can now be delineated that were previously fuzzy due to location

errors. Earthquake interaction is observed to occur in some of these structures in that many events appear to be triggered by nearby events. The discovery of many repeating events, which occur essentially at a point with most of their source areas overlapping, gives "recurrence interval" an unambigous meaning. Because these events are repeating aftershocks they permit excellent postseismic sampling of the velocity change signal, which we can determine heals logarithmically in time. The existence of pre-mainshock events also enables the only coseismic velocity change measurements to date. To borrow from the terminology of our friends in reflection seismology, we have been able to substantially increase the 4D resolution in earthquake seismology applying novel techniques and careful analysis to existing data.

One thing I remember from Simon Klemper's "Reflection seismology" course is that one man's signal is another man's noise. By this he meant using natural sources obscured some of the earth structure he was trying to look at. Conversely, an earthquake seismologist attempts to remove the effects of the earth to learn more about the source. For the first half, we examine the repeating events from both vantage points: in Chapter 2 at their source parameters and in Chapter 3 as a source for waves.

Chapter 2 has identified several large clusters containing between 10 to 19 repeating events. Their recurrence intervals are observed to follow Omori's law $1/t$ decay. A model that can explain the repeated set-up of identical initial conditions necessary for these events to occur is stuck patches embedded in a sea of creep. Logarithmic velocity strengthening friction predicts the observed $1/t$ decay in the creep loading rate following the stress step of the mainshock. This time signature distinguishes it from a viscous mechanism, which predicts an exponential decay.

In Chapter 3, we take advantage of the fact that repeating events occuring at the same spot but at different times produce nearly identical waveforms that can be used to measure velocity changes associated with major earthquakes. Because the rays traverse the same path through the earth, any changes observed in the waveforms can be attributed solely to changes in the medium. In the past, there was great excitement surrounding reported premonitory velocity changes before large earthquakes of as much as 20%. But it was subsequently proved, that not using earthquakes in the same spot led to erroneous conclusions

because of the effect of unknown earth structure. We present here the first reliable evidence of large velocity changes (up to 3.5% coseismically) measured by natural sources. The sign of the velocity change is uniformly the same across stations and the largest magnitude variations appear correlated to stations overlying soft sediments compared to hard rock sites. The logarithmic postseimic healing matches fault healing relations derived in the lab. At some stations the recovery is complete. If the source of the changes are shallow the time signature may also be indicative of a non-linearity in mainshock strong ground motion. Low effective pressures are implied by the magnitude of the path-averaged velocity variations. Pore fluids may be present, since the change in S-wave velocity is greater than P-wave. If the source is deep, high pore pressures are implied and may be involved in the earthquake nucleation process.

Application of correlation techniques to reduce measurement error for the purpose of earthquake location on the Calaveras Fault is presented in Chapter 4. The fault is observed to be quite thin (less than 75 m) even at depth. Areas of high slip in the 1984 Morgan Hill earthquake anti-correlate spatially with aftershock activity as well as pre-mainshock background seismicity suggesting the distributions are primarily influenced by fault geology. Numerous resolved off-fault structures, whose focal mechanisms offer independent evidence of the plane that slipped, allow a stress inversion to be performed where the orientation of the fault and slip direction are known. The best fitting maximum compressive stress is seen to be at a high angle to the fault consistent with the interpretation that the fault is weak. Because the structures are active to within a few hundred meters of the Calaveras fault, it implies no stress rotations occur approaching the fault at these distances.

Chapter 5 describes details of the unifying technique of waveform-based cross correlation that has made all the research in the prior chapters possible. In some sense, it can be considered a big appendix. Specifically, it addresses issues of correlation measurements for the general earthquake location problem. One end member is the case of repeating earthquakes for which correlation measurements derive the most benefit. It always becomes desireable, however, to apply the method on a larger scale and for more events other than repeating events, even though similarity is known to degrade with separation distance. In these situations, the essential question becomes when do correlation measurements provide an improvement over the arrival times in the catalog phase data. Presented is a means to

quantify when correlations are introducing more measurement error than the catalog pick error. For the specific example of a streak on the Calaveras fault, we demonstrate that correlation data performs better than catalog data out to 2 km separation distances and up to magnitude 3.5.

Some of the major contributions to the field this thesis represents can be summarized as follows. Large clusters of repeating earthquake sequences (approaching 40 events in some) were not known to exist so abundantly in the aftershock zones of the Morgan Hill and Loma Prieta earthquakes. The $1/t$ decay in frequency of Omori's law has been observed for collections of aftershocks before but never for a single repeating event. Substantial velocity variations caused by large earthquakes have been recorded reliably for the first time using natural sources. The power of cross correlation data has been shown to be useful over a wide range of scales and for a variety of different problems. Specific application to relocation of Calaveras fault seismicity produces dramatic one to two order of magnitude improvement in event locations over those determined routinely in the catalog.

Chapter 2 has been published in *Geophysical Research Letters, 25*, p. 4,549-4,552, 1998, with Greg Beroza and Bruce Shaw as co-authors.

Chapter 3 will be submitted to *Journal of Geophysical Research* co-written by my advisor, Greg Beroza.

Chapter 4 will be submitted to *Journal of Geophysical Research* with Götz Bokelmann, Greg Beroza, Felix Waldhauser, and Bill Ellsworth as co-authors.

Chapter 5 will be submitted to *Journal of Geophysical Research* with all of the "relocation gang" as co-authors: Götz Bokelmann, Eva Zanzerkia, Greg Beroza, Felix Waldhauser, and Bill Ellsworth.

1.1 References

Ellsworth, W.L., Cole, A.T., Beorza, G.C. and M.C. Verwoerd, Changes in crustal wave propagation associated with the 1989 Loma Prieta, California, earthquake, *EOS Tran. AGU, 73*, 360, 1992.

Nur, A., and J.R. Booker, Aftershocks caused by pore fluid flow? *Science, 175*, 885-887, 1972.

Waldhauser, F., and W.L. Ellsworth, A double-difference earthquake location algorithm: method and application to the northern Hayward Fault, California, *Bull. Seismol. Soc. Am., 90*, 1,353-1,368, 2000 .

Chapter 2

Postseismic response of repeating aftershocks

Abstract. The recurrence intervals of repeating earthquakes on the San Andreas Fault in the Loma Prieta aftershock zone follow the characteristic $1/t$ decay of Omori's law. A model in which these earthquakes occur on isolated patches of the fault that fail in stick-slip with creep around them can explain this observation. In this model the recurrence interval is inversely proportional to the loading rate due to creep. Logarithmic velocity strengthening friction predicts $1/t$ decay in creep rate following the mainshock. The time dependence of recurrence is inconsistent with a simple viscous constitutive relationship, which predicts an exponential decay of loading rate. Thus, our observations imply post-seismic slip at seismogenic depth under a power law rheology. The time dependence of postseismic deformation measured geodetically may be diagnostic of whether postseismic deformation is caused by creep or possible viscoelastic deformation at greater depths.

2.1 Introduction

Omori's law of aftershock decay holds that the frequency of aftershocks decays as the reciprocal of time following the mainshock [*Scholz*, 1990]. Elastic stress changes, such as those exerted on a fault by a large earthquake, act instantaneously and by themselves can not explain the time dependence of aftershocks; however, there are several possible physical mechanisms that can give rise to the observed time-dependence.

Failure triggered by pore fluid diffusion provides an explanation of aftershock decay

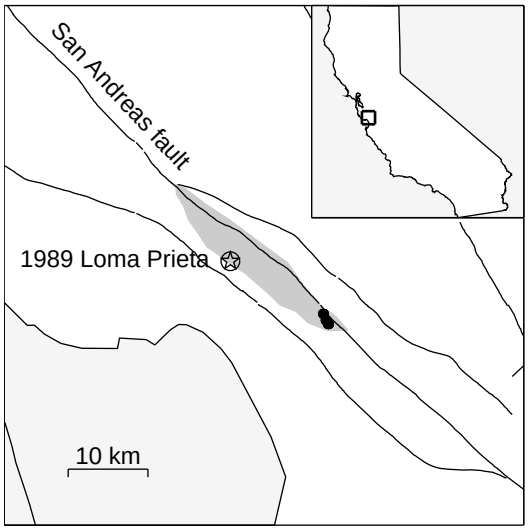

Figure 2.1: Six multiplets (dots) on the San Andreas fault in the aftershock zone (shaded) of the 1989 Loma Prieta earthquake.

[*Nur and Booker,* 1972]. After the mainshock, pore pressure varies spatially and decays as $e^{-1/t}$ with time [*Booker,* 1974], but accounting for all the contributions along the length of the fault leads to $1/t$ behavior for the overall decay of aftershock frequency.

Rate- and state-variable friction has also been shown to give rise to the observed decay rate of aftershocks [*Dieterich,* 1994]. In this model stress changes are assumed to lead to time-dependent nucleation of a population of earthquakes on adjacent parts of the fault. A similar dynamic model of rapidly accelerating crack growth also reproduces Omori's law [*Shaw,* 1993].

In this paper we consider the recurrence intervals of repeating micro-earthquakes on the San Andreas Fault in the aftershock zone of the 1989 Loma Prieta earthquake (Figure 2.1). We find that the repeat times of individual repeating earthquake sequences follow Omori's law. We hypothesize that the repeating earthquakes occur on relatively isolated patches on a fault that is otherwise creeping. This suggests that the recurrence interval is inversely proportional to the loading rate due to creep and that the observed $1/t$ behavior reflects the creep response of the San Andreas fault to the stress step from the Loma Prieta mainshock. Logarithmic velocity strengthening friction predicts the observed $1/t$ response. This represents a new mechanism whereby aftershocks follow Omori's law.

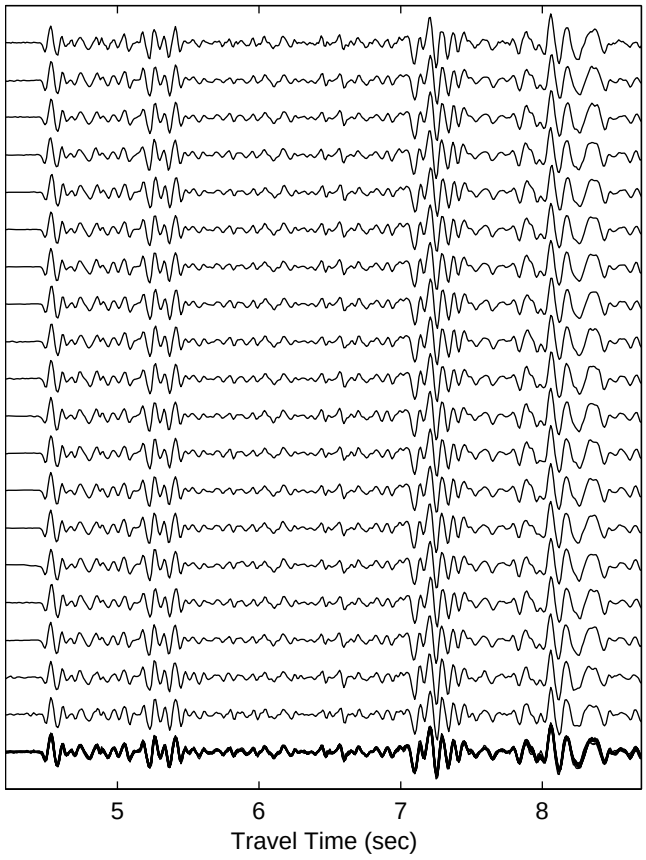

Figure 2.2: Unfiltered seismograms of 19 events within one of the six multiplets. Bottom trace shows all events superposed.

2.2 Repeating Earthquakes

We use the same criterion as in a previous study of temporal variation in coda-Q [*Beroza et al.,* 1995] to identify six sets of repeating earthquakes. Events within a multiplet have relative location precision of ± 7 m and are generally separated by less than 20 m. The average magnitude of the earthquakes is 1.5, correponding to a source radius of about 30 m for a 3 MPa stress drop and so represents approximate repeated rupture of the same fault patch. The multiplets contain from 10 to 19 events and are separated from each other by up to 3 km. The depths of these sequences range from 8 to 9 km. Figure 2.2 shows the similarity of seismograms from one multiplet recorded at Calnet station HCA.

2.3 Time-Dependent Recurrence

The aftershocks in each multiplet occur most frequently right after the mainshock. Figure 2.3 shows inverse recurrence interval for the six multiplets as a function of time on log-linear and log-log plots. Exponential time decay should appear as a straight line on the log-linear graph (upper panel) where the slope is the coefficient of t in the exponent. Power law decay should appear as a straight line on a log-log graph (lower panel) where the slope is equal to the power, p, of t^p. In each case the recurrence interval of the repeating aftershock sequences follows a power law rather than exponential decay. The repeating aftershock sequences also match the t^p decay in frequency for the whole collection of Loma Prieta aftershocks for which $p = -1.01$, i.e. Omori's law. Values of the exponent, p, for individual repeating aftershock sequences are: -0.78, -0.89, -0.90, -0.96, -0.98, and -1.04, with average standard errors of ± 0.05.

2.4 Velocity-Dependent Friction and Creep

We believe that the repeating earthquakes occur on relatively isolated patches of the fault that is otherwise creeping aseismically. It is difficult to understand how the fault could otherwise repeatedly set up conditions for the recurrence of the same micro-earthquake. This suggests that the frequency of recurrence is proportional to the loading rate due to creep and that the observed $1/t$ behavior reflects the creep response of the San Andreas fault to the stress step from the Loma Prieta mainshock. A simple viscous fault zone rheology, in which resistance to slip is linearly proportional to velocity, is inconsistent with our observations because it predicts that fault slip will decay exponentially under external stress.

Pore fluid diffusion can explain Omori's law for all the events within the volume surrounding the fault [*Booker*, 1974]; however, change in pore pressure, and therefore stress, is a complicated function of space and time and so does not offer a simple explanation of our observations for repeating aftershock sequences at a fixed location.

A logarithmic velocity strengthening friction law [*Dieterich*, 1978], on the other hand, predicts the observed $1/t$ decay in loading rate for creep as follows. Assume that stress

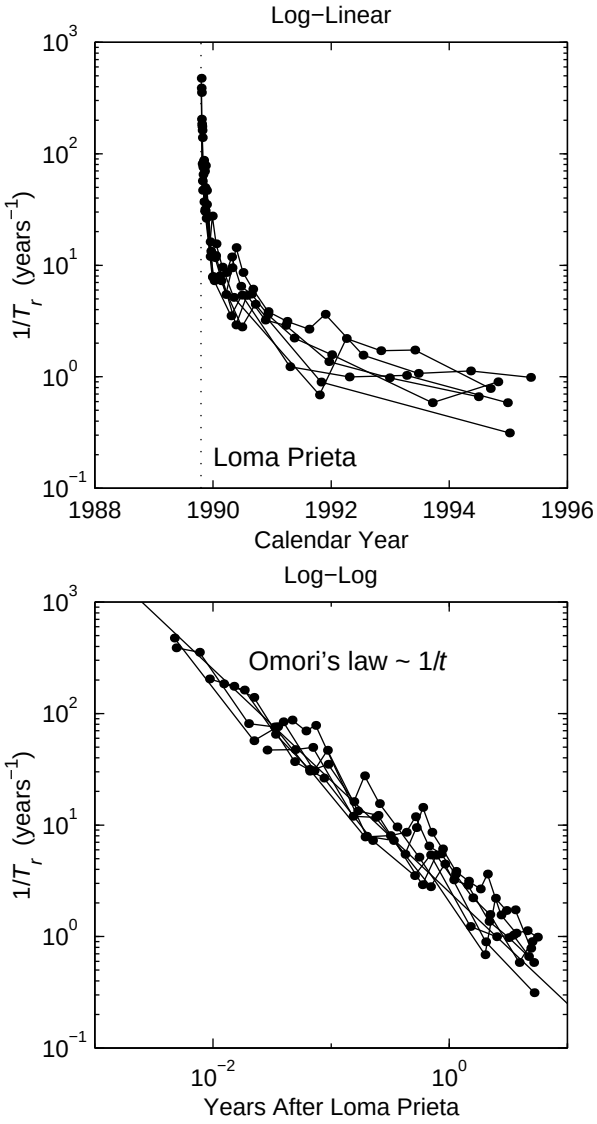

Figure 2.3: Inverse recurrence interval as a function of time on log-linear and log-log plots, displaying power law time decay for each of the six multiplets.

drop, $\Delta\tau$, for each event is constant. This implies that shear stress rate, $\dot{\tau}$, is inversely proportional to recurrence interval, T_r,

$$\dot{\tau} = \frac{\Delta\tau}{T_r} \sim \frac{1}{T_r}. \tag{2.1}$$

Consider a stably sliding zone subjected to the static stress increase of the mainshock. As creep continues this region will be destressed proportional to the amount of total slip. Therefore stress rate decay is proportional to the sliding velocity, V,

$$\dot{\tau} \sim -kV, \tag{2.2}$$

where k is a coupling constant dependent on the geometry of the stuck patch and the creeping region. For quasistatic sliding, the frictional resistance Φ will equal the shear stress, and so,

$$\dot{\tau} = \dot{\Phi}. \tag{2.3}$$

For a creeping fault, we adopt a velocity strengthening steady-state friction [*Rice and Gu,* 1983].

$$\mu_{ss} = \mu_0 + (a-b)\ln\left(\frac{V}{V_0}\right), \tag{2.4}$$

$$\Phi = \mu_{ss}\sigma_n, \tag{2.5}$$

The frictional coefficient, μ_0, corresponds to a reference velocity, V_0, and σ_n is the normal stress. Assuming constant normal stress,

$$\dot{\Phi} = \sigma_n \frac{d\mu_{ss}}{dt} = \sigma_n \frac{d\mu_{ss}}{dV}\frac{dV}{dt}. \tag{2.6}$$

Differentiating equation (2.4) with respect to velocity yields,

$$\frac{d\mu_{ss}}{dV} \sim \frac{1}{V}. \tag{2.7}$$

Relating equations (2.2), (2.3), (2.6), and (2.7) obtains:

$$\frac{dV}{dt} \sim -V^2, \tag{2.8}$$

which yields,

$$V \sim 1/t. \tag{2.9}$$

While creep progresses and the sliding regions are destressed according to (2.2), stuck patches that fail in repeating earthquakes are loaded proportionally but with opposite sign. So from (2.1) and (2.9), the predicted stress rate measured by the recurrence interval of the earthquakes will vary as,

$$\dot{\tau} \sim kV \sim 1/t, \tag{2.10}$$

consistent with our observations.

Experiments record similar $1/t$ relaxation during slide-hold tests and show that rate effects dominate state effects at low slip velocities, comparable to stable fault creep [*Reinen et al.,* 1994]. In a separate study of repeating earthquakes on the Calaveras fault, the variation of seismic moment with recurrence interval was interpreted as showing state dependence [*Vidale et al.,* 1994] manifested as greater fault healing for longer contact time. Unlike our study, their observation applies to the stuck part of the fault rather than the part that is creeping. Earthquakes necessarily occur in zones of velocity weakening, whereas velocity strengthening gives rise to stable creep.

We have also identified sets of repeating aftershocks of the 1984 Morgan Hill, California earthquake, which occurred on the Calaveras fault. These sequences show power law behavior as well, but with greater variability in the value of p (from -0.6 to -1.0). This greater variability may be due to the large postseismic transient (greater than the coseismic change) observed geodetically following this event [*Prescott et al.,* 1986]. That is, the creep response of this fault may involve more than the response to a stress step imposed by the mainshock. Alternatively, it may reflect the fact that the distribution of repeating aftershocks studied on the Calaveras fault are separated by much greater distances than the events studied on the San Andreas fault and that different parts of the fault exhibit different rheologies (i.e. plastic behavior for $p \neq 1$).

It is interesting to note that detailed creepmeter measurements of afterslip following earthquakes reveal it is the accumulation of smaller creep events [*Smith and Wyss,* 1968; *Bilham,* 1989]. The events show similar Omori's law decay in frequency as our aftershocks, slipping roughly equal amounts, and so may be considered aseismic analogs of our repeating earthquakes. Individual creep events are universally observed to slip according to a power law [*Wesson,* 1988]. Geodetic and creep measurements of postseismic transients for the 1966 Parkfield [*Smith and Wyss,* 1968], 1968 Borrego Mountain [*Burford,* 1972], 1976 Guatemala [*Bucknam et al.*, 1978], 1979 Imperial Valley [*Harsh,* 1982], 1987 Superstition Hills [*Bilham,* 1989], and 1992 Landers earthquakes [*Shen et al.,* 1994] all show power law decay. To our knowledge, there does not yet exist an example of a postseismic transient that exhibits exponential decay.

2.5 Conclusions

We find that recurrence intervals of individual repeating earthquake sequences in the aftershock zone of the 1989 Loma Prieta earthquake follow Omori's law. This behavior is predicted by the creep response to a stress step for a logarithmic velocity strengthening friction law. Thus, there are two mechanisms whereby Dieterich-Ruina friction can lead to Omori's law. The first mechanism is that earthquake nucleation occurs by self-driven accelerated runaway to failure, which is controlled by friction on the fault patch itself [*Dieterich,* 1994]. The second mechanism, proposed in this paper, is that Omori's law can arise from repeated rupture on the same fault patch when rate-dependent friction controls the loading velocity of the creep on the surrounding fault. Both mechanisms may be expected to operate in aftershock sequences.

This $1/t$ behavior arising from logarithmic velocity strengthening has been pointed out previously for laboratory [*Reinen et al.,* 1994] and surface-based measurements [*Marone et al.,* 1991]. What is new in our work is we have used the time dependence of repeating aftershocks to probe these properties at depth. Our method provides a local measure of the rheology at depth; here at 8 to 9 km on this portion of the San Andreas, although the exact spatial location is not constrained. The occurrence of these repeating events indicates significant postseismic creep and suggests the existence of velocity strengthening

and velocity weaking zones interspersed at seismogenic depths. Earthquake rupture may therefore be arrested or retarded as it propagates into velocity strengthening zones.

It is often difficult to distinguish postseismic slip at seismogenic depths from viscous postseismic slip in the deeper, ductile regime [*Nur and Mavko,* 1974] with available geodetic measurements. A non-linear "hot-friction" model using the same constitutive law as (2.4) proposes that transients may be explained by creep below a locked seismogenic zone [*Linker and Rice,* 1997]. Our results suggest that the time-dependence of postseismic deformation may help to discriminate between aseismic creep — either at seismogenic depths or deeper — and viscous deformation.

Acknowledgments. We are grateful to Nick Beeler, Mike Blanpied, Chris Marone, Paul Segall, Mark Murray, Amos Nur, Juliet Crider, and Bill Bosl for helpful discussions. DPS and GCB were supported by NSF Grant No. EAR-9725238 and BES was supported by USGS Grant 1434-HQ-97-GR03074.

2.6 References

Beroza, G. C., A. T. Cole, and W. L. Ellsworth, Stability of coda wave attenuation during the Loma Prieta, California, earthquake sequence, *J. Geophys. Res., 100,* 3977-3987, 1995.

Bilham, R., Surface slip subsequent to the 24 November 1987 Superstition Hills, California, earthquake monitored by digital creepmeters, *Bull. Seismol. Soc. Am., 79,* 424-450, 1989.

Booker, J. R., Time dependent strain following faulting of a porous medium, *J. Geophys. Res., 79,* 2037-2044, 1974.

Bucknam, R. C., G. Plafker, and R. V. Sharp, Fault movement [afterslip] following the Guatemala earthquake of February 4, 1976, *Geology, 6,* 170-173, 1978.

Burford, R. O., Continued slip on the Coyote Creek fault after the Borrego Mountain earthquake, in The Borrego Mountain Earthquake of April 9, 1968, *U.S. Geol. Surv. Prof. Pap., 787,* 105-111, 1972.

Dieterich, J. H., Time-dependent friction and the mechanics of stick-slip, *Pure Appl. Geophys., 116,* 790-806, 1978.

Dieterich, J. H., A constitutive law for rate of earthquake production and its application to earthquake clustering, *J. Geophys. Res., 99,* 2601-2618, 1994.

Harsh, P. W., Distribution of afterslip along the Imperial Fault, in The Imperial Valley Earthquake of October 15, 1979, *U.S. Geol. Surv. Prof. Pap., 1254,* 193-203, 1982.

Linker, M. F., and J. R. Rice, Models of postseismic deformation and stress transfer associated with the Loma Prieta earthquake, in The Loma Prieta Earthquake of October 17, 1989, *U.S. Geol. Surv. Prof. Pap., 1550-D,* 253-275, 1997.

Marone, C.J., C.H. Scholz, R. Bilham, On the mechanisms of earthquake afterslip, *J. Geophys. Res., 96,* 8441-8452, 1991.

Nur, A., and J. R. Booker, Aftershocks caused by pore fluid flow? *Science, 175,* 885-887, 1972.

Nur, A., and G. M. Mavko, Postseismic viscoelastic rebound, *Science, 183,* 204-206, 1974.

Prescott, W. H., N. E. King, and G. Guohua, Presiesmic, coseismic, and postseismic deformation associated with the 1984 Morgan Hill, California, earthquake, in *The 1984 Morgan Hill, CA earthquake,* edited by J. H. Bennett and R. W. Sherburne, pp. 137-148, Cal. Div. Mines and Geo. Spec. Pub. 68, 1986.

Rice, J. R., and J.-C. Gu, Earthquake aftereffects and triggered seismic phenomena, *Pure Appl. Geophys., 121,* 187-219, 1983.

Reinen, L. A., J. D. Weeks, and T. E. Tullis, The frictional behavior of lizardite and antigorite serpentinites: experiments, constitutive models, and implications for natural faults, *Pure Appl. Geophys., 143,* 317-358, 1994.

Scholz, C. H., *The Mechanics of Earthquakes and Faulting,* 439 pp., Cambridge Univ. Press, New York, New York, 1990.

Shaw, B. E., Generalized Omori law for aftershocks and foreshocks from a simple dynamics, *Geophys. Res. Lett., 20,* 907-910, 1993.

Shen, Z., D. Jackson, Y. Feng, M. Cline, M. Kim, P. Fang, and Y. Bock, Postseismic deformation following the Landers earthquake, California, 28 June 1992, *Bull. Seismol. Soc. Am., 84,* 780-791, 1994.

Smith, S. W., and M. Wyss, Displacement on the San Andreas fault subsequent to the 1966 Parkfield earthquake, *Bull. Seismol. Soc. Am., 58,* 1955-1973, 1968.

Vidale, J. E., W. L. Ellsworth, A. Cole, and C. Marone, Variations in rupture process with recurrence interval in a repeated small earthquake, *Nature, 368,* 624-626, 1994.

Wesson, R. L., Dynamics of fault creep, *J. Geophys. Res., 93,* 8929-8951, 1988.

Chapter 3

Coseismic and postseismic velocity changes

Abstract. Repeating earthquakes that rupture approximately the same fault patch and have nearly identical waveforms are a useful tool for measuring temporal changes in wave propagation in the earth's crust. Since source and path effects are common to all earthquakes in a repeating earthquake sequence (multiplet), differences can be attributed to changes in the characteristics of the medium. We have identified over 20 multiplets containing between 5 and 40 repeating events in the aftershock zones of the Loma Prieta and Morgan Hill earthquakes. Several of the multiplets have events before the Loma Prieta mainshock. Post-mainshock events reveal delays of phases in the early S-wave coda of as much as 0.2 seconds relative to pre-mainshock events. The delay amounts to a path-averaged coseismic velocity decrease of about 1.5% for P-waves and 3.5% for S-waves. Since most of the multiplets are aftershocks and follow Omori's law, we have excellent temporal sampling in the immediate post-mainshock period. The amplitude of the velocity decrease decays logarithmically in time following the mainshock. In some cases it returns to the pre-mainshock values, while in others it does not. Similar results are obtained for the Morgan Hill mainshock. Because the fractional change in S-wave velocity is greater than the fractional change in P-wave velocity, it suggests that the opening or connection of fluid-filled fractures may be the underlying cause. Since the magnitude of the velocity change is significant, low effective pressures are indicated. Our results suggest that the changes are predominantly near the stations and shallow but we can not exclude the possibility that changes occur at greater depth as well. If the variations are shallow, we may be detecting the lingering effects of nonlinearity during mainshock strong ground motion. If the variations are deep, it suggests that pore pressures at seismogenic depths are high, and likely play a key role in the earthquake process.

3.1 Introduction

Temporal variations in properties of the earth's crust related to earthquakes have been sought for decades. In the early 1970's, premonitory changes in seismic wave velocity as large as 10 to 20% before earthquakes in Russia [*Savarensky,* 1968; *Semenov,* 1969], New York [*Aggarwal et al.,* 1973, 1975], and California [*Whitcomb et al.,* 1973] were reported. These studies suggested that reliable earthquake prediction was imminent; however, the measurements used in them were based on travel time changes for naturally occurring earthquakes whose position and origin time were poorly known. The initial excitement was deflated when subsequent analysis of quarry blasts and man-made explosions, for which the location and origin time were known, showed no detectable changes in seismic velocity down to 1% for moderate earthquakes up to magnitude 5.4 [*McEvilly and Johnson,* 1974; *Boore et al.,* 1975; *Kanamori and Fuis,* 1976; *Bolt,* 1977; *Chou and Crosson,* 1978]. Closer examination of the original data and techniques revealed that the apparent signals could be explained by differences in event location and unwanted effects of unknown earth structure [e.g. *Lindh et al.,* 1978; *Got and Coutant,* 1995].

The discovery of repeating events (doublets) allowed natural seismicity to be used again as a source for waves, but eliminated virtually all of the unwanted path effects from the measurement. These studies appeared to confirm that velocity variations were non-existent or very much smaller than found previously, on the order of 0.1% [*Poupinet et al.,* 1984; *Aster et al.,* 1990; *Nadeau et al.,* 1994a, 1994b; *Haase et al.,* 1995]. Studies of repeating earthquakes also showed that Coda Q, was quite stable within the noise and limitations of the measurement techniques [*Beroza et al.,* 1995; *Hellweg et al.,* 1995; *Antolik et al.,* 1996].

Controlled source experiments have found that measureable velocity variations do occur in the crust. An active seismic survey conducted after the 1992 M 7.3 Landers earthquake found a 0.5 to 1.5% increase in P- and S-wave travel times from 1994 to 1996 [*Li et al.,* 1998] for waves propagating through the shallow fault zone. At Parkfield, Vibroseis monitoring found travel time changes in the S-wave coda up to 50 msec, which were

modeled as a 6% velocity increase where previous M 6 earthquakes have nucleated [*Karageorgi et al.,* 1992, 1997; *Korneev et al.,* 2000]. In Germany at the 9 km deep KTB borehole, a hydraulic fracturing induced-seismicity experiment measured a $\sim$ 0.2% decrease in S-wave velocity at depth [*Bokelmann and Harjes*, 2000].

Closer analysis of natural sources in the form of earthquake multiplets produced reliable evidence of substantial velocity changes associated with a volcanic eruption ($\sim$ 1.2%) [*Ratdomopurbo and Poupinet,* 1995] and with earthquakes ($\sim$ 5%) [*Beroza et al.,* 1997]. In this paper we build on earlier results of [*Ellsworth et al.,* 1992; *Beroza et al.,* 1997] and demonstrate consistent, reproducible behavior for both the 1984 M 6.2 Morgan Hill and 1989 M 6.9 Loma Prieta earthquakes. We find that the velocity decreases co-seismically, and that the amplitude of the change then heals postseismically as the logarithm of elapsed time after the mainshock. The magnitude of the S-wave velocity change is much larger than that of the P-wave change suggesting that fluids are present.

Most of the evidence points towards a shallow origin for the observed velocity change. The fact that the change is a decrease in velocity for all stations, the logarithmic recovery of velocity with time, and the association of the strongest signals with stations located in sedimentary environments suggest that the anomalies we observe may represent the lingering memory of nonlinearity during near-source strong ground motion.

3.2 Data

In this study we use microearthquakes to study the effects of large earthquakes on the Earth's crust. These microearthquakes are detected by the Northern California Seismi Network (NCSN), for which high-gain, vertical-component, digital waveforms are available at the Northern California Earthquake Data Center since 1984. The period from 1984 to present saw two large earthquakes in the midst of the NCSN, the 1984 Morgan Hill and 1989 Loma Prieta events. A benefit of using natural sources is that the waves emanate from the depths at which earthquakes occur, whereas field surveys are restricted to the near surface. As earthquake sources they are also rich in both P and S waves. A disadvantage over controlled sources is that the locations of these small earthquakes is not known.

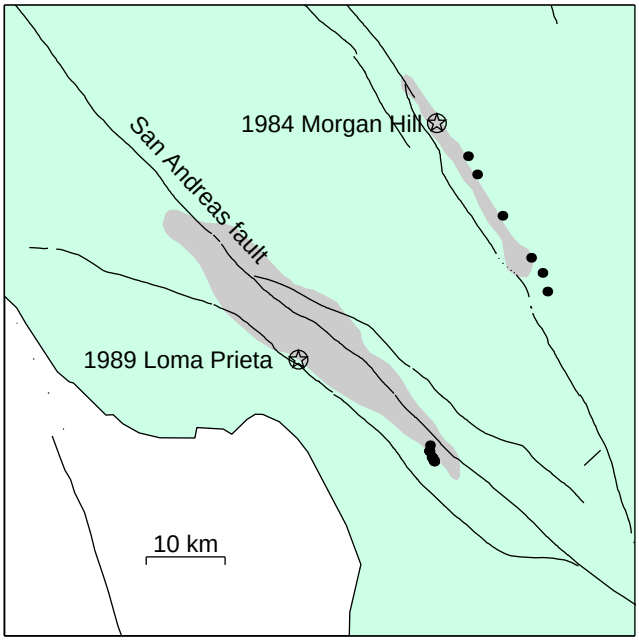

Figure 3.1: Multiplet clusters denoted by dots in the shaded aftershock zones of the 1984 Morgan Hill and 1989 Loma Prieta earthquakes.

Because earthquakes themselves are located within a crust with an incompletely known velocity structure, any changes in the real velocity over time may be mapped into a translation of earthquake hypocenters.

Fortunately the existence of large clusters of repeating earthquakes, or ”multiplets,” is close to the ideal of having repeatable sources that occur at the same spot but at different times. Because source and path effects are common to all events in a multiplet, any changes observed may be assumed to be caused by changes in the medium. We have identified large multiplets containing between 5 and 40 events in the aftershock zones of the 1984 Morgan Hill and 1989 Loma Prieta earthquakes (Figure 3.1). Precise relative relocation of these events reveals they rupture approximately the same fault patch in each case (Figure 3.2). Four of the mulitplets at the southern end of the 1989 Loma Prieta earthquake also have a pre-mainshock event enabling a coseismic measurement of velocity change. Because the majority of the events are aftershocks, there is excellent postseismic temporal sampling when the change in velocity signal is observed to vary rapidly and strongly. Note the frequency and time duration of several years for these measurements may be economically prohibitive for most controlled-source experiments.

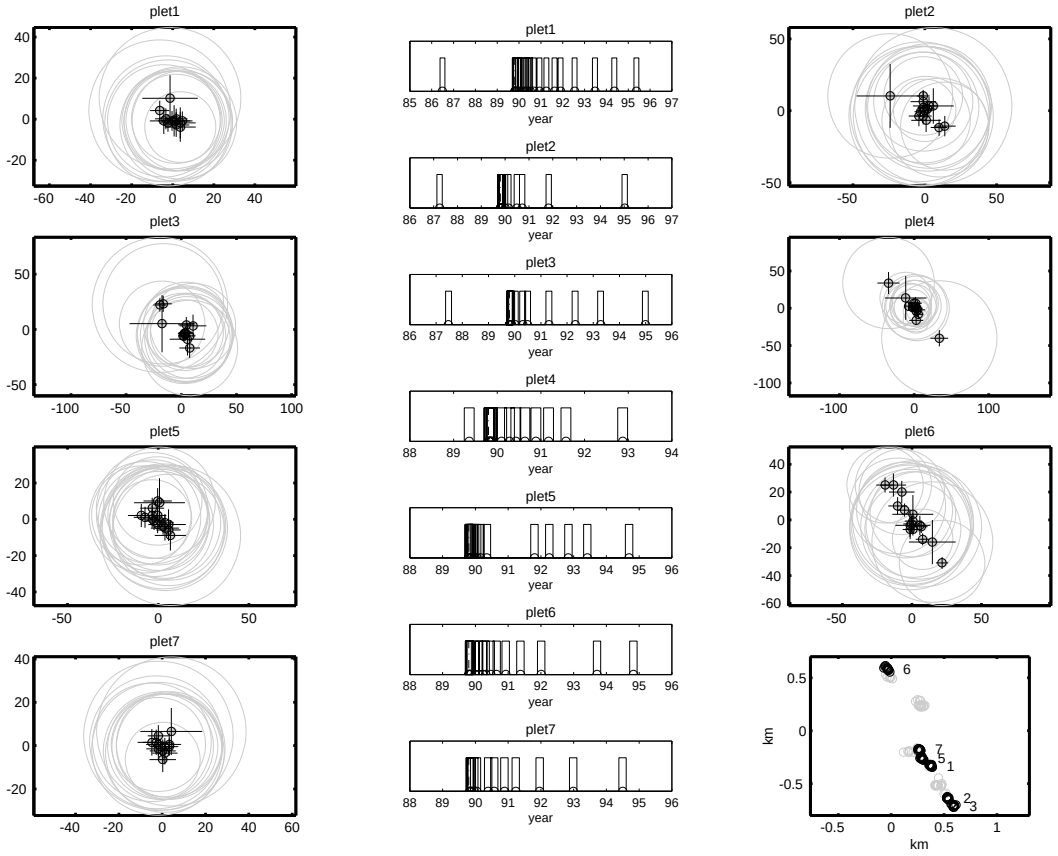

Figure 3.2: Approximate source dimensions and location errors for some example mutiplets on the San Andreas fault at the southern tip of the Loma Prieta rupture zone. The first four multiplets each have a pre-Loma Prieta event.

An examination of the seismograms at a station (Figure 3.3) reveals nearly identical waveforms, confirming source and path effects for all events are common. The high degree of similarity throughout the seismogram also enables the tracking of individual phases. If a velocity change has occurred between events a delay or advance of these phases may be expected.

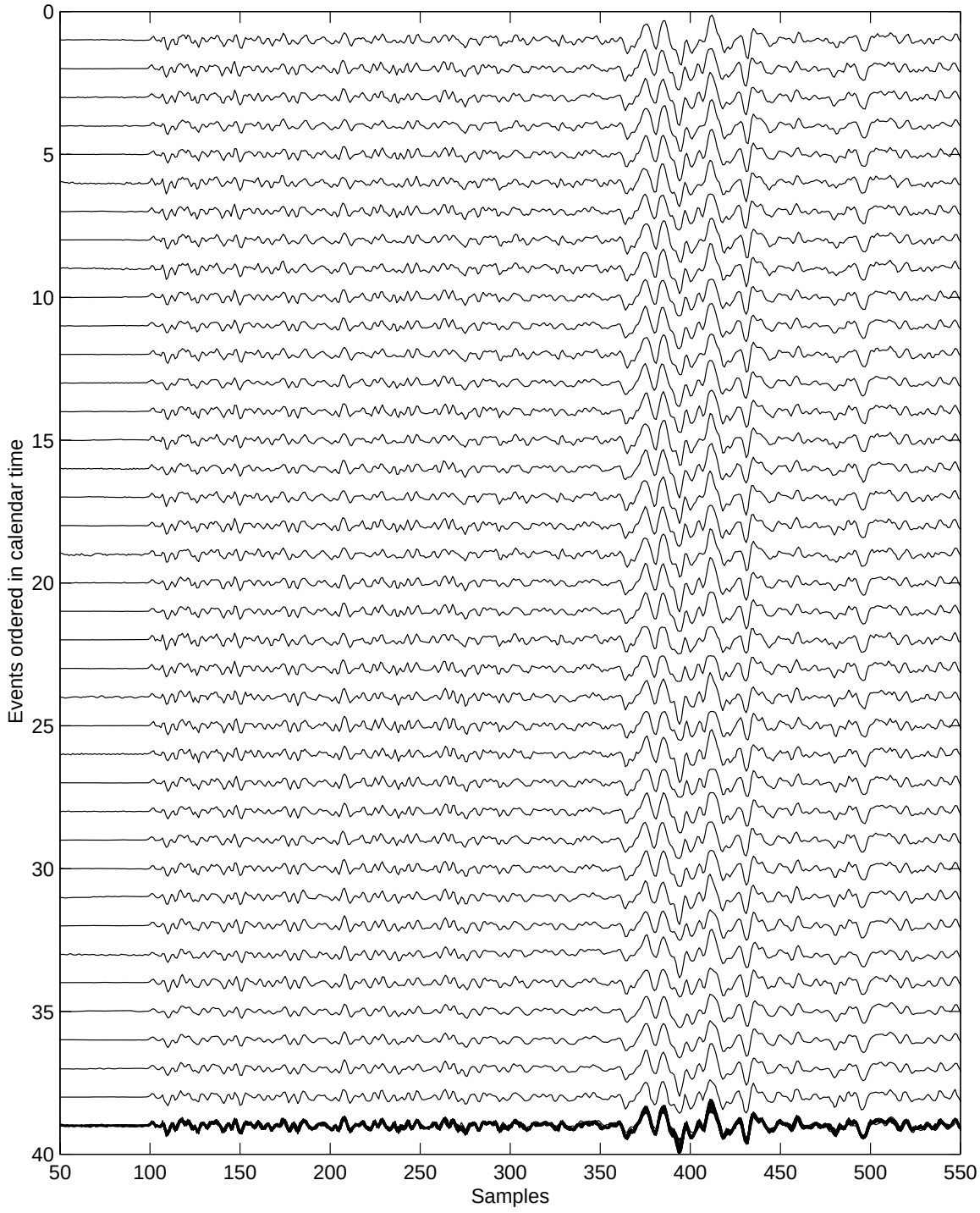

Figure 3.3: Unfiltered seismograms at station JST for 38 different events in a multiplet cluster on the Calaveras fault exhibiting nearly identical waveforms throughout the entire coda. The last trace shows all the events superposed.

3.3 Technique

We use the method of *Poupinet et al.,* [1984] to measure delay as a function of time in the seismogram. If a velocity change has occurred between the origin time of two events, a stretching in one of the seismograms may be observed if later phases in the coda spend a longer time in an altered medium (see top panel of station JPL in Figure 3.4). Slightly mislocated hypocenters, on the other hand, would cause a translation of the waveforms, for a given phase. Consider the travel time of the same phase on two different repeating events, t_1 and t_2, which has been shifted by delay, dt, due to a change in velocity, dv, between the two times, v_1 and v_2.

$$t_2 = t_1 + dt \tag{3.1}$$

$$v_2 = v_1 + dv \tag{3.2}$$

$$d = v_1 t_1 = v_2 t_2 = v_2(t_1 + dt) \tag{3.3}$$

The distance traveled by the phase is given by, d. Rearranging terms,

$$dt = \frac{v_1 - v_2}{v_2} t_1 = \frac{-dv}{v_2} t_1 \tag{3.4}$$

Expressed in terms of fractional slowness,

$$dt = \frac{d\eta}{\eta_1} t_1 \tag{3.5}$$

So the slope of delay vs. time in the seismogram gives the fractional slowness change, which can also be expressed as a percentage.

The top panels in Figure 3.4 display the seismograms for a pre-89 event and the first event following the mainshock for a multiplet containing 14 events at the southern edge of the Loma Prieta rupture zone. At station HFP far from the mainshock (Figure 3.5), the seismograms overlay cleanly indicating no temporal variation. At station JPL within the Loma Prieta rupture zone, a delay of phases is observed for the same events. Coherence is also seen to systematically decrease for stations in the rupture zone [*Baisch and Bokelmann,* 2000].

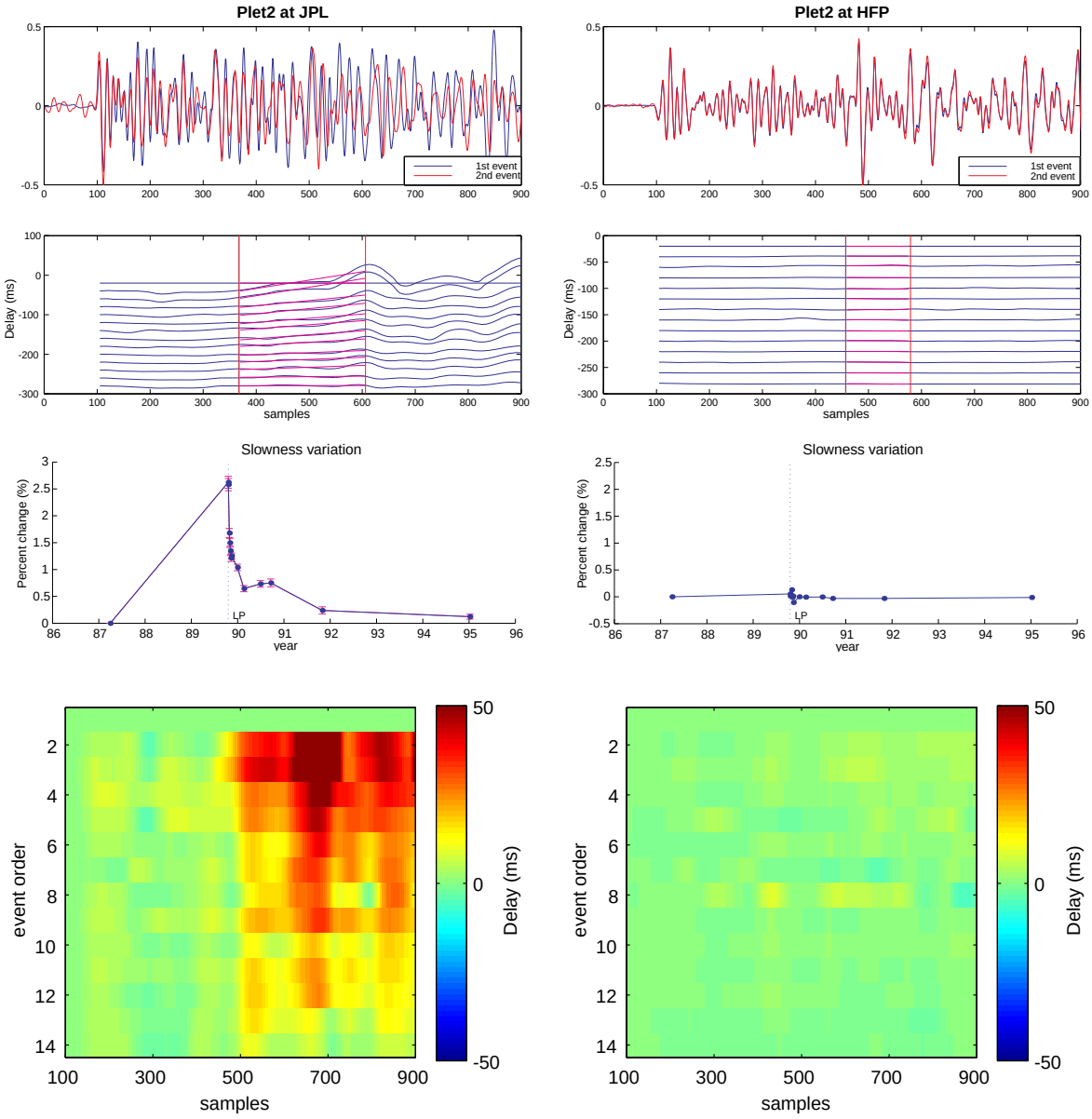

Figure 3.4: Comparison of a station that does show velocity changes (left) and one that does not (right) for plet2. See text for explanation.

The second panels quantify the delay of phases as a function of time in the seismogram for all 14 events in the multiplet. These are computed by stepping through the seismogram a sample at a time using 1.4 second window lengths. All values are referenced to the first event, which appears as a flat line. Since correlations operate on event pairs we can take advantage of all possible measurement combinations, Δt_{ij}, and use the redundancy in the multiplet to invert for the relative delays, t_i, that are most consistent with all of the measurements [*VanDecar and Crosson,* 1990].

$$\begin{pmatrix} 1 & -1 & 0 & 0 \\ 1 & 0 & -1 & 0 \\ 1 & 0 & 0 & -1 \\ 0 & 1 & -1 & 0 \\ 0 & 1 & 0 & -1 \\ 0 & 0 & 1 & -1 \\ 1 & 1 & 1 & 1 \end{pmatrix} \begin{pmatrix} t_1 \\ t_2 \\ t_3 \\ t_4 \end{pmatrix} = \begin{pmatrix} \Delta t_{12} \\ \Delta t_{13} \\ \Delta t_{14} \\ \Delta t_{23} \\ \Delta t_{24} \\ \Delta t_{34} \\ 0 \end{pmatrix} \tag{3.6}$$

The inverted relative delays, t_i, are in fact what is plotted in the second panels of Figure 3.4. For stations that have no velocity changes, using all the data will provide more stable estimates. For stations that do have a velocity change, the closure assumption of equation 3.6 may be violated since waveform similarity begins to break down (i.e., $\Delta t_{12} + \Delta t_{23} = \Delta t_{13}$), but more stable results should still be obtained because each measurement is weighted by its correlation coefficient [*Schaff et al.,* 2001]. A window around the expected S-wave arrival time is marked by vertical lines. The accumulated delays in the early S-wave coda can be quite large (up to 200 ms) for stations near the rupture zone.

Care must be taken when interpreting results from such moving window analyses. 100 ms delays have been observed later in the coda (between 2 and 3 times the S-wave travel time) for events separated by as little as 500 m, due to geometrical propagation effects rather than true velocity changes [*Got and Coutant,* 1997]. For example, if the S-wave velocity at depth between two events separated by 500 m is 3.5 km/s, then the travel time difference will vary sinusoidally with azimuth reaching a maximum of 143 ms. Since phases later in the coda may leave the source at different azimuths, delays in this example could range from -100 to 100 ms depending on how different the take-off and azimuth are from the direct arrivals. Hence it is essential that the events in Figure 2 are co-located to

10 meter precision to remove most of the path effects $(10\mathrm{m} \times 1\mathrm{ms}/3.5\mathrm{m} = 3\mathrm{ms})$. This means the delay, dt, in equation 3.1 occurs only from a change in velocity of the medium and not from earth structure due to different source locations.

Many of the multiplets we use occur at a point within the resolution of the location errors. The delays we find are large in the early coda (right after the S-wave onset). Most stations far from the mainshock epicenters show no appreciable delays. These results are consistent for all the different multiplet clusters we find for both the Morgan Hill and Loma Prieta earthquakes. For these reasons and the fact that coincident coseismic and postseismic temporal decay could not systematically be produced by earth structure or hypocenter differences, we are confident that the observed changes are real temporal variations in the crust associated with these large earthquakes.

The third panels of Figure 3.4 display the estimated slowness changes obtained from the slope of the line fits in the second panels. Station JPL records a large $\sim 2.5\%$ coseismic increase in slowness (velocity decrease), which subsequently heals over time returning to close its original value before the Loma Prieta earthquake. From equations 3.1–3.5 the slope constitutes a measure of the path-averaged slowness assuming a constant velocity change over the entire volume where the affected rays have traveled.

The average error bars for the slowness change at JPL are 0.07% in Figure 3.4. These are computed as the formal standard errors of the slope from the line fit, but do not entirely reflect the potential sources for error. The choice of the window to make the line fit is a subjective decision which influences the measurements, but is hard to quantify. Usually, the windows are chosen where the delay varies linearly with time in the seismogram, because the model is most likely valid under these conditions. The window can significantly affect the amplitude of the velocity change measurement. The relative velocity change with respect to other events, however, is much more reliable and so the observed temporal decay is robust. Another source of error is due to the choice of the reference event. Any errors associated with this event will be transmitted entirely to the other events, because its delays as a function of time in the seismogram are zeroed out (no error). Therefore the error estimates for all the other events represent some kind of upper bound: their individual error plus the error of the reference event.

The bottom panels of Figure 3.4 are a color representation of the identical delay vs.

time data as in the second panels, where each row corresponds to an event in the multiplet and the x-axis is time into the seismogram. The first event is used as a reference event, which appears as a green band (no change). The color gradation reveals the postseismic decay and recovery back towards the original state. We use these plots to display the spatial distribution of the travel time changes in the next section.

3.4 Spatial Distribution of Velocity Changes

The strongest velocity change signal is confined to stations near the rupture zones of both the Morgan Hill and Loma Prieta earthquakes. Figures 5 through 7 display the raw delay measurements for three representative multiplets. The origin on each map denotes the location of each multiplet source. Blank rows indicate events missing from the multiplet at the given station. Listed next to each station name is the mean cross-correlation coefficient determined as an average over all measurement combinations, Δt_{ij}, in equation 3.6 and for all time steps in the seismograms. Approximate rupture zones determined from the aftershock distribution for Morgan Hill and Loma Prieta are shaded.

Figure 3.5 shows all the stations for plet2 examined in detail for JPL and HFP in Figure 3.4. Positive delays represent an increase in slowness (lower velocity) relative to the pre-Loma Prieta event. The sign of these changes are predominantly in the same sense, indicating a coseismic decrease in velocity everywhere. Stations missing the first event are referenced to the last available event. A black tick in the upper left hand corner for each station represents the occurrence of Loma Prieta. A fixed color scale from -60 to 60 ms illuminates a widely distributed travel time change signal over stations sensitive to smaller variations. If the scale ranges from -100 to 100 ms, only stations JEC, JBZ, JTG, JPL, HPR, and HCB show any significant color. It is interesting that the smaller signal is measured at even some distant stations, which are mainly clustered near the San Andreas or Calaveras faults. For most of these stations, the coseismic velocity decrease recovers completely by the later events in the multiplet (i.e. HSF HBT HAZ HSP JCB JRR HGW JSS JRG). Stations JBZ and JEC have not yet fully healed, perhaps indicative of permanent, irreversible deformation. Stations JAL and JHL, which should have experienced very strong shaking

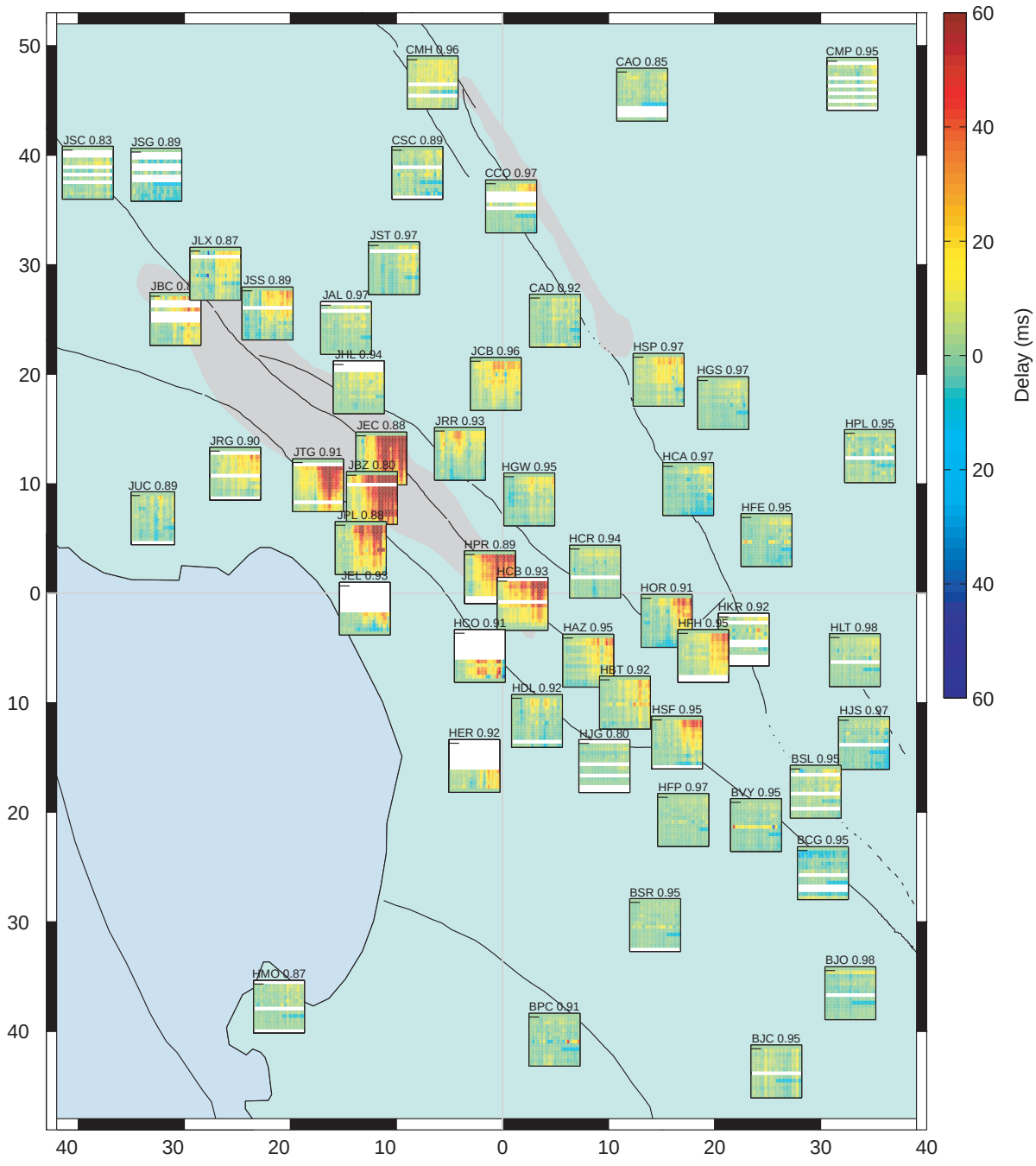

Figure 3.5: Travel time delays due to Loma Prieta measured by plet2 (see text for explanation). Map axes are in kilometers.

in the mainshock, exhibit almost no velocity change and the waveform data are highly coherent with time. The reason for this may be that they are on hard rock sites [*Phillips and Aki*, 1986; *Seekins* personal comm.] whereas stations such as JEC are on softer sediments. The other six San Andreas multiplets in Figure 3.2 display the same general travel travel time change pattern as that recorded in Figure 3.5.

This same multiplet was anaylzed by [*Baisch and Bokelmann*, 2000] who similarily observed the largest decrease in coherence at stations JEC, JBZ, JPL, and HPR. A measured signal at HAZ and JSS, they interpret as back scatter and forward scatter, respectively, off an anomalous region below station JBZ. They argue that a change in coherence may provided complementary information for scattered phases compared to velocity change analysis, which measures delayed phases. A difference in the measured patterns for these reflected and transmitted waves may therefore help to constrain spatially where the changes have occurred. However, since we also observe a travel time change at HAZ and JSS, it appears these phases have a significant portion of their ray path that traverses an altered region.

In Figure 3.6, we repeat the analysis for the 1984 Morgan Hill earthquake using a multiplet cluster on the Calaveras fault and only events before Loma Prieta. In this case all stations are referenced to the last event since no pre-mainshock reference event was available for Morgan Hill. This velocity increase with time is exactly consistent with the postseismic healing observed for Loma Prieta. Again the strongest signal is for stations CCO and HSP close to the rupture zone. This time measured with very high coherence, however. The sign of the changes is also everywhere the same within the resolution of the technique. Interestingly, stations JEC, JBZ, JTG, and JPL show a detectable Morgan Hill signal even though this event was only a magnitude 6.2 and the shaking would have been relatively modest at these distances. The other stations close to major faults that showed a smaller signal for Loma Prieta (i.e. HSF HOR HCB HPR). also show a change associated with the Morgan Hill earthquake.

Analyzing the two events in this same multiplet before Loma Prieta and the four others that follow show travel time changes associated with the Loma Prieta earthquake as measured from a Calaveras fault mulitplet (Figure 3.7). All stations are referenced to the first event in the sequence. Black ticks on the y-axis for each subplot demark the occurence of

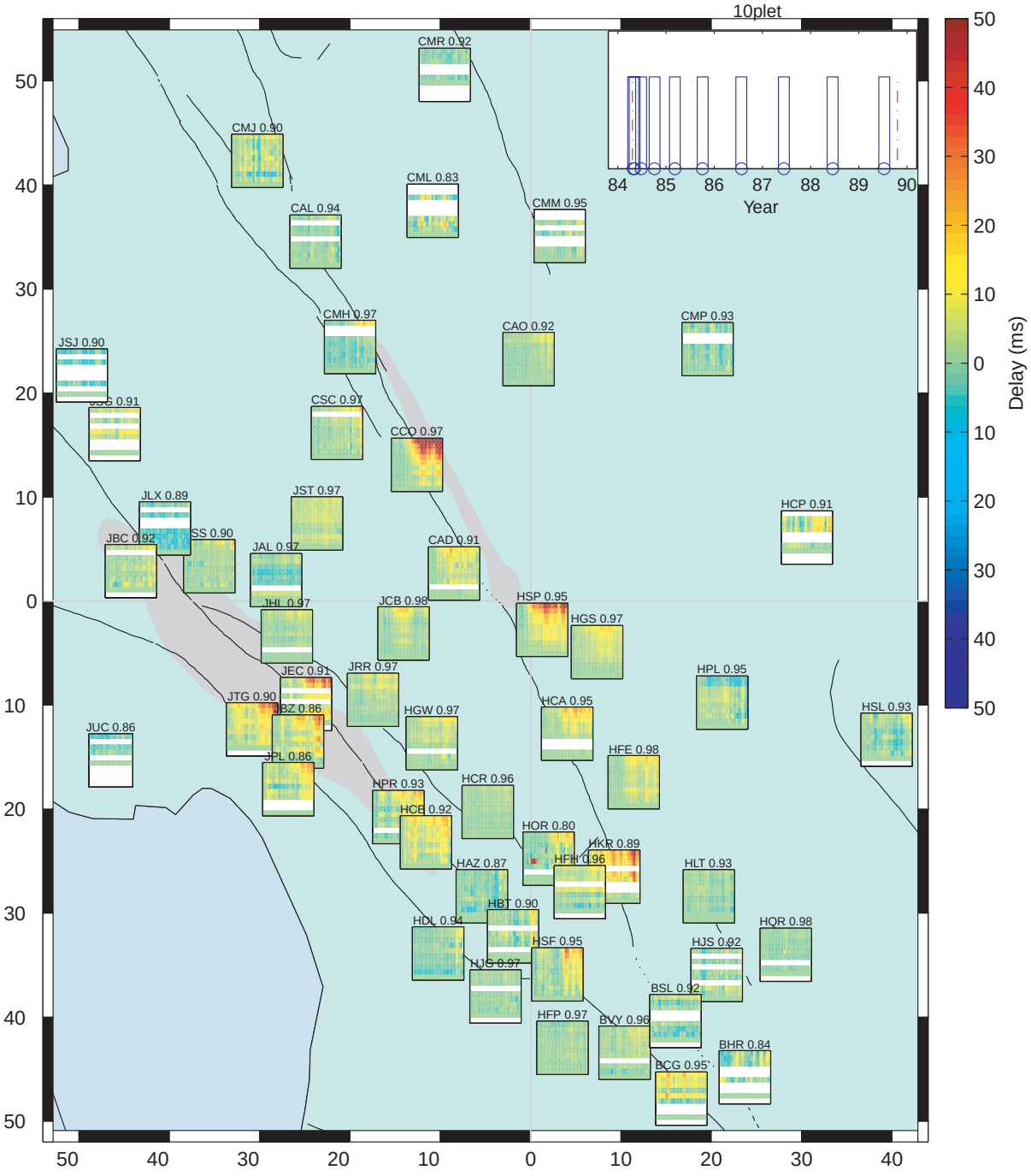

Figure 3.6: Travel time delays due to Morgan Hill measured by plet8 (see text for explanation). Map axes are in kilometers, but aspect ratio is skewed to display the most data.

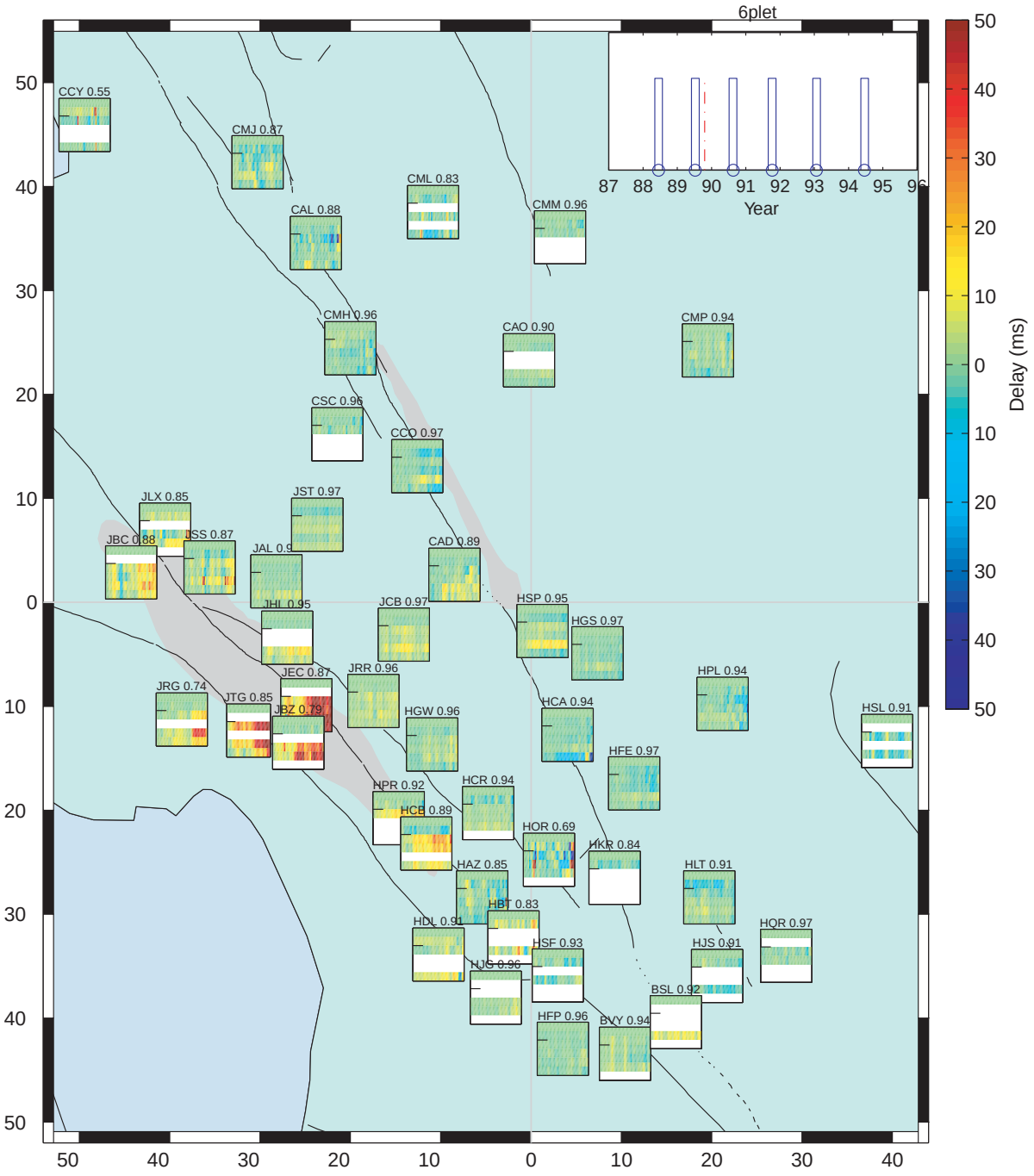

Figure 3.7: Travel time delays due to Loma Prieta measured by the rest of the events in plet8 on the Calaveras fault (see text for explanation). Red dashed line on timeline indicates occurrence of Loma Prieta as well as black ticks on each subplot. Map axes are in kilometers, but aspect ratio is skewed to display the most data.

Loma Prieta. Stations JEC, JBZ, JTG, HPR, and HCB measure the strongest changes and in the same sense as in Figure 3.5. The absence of the weaker signal seen before at other stations may be due to the inadequate temporal sampling in the months after Loma Prieta because the velocity anomaly may have subsided already. As noted earlier, if the color scale is changed from -100 to 100 ms in Figure 3.5, the pattern looks very much like that in Figure 3.7.

Because the travel time changes measured from these two different azimuths are localized to the same stations, it appears that to first order the velocity variations occur largely close to the stations. Several supporting lines of evidence suggest this is the case. Velocity changes show some correlation with underlying geology [*Phillips and Aki*, 1986; *Seekins* personal comm.] although the correspondence is not one-to-one. Previous studies have also suggested that the coda is primarily generated near the station [*Blakeslee and Malin.*, 1990; *Leary and Abercrombie*, 1994]. Supporting evidence from other studies indicates that most phases in the coda appear to leave the source at angles close to the path of the direct wave [*Spudich and Bostwick*, 1987; *Scherbaum et al.*, 1991; *Dodge and Beroza*, 1997]. While our observations indicate the dominant changes occur near the stations and perhaps shallow, we do find some evidence that velocity changes may also occur near the sources at depth. For example while the seven multiplets in Figure 3.2 all demonstrate the same general character, there are some variations in the delays measured from the different multiplets. Since they occur close to each other compared to the station distance, the rays near the station will be approximately co-linear. Therefore these minor differences may be attributable to changes near the source. Much greater variations are observed for the Calaveras multiplets, which are distributed throughout the Morgan Hill aftershock zone. If the changes were only occurring right under the stations, such behavior might not be observed. Because of the large uncertainty in knowing exactly where the coda waves are traveling, spatial constraint of velocity changes is perhaps the most difficult thing to pin down using multiplet data. What repeated wave sources at a point are most suited for, however, is measurement of a temporal signal because all the path unknowns are common and therefore contribute nothing to the delays.

3.5 Temporal Behavior of Velocity Changes

The velocity changes we find are quite large compared to earlier studies. An important reason why we find large amplitude temporal variations for the Loma Prieta earthquake relative to earlier studies is due to dense temporal sampling from our multiplet sources immediately following the mainshock. In earlier studies, most of the repeating earthquake sources were doublets [*Ellsworth et al.*, 1992; *Beroza et al.*, 1997]. Through a systematic search of the catalog, we have found that these doublets are in fact members of much more extensive repeating earthquake sequences. The temporal variations we observe change rapidly in the early postseismic period and the improved temporal sampling of the large multiplets during this interval has revealed large velocity changes. The events in the larger clusters are repeating aftershocks, and hence there is a fortunate high density of measurements in the months that follow the Loma Prieta mainshock when the velocity change signal is the strongest. Not only do these multiplets have excellent temporal sampling after the mainshock, but they also span a long duration. Another factor that can reduce the size of the measured velocity change is the length of the window used for the measurement. If the windows for the line fits (i.e. 2nd panels in Figure 3.4) are chosen to be long it will tend to average out the stronger variations observed for coda arrivals over short durations.

Figure 3.8 shows slowness estimates for the four multiplets on the San Andreas fault that had an event before the Loma Prieta mainshock. These exhibit a coseismic increase in slowness up to 3%. The lower panel shows subsequent logarithmic decay of the anomaly with time (velocity increase) but does not return to the initial value suggesting some permanent alteration of the crust near this station (JEC). A similar postseismic decay in slowness is observed at station CCO for the Morgan Hill earthquake. The $\sim$ 2% change in slowness is less for this event perhaps due to its smaller magnitude of 6.2. For the 38-plet in Figure 3.3 at station CCO, however, the velocity change signal decays by 4%. The reason for this may be denser temporal sampling or perhaps a stronger site response. Again in the lower panel the slowness change is observed to decay logarithmically with time. The contolled source experiment for the 1992 Landers earthquake [*Li et al.*, 1998] finds a postseismic increase in P- and S-wave velocity or healing, consistent with out observations. Since the controlled source surveys were conducted in 1994 and 1996, however, they are

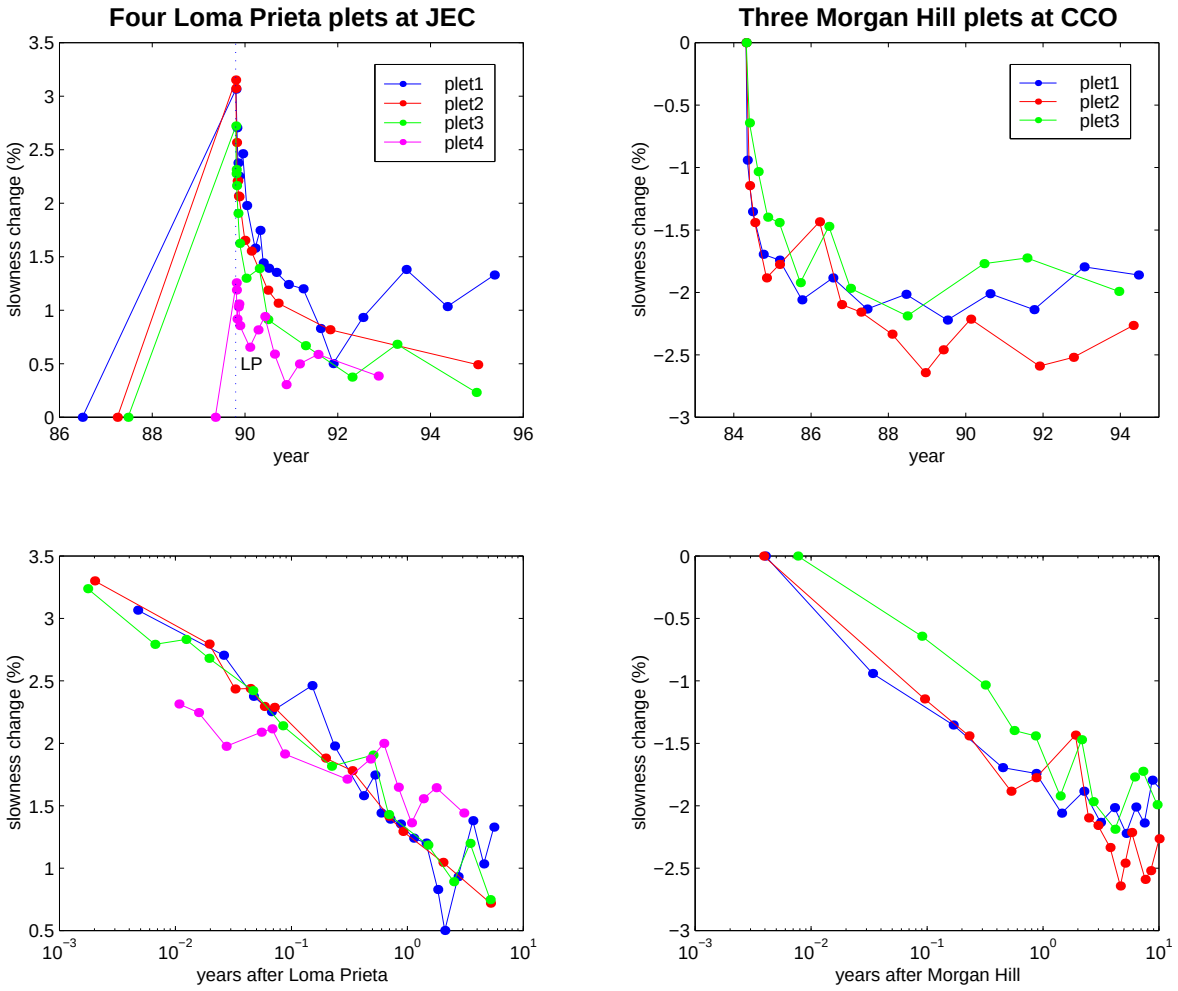

Figure 3.8: Slowness changes for Loma Prieta (left) and Morgan Hill (right). Estimates are shown as a function of calendar time (top) and elapsed time after the mainshock on a logarithmic scale (bottom).

not able to determine the temporal dependence of the velocity change.

The logarithmic time signature we measure is consistent with fault healing relationships determined in the lab [*Dieterich* 1992; *Beeler et al.*,1994]. The time decay may represent a nonlinear response of the crust after the strong shaking of the main shock. If the rocks behaved entirely elastically we would expect instantaneous changes that don't vary with time. The fact that there is a time dependence suggests the rocks have some memory of

higher strains. *TenCate et al.,* [2000] describe this logarithmic decay as a universal feature of relaxation following many processes. In measuring the nonlinear elasticity of widely different rock samples in the lab, they found that after being driven for a period at high oscillatory strains, velocities of the sample were observed to decrease. In all cases velocity recovered logarithmically with time after the large strains were applied. Both of these laboratory observations are consistent with our observations in the earth. The typical onset of nonlinearity in the lab occurs at strains in excess of $\sim 10^{-6}$ for ambient conditions e.g., *TenCate et al.,* 1996. These strains are easily exceeded in the near field of an earthquake, where strains of ($\sim 10^{-4}$) are typical, so a nonlinear response should not be too surprising.

3.6 Physical Model

The fractional changes in S-wave coda slowness are typically twice as large as in the P-wave coda for both the Loma Prieta (Figure 3.9) and the Morgan Hill (Figure 3.10) earthquakes. In some cases, the P-wave coda slowness change is negligible. *Dodge and Beroza* [1997] showed that the P-wave coda and early S-wave coda in this region are primarily composed of scattered P- and S-waves respectively. These observations suggest that fracturing of a fluid saturated medium may be the mechanism underlying the observed velocity changes. The opening of dry cracks will cause a nearly equal decrease in P- and S-wave velocities (Figure 3.11). If the cracks are initially filled with water, however, the P-wave velocity will be much less affected because the bulk modulus will change less. The S-wave velocity change will be relatively larger because fluids can't support shear stress [*Mavko et al.,* 1998].

Diffusion of pore fluids may also provide an explanation for the time dependence of the slowness decay. The large amplitude of the observed velocity change implies low effective pressures because at high normal stress it is difficult to affect a change in velocity. This suggests pore pressures are high if the changes arise at substantial depth. The observation that all the velocity changes are of the same sign, however, is inconsistent with the four-lobed mean stress variation expected after an earthquake. If the velocity change were due to the opening and closing of cracks in reponse to a change in mean stress [*Nur,* 1971] it would have a four lobe pattern as well [*Dodge and Beroza,* 1997]. Rays from the Calaveras

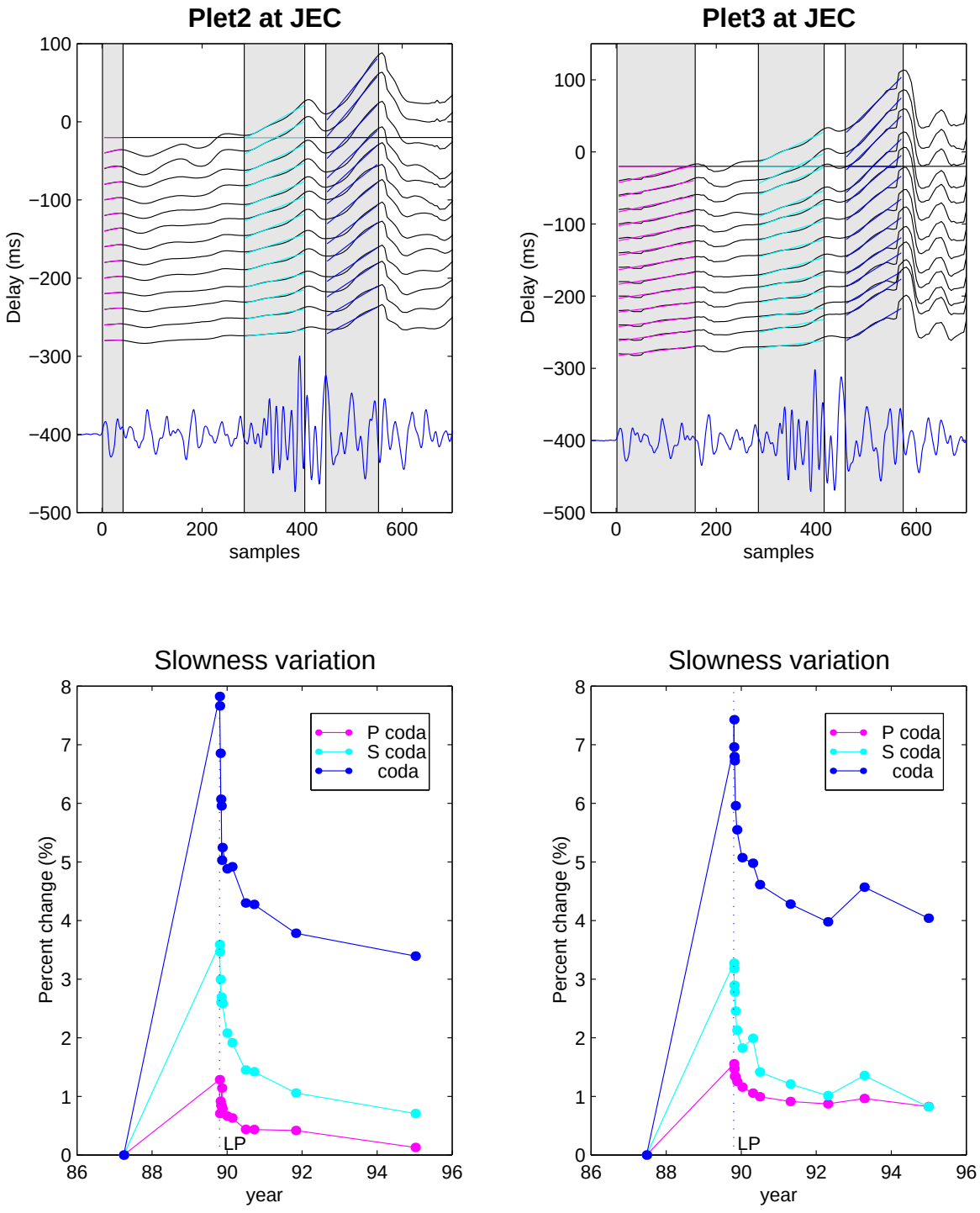

Figure 3.9: Slowness changes due to Loma Prieta for different phases in the coda. Notice incomplete recovery in most cases.

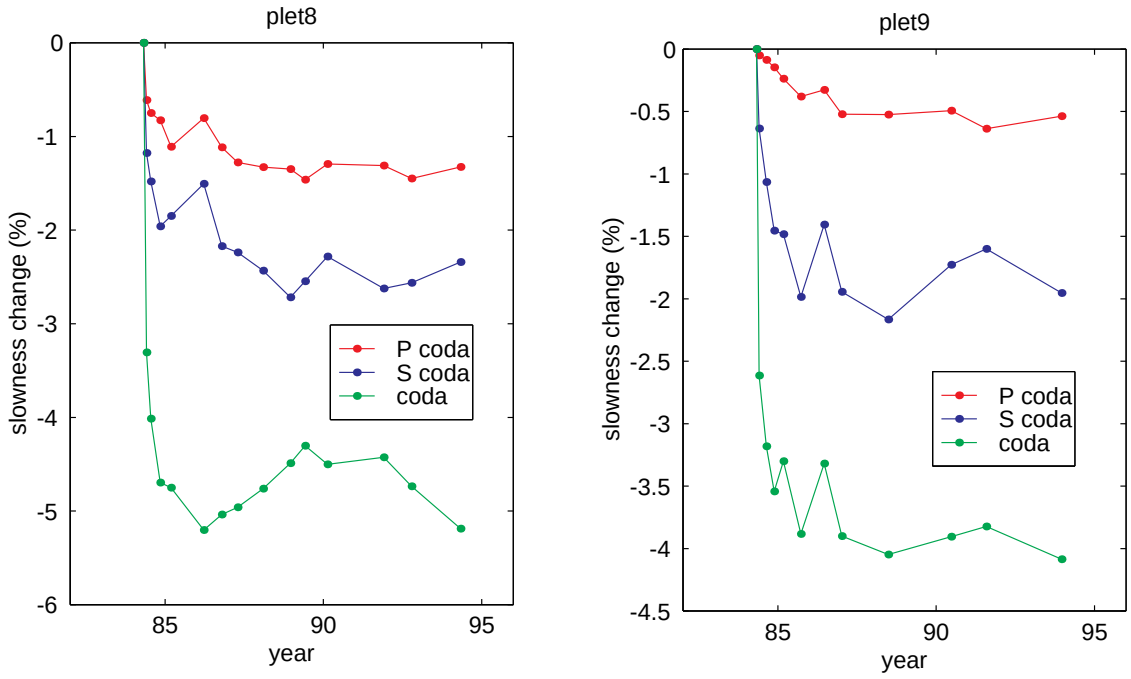

Figure 3.10: Same velocity changes observed in the P coda, S coda, and later coda arrivals due to the Morgan Hill earthquake at station CCO.

fault for the Loma Prieta case should sample both compressional and dilatational quadrants and yet show only positive delays. Similarly, multiplets at both ends of the Morgan Hill rupture indicate that the velocity change is always of the same sign, a co-seismic decrease of velocity.

Independent evidence for the presence of fluids and fracturing of the shallow crust comes from the observation of widespread increased stream flow after the Loma Prieta earthquake [*Rojstaczer et al.,* 1995]. They propose enhanced permeability due to the shaking of the mainshock to explain the increased flow found in both the compressional and dilatational quadrants. The fact that the stream chemistry does not change over time suggests that the fluids are not derived from considerable depth. They conclude that upper to mid-crust expulsion of water due to elastic compression is not supported by the observations [*Rojstaczer et al.,* 1995]. Our results are consistent with their model of enhanced

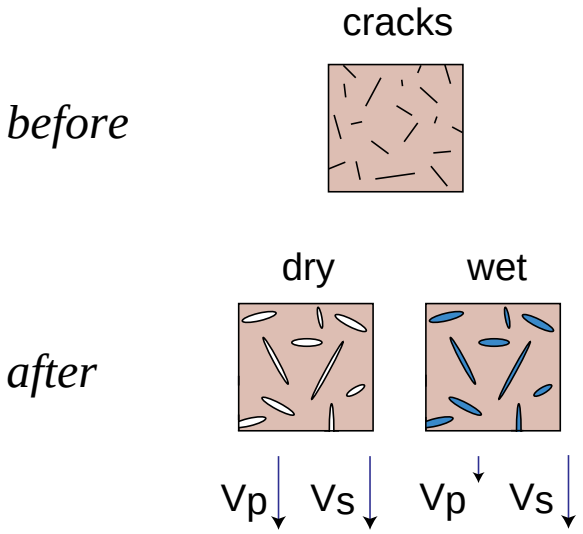

Figure 3.11: Cartoon demonstrating possible mechanism for observed differences in P- and S-wave velocity change behavior.

near-surface permeability caused by the Loma Prieta mainshock.

It is interesting that the strongest velocity changes we record occur for some phases in the early coda shortly after the direct S-wave (Figures 9 & 10). This is true for both the Loma Prieta and Morgan Hill earthquakes. Although we have not been able to localize the source of the velocity changes, their arrival shortly after the direct phase and their association with stations proximal to fault zones suggest that in some cases they might be fault-zone guided waves. The possibility that they are fault-zone guided waves is especially interesting since they would then reflect time-dependent fault-zone properties. *Li et al.* [1998] measured P- and S-travel time changes of the direct waves, which they know travel in the shallow reaches of the Landers fault zone. Since our results are consistent with theirs we may expect that similar changes have occurred in the Morgan Hill and Loma Prieta fault zones; however, unlike the Landers earthquake, these earthquakes did not rupture to the surface. Thus if fault-zone guided waves are responsible for the anomalies, then the changes would likely occur at greater depth.

3.7 Conclusions

A large coseismic velocity decrease is measured for the 1989 Loma Prieta earthquake followed by a postseimic recovery, which varies as the logarithm of time after the mainshock. The magnitude of the path-averaged velocity changes are as much as 1.5% for P-waves and 3.5% for S-waves. Similar results are also obtained for the 1984 Morgan Hill earthquake. Repeating event clusters provide an excellent tool to measure this temporal signal but are not well suited for constraining where these changes occur. Future work will attempt to determine whether these changes take place shallow or deep. Since the S-wave velocity change is greater than the P-wave change it suggests that fluids are present. Because the magnitude of the velocity changes is high, low effective pressures are indicated. If the changes are deep it implies high pore pressures, which would likely influence other aspects of earthquake behavior.

We think it most likely that the changes are shallow, and that a nonlinear response of the crust to mainshock strong ground motion explains our observations. The sign of the velocity changes is everywhere the same, which is inconsistent with a model where velocity changes follow the mean stress variation due to the mainshock. The observed co-seismic velocity decrease, which subsequently recovers, is consistent with a damage/recovery mechanism where strong shaking opens cracks. The logarithmic time signature matches fault healing relations obtained in the lab. Such behavior would result if damage occurs, which heals with increased contact time. Nonlinear elastic effects also arise from the creation of micro-cracks and flaws. A velocity change due to straining of samples beyond the linear regime in the lab leads to velocity decreases that recover logarithmically in time once the stressing source is removed. Our observations show that stations on softer sediments have the largest velocity changes, which may also be expected to experience higher strains and hence nonlinear site response. There is some evidence for nonlinearity in other earthquake sequences *Field et al.,* [1997] based on a comparison of mainshock strong ground motion and predictions of mainshock strong ground motion based on aftershock recordings. Those observations have been challenged recently *O'Connell*, [1999], but our observations provide independent evidence that nonlinearity may be important in strong ground motion. Moreover, if we are able to localize the source of nonlinearity through, for example, array

analysis, we would be able to place constraints on the extent and mechanism behind it.

Acknowledgments. We are grateful to Doug Dodge, Bill Ellsworth, Amos Nur, Bill Bosl, Paul Segall, and Nick Beeler for helpful discussions. David Oppenheimer and Linda Seekins provided guidance on the local geology. DPS and GCB were supported by NSF Grants No. EAR-9725238 and EAR-0074084.

3.8 References

Aggarwal, Y.P., L.R. Sykes, J. Armbruster, and M.L. Sbar, Premonitory changes in seismic velocities and prediction of earthquakes, *Nature, 241*, 101-104, 1973.

Aggarwal, Y.P., L.R. Sykes, D.W. Simpson, and P.G. Richards, Spatial and temporal vaiations in ts/tp and in P wave residuals at Blue Mountain Lake, New York: application to earthquake prediction, *J. Geophys. Res., 80*, 718-732, 1975.

Antolik, M., R.M. Nadeau, R.C. Aster, and T.V. McEvilly, Differential analysis of coda Q using similar microearthquakes in seismic gaps, part 2: application to seismograms recorded by the Parkfield High Resolution Seismic Network, *Bull. Seismol. Soc. Am., 86* 890-910, 1996.

Aster, R.C., P.M. Shearer, and J. Berger, Quantitative measurements of shear wave polarizations at the Anza Seismic Network, southern California: implications for shear wave splitting and earthquake prediction, *J. Geophys. Res., 95*, 12,449-12,473, 1990.

Baisch, S., and G.H.R. Bokelmann, Seismic waveform attributes before and after the Loma Prieta earthquake: scattering change near the earthquake and temporal recovery, *J. Geophys. Res.,* , submitted 2000.

Beeler, N.M., T.E. Tullis, and J.D. Weeks, The roles of time and displacement in the evolution effect in rock friction, *Geophys. Res. Let., 21*, 1987-1990, 1994.

Beroza, G.C., A.T. Cole, and W.L. Ellsworth, Stability of coda wave attenuation during the Loma Prieta, California, earthquake sequence, *J. Geophys. Res., 100*, 3,977-3,987, 1995.

Beroza, G.C., D.P. Schaff, W.L. Ellsworth, A.T. Cole, and D.A. Dodge, Temporal changes in seismic velocities observed in the shear wave coda related to the 1989 Loma Prieta, California, earthquake, *EOS, Trans. AGU, 78*, 482, 1997.

Blakeslee, S. N., and P.E. Malin, A comparison of earthquake coda waves at surface versus subsurface seismometers, *J. Geophys. Res., 95*, 309-326, 1990

Bokelmann, G.H.R., and H-.P. Harjes, Evidence for temporal variation of seismice velocity within the upper continental crust, *J. Geophys. Res., 105*, 23,879-23,894, 2000.

Boore, D.M., A.G. Lindh, T.V. mcEvilly, and W.W. Tolmachoff, A search for travel time changes associated with the Parkfield earthquake of 1966, *Bull. Seismol. Soc. Am., 65*, 1407-1418, 1975.

Bolt, B., Constancy of P travel times from Nevada explosions to Oroville Dam station 1970-1976, *Bull. Seismol. Soc. Am., , 67*, 27-32, 1977.

Chou, C.W., and R.S. Crosson, Search for time-dependent seismic P travel times from mining explosions near Centralia, Washington, *Geophys. Res. Let., 5*, 97-100, 1978.

Dieterich, J.H., Time-dependent friction in rocks, *J. Geophys. Res., 77*, 3690-3697, 1972.

Dodge, D.A., and G.C. Beroza, Source array analysis of coda waves near the 1989 Loma Prieta, California, mainshock: Implications for the mechanism of coseismic velocity changes, *J. Geophys. Res., 102*, 24,437-24,458, 1997.

Ellsworth, W.L., Cole, A.T., Beorza, G.C. and M.C. Verwoerd, Changes in crustal wave propagation associated with the 1989 Loma Prieta, California, earthquake, *EOS Tran. AGU, 73*, 360, 1992.

Field, E.H., P.A. Johnson, I.A. Beresnev, and Y. Zeng, Nonlinear ground-motion amplification by sediments during the 1994 Northridge earthquake, *Nature, 390,* 599-601, 1997.

Got, J-.L., and O. Coutant, Anisotropic scattering and travel time delay analysis in Kilauea volcano, Hawaii, earthquake coda waves, *J. Geophys. Res., 102*, 8,397-8,410, 1997.

Haase, J.S., P.M. Shearer, and R.C. Aster, Constraints on temporal variations in velocity near Anza, California, from analysis of similar event pairs, *Bull. Seismol. Soc. Am., 85*, 194-206, 1995.

Hellweg, M., P. Spudich, J.B. Fletcher, and L.M. Baker, Stability of coda Q in the region of Parkfield, California: view from the U.S. Geological Survey Parkfield Dense Seismograph Array, *J. Geophys. Res., 100*, 2,089-2,102, 1995.

Kanamori, H. and G. Fuis, Variation of P wave velocity before and after the Galway Lake earthquake ($M_L = 5.2$) and the Goat Mountain earthquakes ($M_L = 4.7$,4.7), 1975, in the Mojave desert, California, *Bull. Seismol. Soc. Am., 66*, 2,027-2,037, 1976.

Karageorgi, E.D., R.Clymer, and T.V. McEvilly, Seismological studies at Parkfield II: search for temporal variations in wave propagation using Vibroseis, *Bull. Seismol. Soc. Am.,* , *82,* 1,388-1,415, 1992.

Karageorgi E.D., T.V. McEvilly, and R.Clymer, Seismological studies at Parkfield IV: variations in controlled-source waveform parameters and their correlation with seismic activity, 1987-1994, *Bull. Seismol. Soc. Am., 87*, 39-49, 1997.

Korneev, V.A., T.V. McEvilly, and E.D. Karageorgi, Seismological studies at Parkfield VIII: modeling the observed travel-time changes, *Bull. Seismol. Soc. Am., 90*, 702-708, 2000.

Leary, P. and R. Abercrombie, Frequency dependent crustal scattering and absorption at 5-160 Hz from coda decay observed at 2.5 km depth, *Geophys. Res. Let., 21*, 971-974, 1994.

Li, Y-.G., J.E. Vidale, K. Aki, F. Xu, and T. Burdette, Evidence of shallow fault zone healing after the 1992 M 7.5 Landers, California, earthquake, *Science*, 1998.

Lindh, A.G. D.A. Lockner, and W.H.K. Lee, Velocity anomalies: an alternative explanation, *Bull. Seismol. Soc. Am., 68*, 721-734, 1978.

Mavko, G., T. Mukerji, and J. Dvorkin, *The Rock Physics Handbook: Tools for Seismic Anlaysis in Porous Media,* 329 pp., Cambridge Univ. Press, Cambridge, UK, 1998.

McEvilly, T.V., and L.R. Johnson, Stability of P and S velocities from central California quarry blasts, *Bull. Seismol. Soc. Am., 64*, 343-353, 1974.

Nadeau, R.M., M. Antolik, P. Johnson, W. Foxall, and T.V. McEvilly, Sesimological studies at Parkfield III: microearthquake clusters in the study of fault-zone dynamics, *Bull. Seismol. Soc. Am., 83*, 247-263, 1994a.

Nadeau, R.M., E.D. Karageorgi, and T.V. McEvilly, Fault-zone monitoring with repeating similar microearthquakes: a search for the Vibrosesi anomaly at Parkfield, *Seis. Res. Lett., 65,* 69, 1994b.

Nur, A., Effects of stress on velocity anisotropy in rocks with cracks, *J. Geophys. Res., 76,* 2,022-2,034, 1971.

O'Connell, D.R.H., Replication of apparent nonlinear seismic response with linear wave propagation models, *Science, 283,* 2,045-2,050, 1999.

Phillips, W.S., and K. Aki, Site amplification of coda waves from local earthquakes in central California, *Bull. Seismol. Soc. Am., 76*, 627-648, 1986.

Poupinet, G., W.L. Ellsworth, and J. Fréchet, Monitoring velocity variations in the crust using earthquake doublets: an application to the Calaveras Fault, California, *J. Geophys. Res., 89,* 5719-5731, 1984.

Ratdomopurbo, A., and G. Poupinet, Monitoring a temporal change of seismic velocity in a volcano: application to the 1992 eruption of Mt. Merapi (Indonesia), *Geophys. Res. Let., 22,* 775-778, 1995.

Rojstaczer, S.A., S.C. Wolf, and R.L. Michel, Permeability enhancement in the shallow crust as a cause of earthquake-induced hydrological changes, *Nature, 373,* 237-239, 1995.

Savarensky, E.F., On the prediction of earthquakes, *Tectonophysics, 6,* 17-27, 1968.

Schaff, D.P., G.H.R. Bokelmann, E. Zanzerkia, F. Waldhauser, G.C. Beroza, and W.L. Ellsworth, Cross correlation arrival time measurements for earthquake location, submitted to *J. Geophys. Res.,* , 2001.

Scherbaum, F., D. Gillard, and N. Deichmann, Slowness power spectrum analysis of the coda composition of two microearthquake clusters in northern Switzerland, *Phys. Earth Planet. Inter., 67,* 137-161, 1991.

Spudich, P., and T. Bowtwick, Studies of the seismic coda using an earthquake cluster as a deeply buried seismograph array, *J. Geophys. Res., 92,* 10,526-10,546, 1987.

Semenov, A.N., Variation in the travel time of transverse and longitudinal waves before violent earthquakes, *Bull. Acad. Sci. USSR, Phys. Solid earth, 3,* 245-248, 1969.

Shearer, P.M., Improving local earthquake locations using the L1 norm and waveform cross correlation: application to the Whittier Narrows, California, aftershock sequence, *J. Geophys. Res., 102,* 8,269-8,283, 1997.

Ten Cate, J.A., and T.J. Shankland, Slow dynamics in the nonlinear elastic response of Berea Sandstone, *Geophys. Res. Let., 23,* 3,019-3,022, 1996.

TenCate, J.A., E. Smith, and R.A. Guyer, Universal slow dynamics in granular solids, *Phys. Rev. Let., 85,* 1020-1023, 2000.

VanDecar, J.C., and R.S. Crosson, Determination of teleseismic relative phase arrival time using mulit-channel cross-correlation and least squares, *Bull. Seismol. Soc. Am., 80,,* 150-169, 1990.

Waldhauser, F., and W.L. Ellsworth, A double-difference earthquake location algorithm with an application to the northern Hayward Fault, CA, *Bull. Seismol. Soc. Am.,* , in prep.

Whitcomb, J.H., J.E. Garmany, and D.L. Anderson, Earthquake prediction: variation of seismic velocities before the San Francisco (sic) earthquake, *Science, 180*, 632-635, 1973.

Chapter 4

Relocations of Calaveras Fault seismicity

Abstract. By measuring relative arrival times between pairs of earthquakes using waveform cross-correlation and the double difference relative relocation technique, we are able to reduce errors in earthquake hypocenters by 1 to 2 orders of magnitude. We have applied this approach to nearly 8000 events distributed along a 35 km section of the Calaveras Fault that includes the rupture zone of the M 6.2 1984 Morgan Hill, California earthquake. The earthquakes that correlate well enough with other events for us to relocate represent approximately 92 percent of all seismicity for which waveforms are available. We find that the relocated seismicity forms highly organized structures that were previously obscured by location errors. There are abundant repeating earthquake sequences as well as linear clusters of earthquakes that are elongated along the strike of the fault. Large voids in seismicity appear with dimensions of kilometers that have been aseismic over the 30-year time interval considered, suggesting that these portions of the fault are either locked or creeping. The area of greatest slip in the Morgan Hill mainshock coincides with the most prominent of these voids, suggesting that this part of the fault may be locked between large earthquakes. We find that the Calaveras fault at depth is extremely thin, with an average upper bound on fault zone width of 75 meters. Given the errors in the locations, however, the inferred fault zone width is not resolvably different from zero. In addition to seismicity on the Calaveras fault, we find active secondary faults. These structures consist of planar alignments of hypocenters that in each case correspond to one of two nodal planes from the focal mechanisms of events that occur within them. This provides an excellent opportunity to solve for the stress field in the immediate vicinity of the Calaveras Fault. We find that the maximum compressive stress is at a high angle to the Calaveras fault, only 13 degrees from the fault normal vector, even within hundreds of meters of the fault trace, supporting previous interpretations that this fault is weak.

4.1 Introduction

The Calaveras fault is one of the most active branches of the San Andreas fault system in northern California (Figure 4.1). In the 20th century there have been a series of moderate magnitude earthquakes some of which have repeated [*Oppenheimer et al.*, 1990]. The largest of these earthquakes was the M 6.2 1984 Morgan Hill earthquake, which appears to have been a repeat of an earthquake in 1911. The long-term slip rate on the Calaveras fault to the south of where the Hayward fault splays from it is thought to be 15 ± 3 mm/yr [*WGCEP,* 1999]. In addition to rupture in moderate earthquakes, this section of the Calaveras fault has been extraordinarily active in microearthquake activity. It is also known to creep with an average rate of approximately 13.5 mm/yr since 1997 [*WGCEP,* 1999]. Because of the combination of a fast slip rate, the presence of creep, and equivocal paleoseismic evidence for large earthquakes in the past, the potential for future large earthquakes on the central section of the Calaveras fault remains uncertain [*WGCEP,* 1999].

Oppenheimer et al. [1990] studied micro-earthquake activity of the Calaveras fault in great detail. They found a correspondence between the areas that slipped in moderate earthquakes with areas that were relatively devoid of microearthquake activity. They also found that small earthquakes had a very similar spatial distribution both before and after moderate earthquakes. They proposed that the areas devoid of seismicity were stuck between moderated earthquakes and used this assumption to identify two likely source zones for future moderate earthquakes on the Calaveras fault.

The geometry of fault zones within the earth is revealed primarily by seismicity. In this study, we greatly improve the earthquake locations on the Calaveras fault. Our ability to resolve fault zone structure and hence to address many essential aspects of earthquake behavior, is limited by our ability to obtain precise earthquake locations. While quantitative earthquake location techniques date back to the early years of the 20th century [e.g. *Geiger,* 1909], our incomplete knowledge of earth structure and the difficulty of measuring arrival times accurately typically limits the accuracy of earthquake locations to 10's of km at teleseismic distances and several km at regional distances even in well instrumented regions like California and Japan.

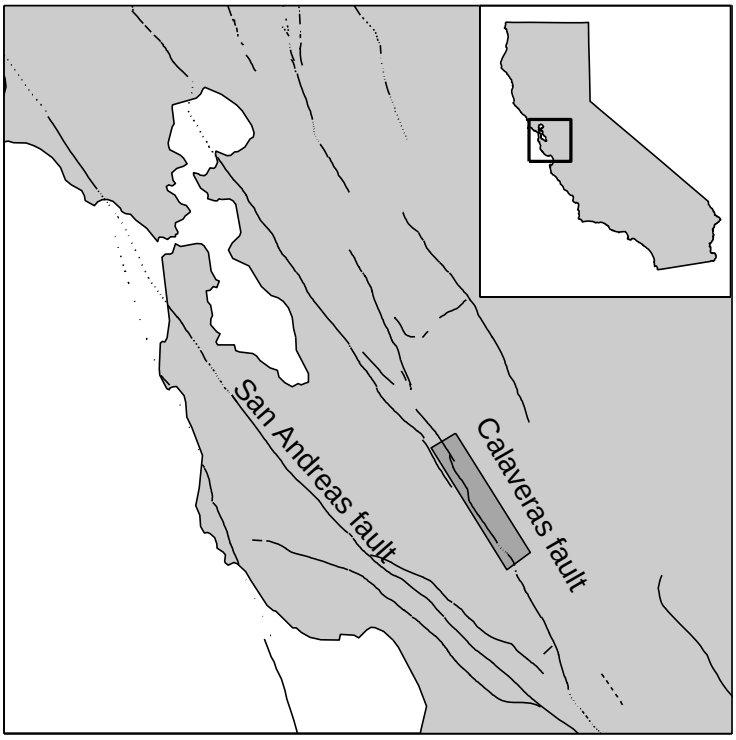

Figure 4.1: Calaveras fault in California. Shaded box denotes study area.

Uncertainty in earthquake locations can be dramatically reduced by aiming for precision, rather than accuracy, in the form of relative earthquake locations [e.g. *Poupinet et al.,* 1984; *Fréchet,* 1985; *Deichmann and Garcia-Fernandez,* 1992; *Got et al.,* 1994]. In this study, we improve the precision of earthquake locations in two principal ways: (1) removing substantial velocity model error with the double difference approach [*Waldhauser and Ellsworth,* 2000] and (2) reducing relative arrival time measurement errors by waveform cross-correlation [*Schaff et al.,* 2001]. The combination allows us to reduce relative location errors by 1 to 2 orders of magnitude for the entire data set.

What emerges from the improved earthquake locations is a highly refined picture of seismicity on the Calaveras fault. Numerous features that were seen as clouds of seismicity are brought into sharp focus. These features include streaks of earthquakes that are elongated in the direction of slip, sets of repeating microearthquakes that recur up to dozens of times, and large areas of little or no seismicity. We are also able to obtain a much clearer

view of a km-scale compressional fault offset and its geometry at depth. Our locations suggest that the two principal offset fault strands may merge near the base of the seismogenic zone. We are also able to resolve secondary fault structures, which were previously suggested by focal mechanisms [*Oppenheimer et al.,* 1988]. Slip on these structures indicate that the maximum compressive stress is at a high angle to the Calaveras fault implying that it is weak. They are also active to within 100's of meters of the main fault trace suggesting that any stress rotation near the Calaveras fault must be confined to the immediate proximity of the fault zone. The improved locations also allow us to constrain the degree of strain localization on the Calaveras fault. We find a very narrow fault-zone width of no more than 75 m at seismogenic depths.

4.2 Data and Technique

The waveforms for the event set of 7857 earthquakes comprise over half a million seismograms. They are recorded on Northern California Seismic Network (NCSN) vertical component, short period stations archived at the Northern California Earthquake Data Center (NCEDC). The correlation-double difference method we use scales differently than traditional relative relocation techniques. If only absolute travel times are used the number of observations goes approximately as: $N_e \times N_s$, where N_e is number of events and N_s is the number of stations. To do all possible correlations, on the other hand, requires on the order of $N_e(N_e - 1)N_s/2$ measurements. For our study of the Calaveras Fault we have chosen Calnet stations within 70 km, which amounts to on average 50 stations per event. For $\sim$ 8000 events, this translates to approximately 3 billion possible unique cross-correlations for both P- and S-waves. The correlation measurements are obtained by a two step procedure: align to the nearest sample using 2.56 second window lengths and then compute to subsample precision with 1.28 second window lengths [*Schaff et al.*, 2001]. We are able to perform about one million correlation measurements per hour, so total computation time including input/output would amount to approximately half a year or the amount of time typically taken to review a geophysical manuscript.

Differential travel times derived from cross-correlation are most accurate for events that occur in close proximity to one another. There are several reasons for this. As the

inter-event distance increases, waveform similarity decreases and undermines the basis for cross-correlation as a means for determining relative arrival times. Moreover, at short inter-event distances, differential arrival time measurements allow one to remove nearly all of the common mode error due to unmodeled path effects. As inter-event distance increases this no longer holds and the advantage of locating earthquakes using differential arrival times is diminished.

Since the events we consider span a 35-kilometer stretch of the Calaveras fault, we can significantly reduce the computational time by recognizing that cross-correlation measurements become less useful at increasing inter-event distances. In this study we perform correlation measurements only for inter-event distances less than 1.5 km in the horizontal and 3 km in the vertical, which limits the number of cross-correlations to 108 million (about 3.4% of the total possible measurements). This selection is based both on the magnitude of location errors in the NCSN catalog, and the observation that cross-correlation derived relative arrival times are only an improvement over catalog phase data up to inter-event distances of about 2 km for this region [*Schaff et al.,* 2001]. Reducing the number of measurements allowed us to complete the cross-correlations in about one week.

Of the 108 million relative arrival time measurements, we retain only 8 million (7.5%). We select only those observations that have both normalized cross-correlation coefficients above 70% and mean coherence above 70%. This criterion is based on the observed levels of post-fit residuals from relocations that included sets of repeating earthquakes [*Schaff et al.,* 2001] and has the effect of removing most of the unreliable measurements from the dataset. After applying this cut-off we are left with a data set comprised of 4.9 million P-wave observations and 3.1 million S-wave observations that are used to estimate hypocentral locations by the double difference technique.

To constrain large scale structures and fill in where there are no good correlation measurements available, we use catalog phase data to form relative arrival time pairs [*Waldhauser and Ellsworth,* 2000]. This adds approximately an additional 1.5 million observations. Inter-event distance weighting functions are applied to both catalog and correlation data and are allowed to vary for different iterations in the linearized least-squares inversion procedure. It is not known *a priori* to what separation distances correlation data is reliable. Because of this they are downweighted with respect to the catalog data (1:100) for the first

ten iterations so as to have minimal effect on the inversion. Using the improved locations, all correlation measurements are subsequently removed for event pairs separated by more than 2 km. The correlation measurements are then weighted more strongly than the catalog data (100:1) to constrain structures at intermediate spatial scales. At iteration 20, correlation data with inter-event distances greater than 500 m are removed to further enhance the fine-scale detail.

One should note that the two data types measure different things. The catalog phase picks on the first break constrain the hypocenter whereas correlation measurements on a windowed wave arrival of some duration will constrain the spatial centroid of moment release. For the majority of these small events, however, the difference between hypocenter and centroid is not resolvable within the errors. For the larger events it may be possible to distinguish the two and hence infer rupture direction [*Waldhauser et al.,* 1999].

4.3 Relocation Results

Figure 4.2 shows earthquake locations on the Calaveras fault from the NCSN catalog in map and side view. Figure 4.3 displays the same events after relocation. The seismicity represents 92% of the events for which waveform data is available from 1984 through 1997 — a data set that includes the aftershocks of the M 6.2 1984 Morgan Hill earthquake. The relocated catalog appears complete down to M 1 and is observed to follow a Gutenberg-Richter magnitude distribution. 7724 of the events (98%) are less than M 3, 133 are greater than or equal to M 3. Off-fault events were removed from the lower panels in side view. Upon relocation, the seismicity becomes highly clustered. It is clear from the comparison that catalog location errors, particularly in hypocentral depths, obscure much of the underlying structure.

Formal errors in the catalog hypocenters for this region give average 95% confidence estimates of 1.2 km in the horizontal and 2.5 km in the vertical. After relocation, the average 95% confidence intervals are 5 m in the horizontal and 9 m in the vertical. These numbers represent formal errors evaluated in the linearized approximation, so there is no guarantee that they fully characterize the true relative location errors. Bootstrap analysis indicates that they are approximately correct within streaks [*Waldhauser and Ellsworth,*

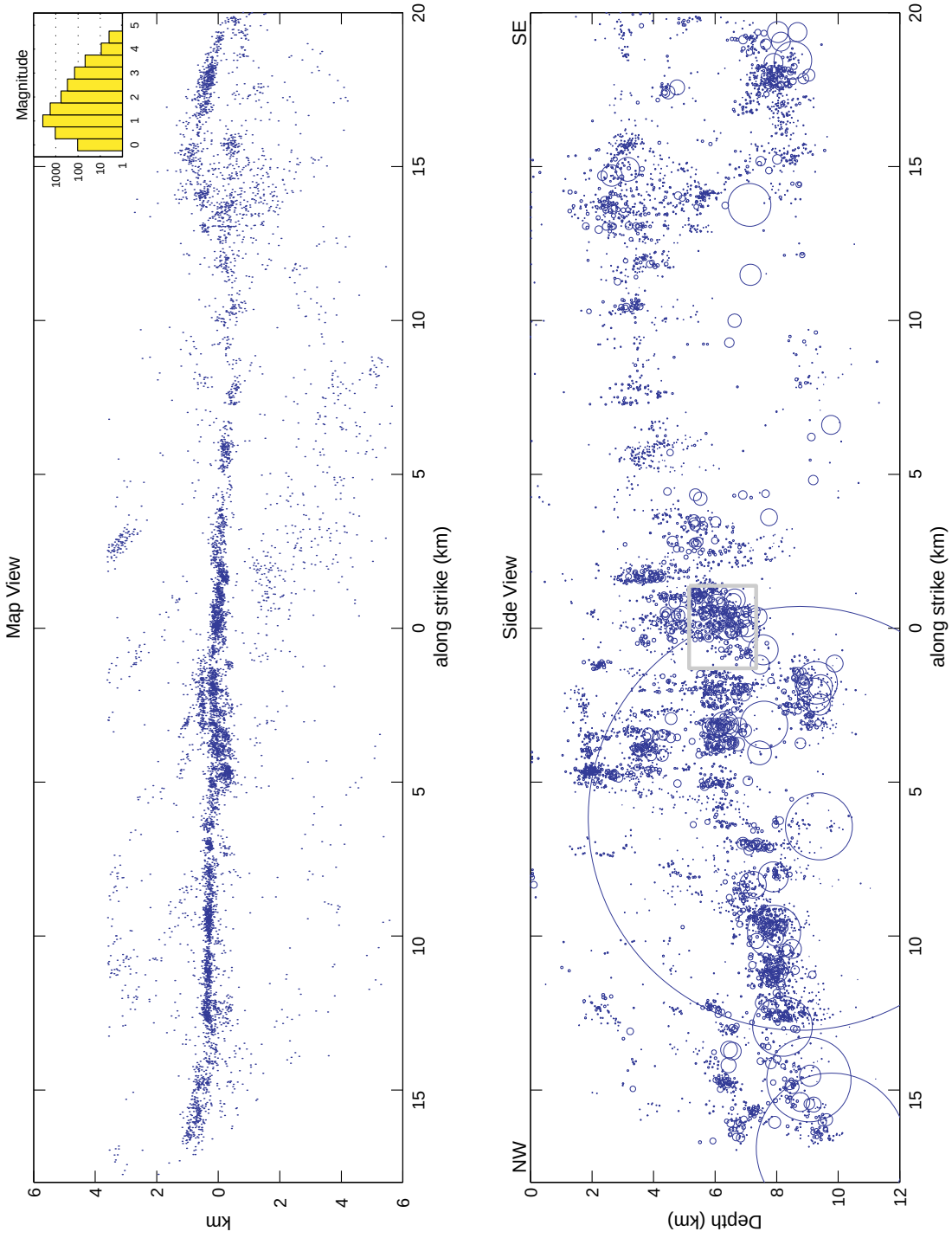

Figure 4.2: Catalog earthquake locations recorded by the NCEDC for the Calaveras fault from 1984 till present, comprising 7857 events. (top) Map view of events along the Calaveras fault (146 degree strike). Inset reveals a Gutenberg-Richter magnitude distribution. (bottom) Fault plane side view displaying only on-fault earthquakes with estimated source sizes based on circular crack model using a 3 MPa stress drop. Largest event is the M 6.2 Morgan Hill mainshock.

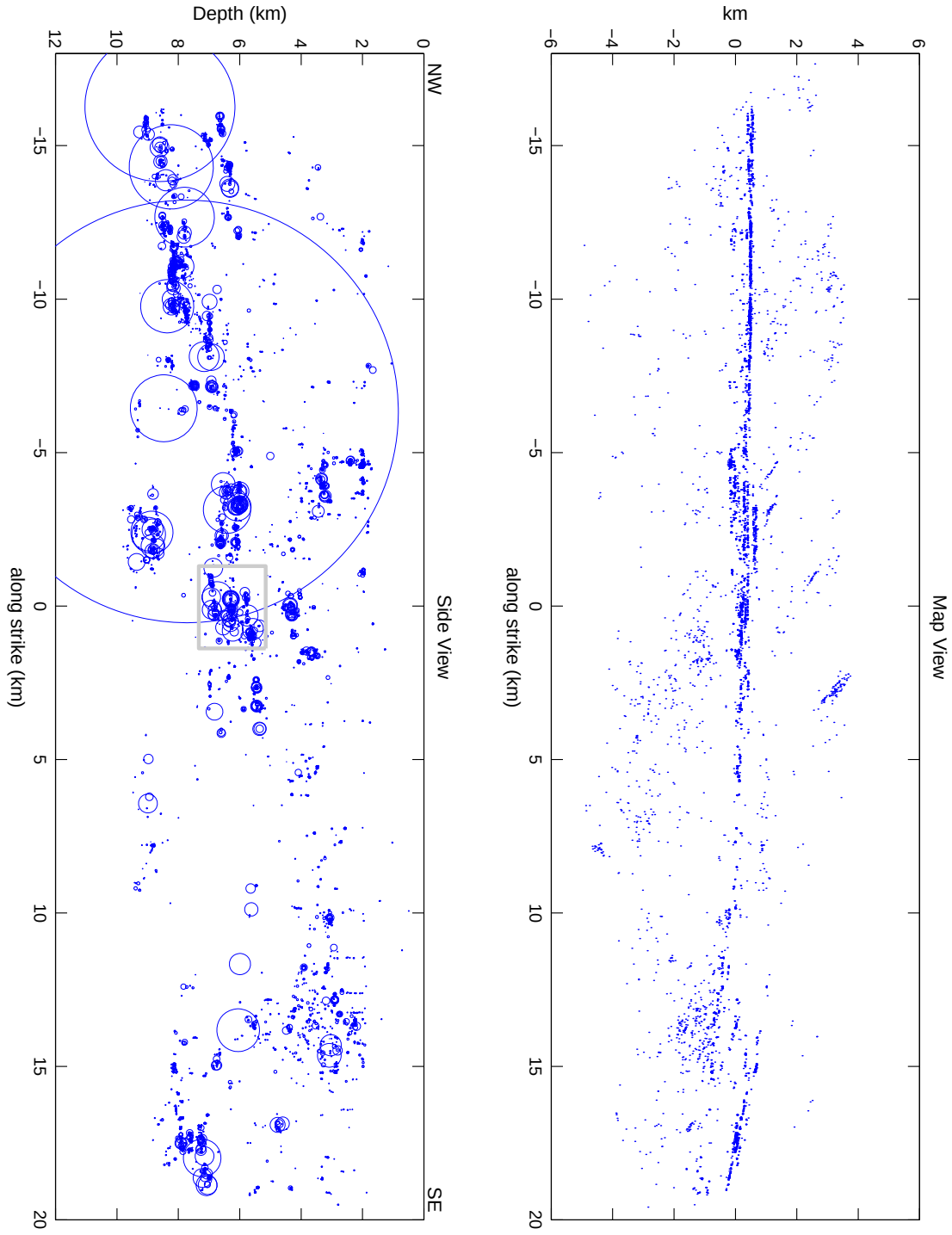

Figure 4.3: Improved relocations using correlation-double difference technique displaying all 7857 events on same length scale. (top) Note fine scale structure that becomes apparent as well as several off-fault structures now resolved. (bottom) Tremendous improvement of vertical errors concentrates seismicity onto several discrete bands containing events of widely varying magnitudes.

2000]. These errors most likely reflect fine-scale precision controlled by the correlation data. It should be noted that our ability to constrain larger scale structures is not as good because of the introduction of catalog phase pick error and additional unknown velocity structure. Therefore single error estimates attached to individual earthquakes do not adequately describe the location precision on different length scales. For instance, larger features constrained only by catalog phase data will have correspondingly higher relative location errors.

The degree to which seismicity coalesces onto discrete structures can be better appreciated by magnifying a small area on the fault. Figure 4.4 shows the effect of relocation on the organization of seismicity on the small scale. The diffuse arrangement of locations characteristic of the initial catalog locations becomes highly clustered. Many smaller events appear to nucleate at the boundaries of larger events, suggesting that they represent failure of stress concentrations at the edges of the larger earthquakes [*Ellsworth*, 1994; *Rubin et al.*, 1999]. This feature is also seen later in the topmost, right panel of Figure 4.7.

It is evident from the side view in Figure 4.3 that events of widely varying magnitudes fall onto prominent linear structures. Similar streaks of seismicity have been observed on the San Andreas and Hayward faults [*Rubin et al.*, 1999; *Waldhauser et al.*, 1999]. On other parts of the fault there is little or no seismicity. This pattern was recognized for the Calaveras fault by *Oppenheimer et al.* [1990], who noted that moderate earthquakes on the Calaveras fault tend to occur in these holes in seismicity. After relocation, the uneven distribution of seismicity on the fault becomes even more dramatic.

Surprisingly, the seismogenic part of the fault zone does not penetrate below 10 km depth in Figure 4.3. It is possible that the lowermost events from -15 to -9 km along strike distance occur at the brittle-ductile transition. The depth of this transition will depend on strain rate [*Sibson*, 1984]. The top panel of Figure 4.5 illustrates that the depth of the brittle-ductile transition might increase due to the higher strain rates immediately following the 1984 Morgan Hill mainshock. The bottom panel displays evidence consistent with this mechanism. Plotted are events between 8.5 and 10 km depth at -2 km along strike (Figure 4.3) as a function of origin time. We observe that the $\sim$ 100 events below 9.1 km follow a steep Omori's law but only occur in the immediate postseismic period up to 1986. The shallower events on the other hand also follow Omori's law but persist until

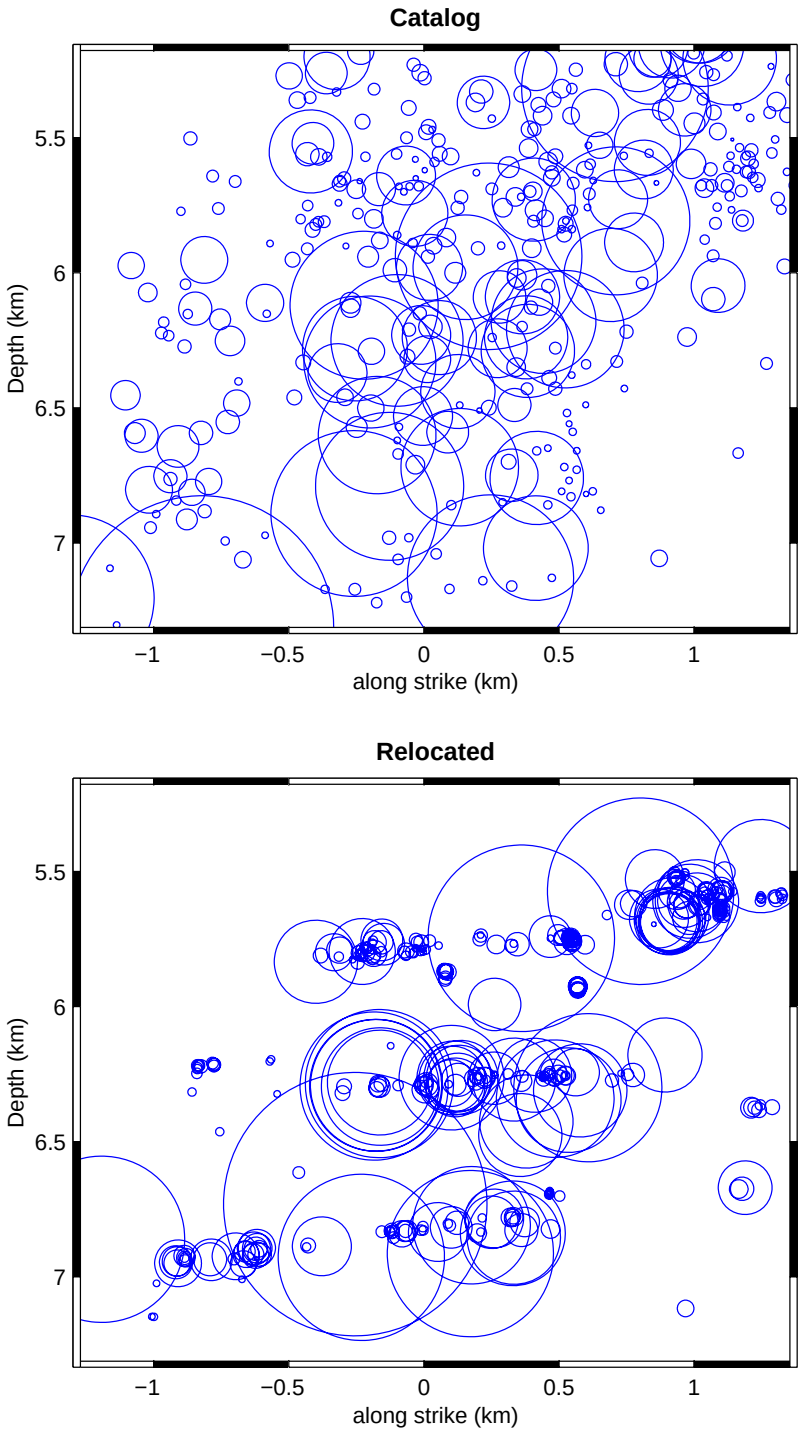

Figure 4.4: Zoom plots of the seismicity contained within the gray boxes on Figures 4.2 & 4.3.

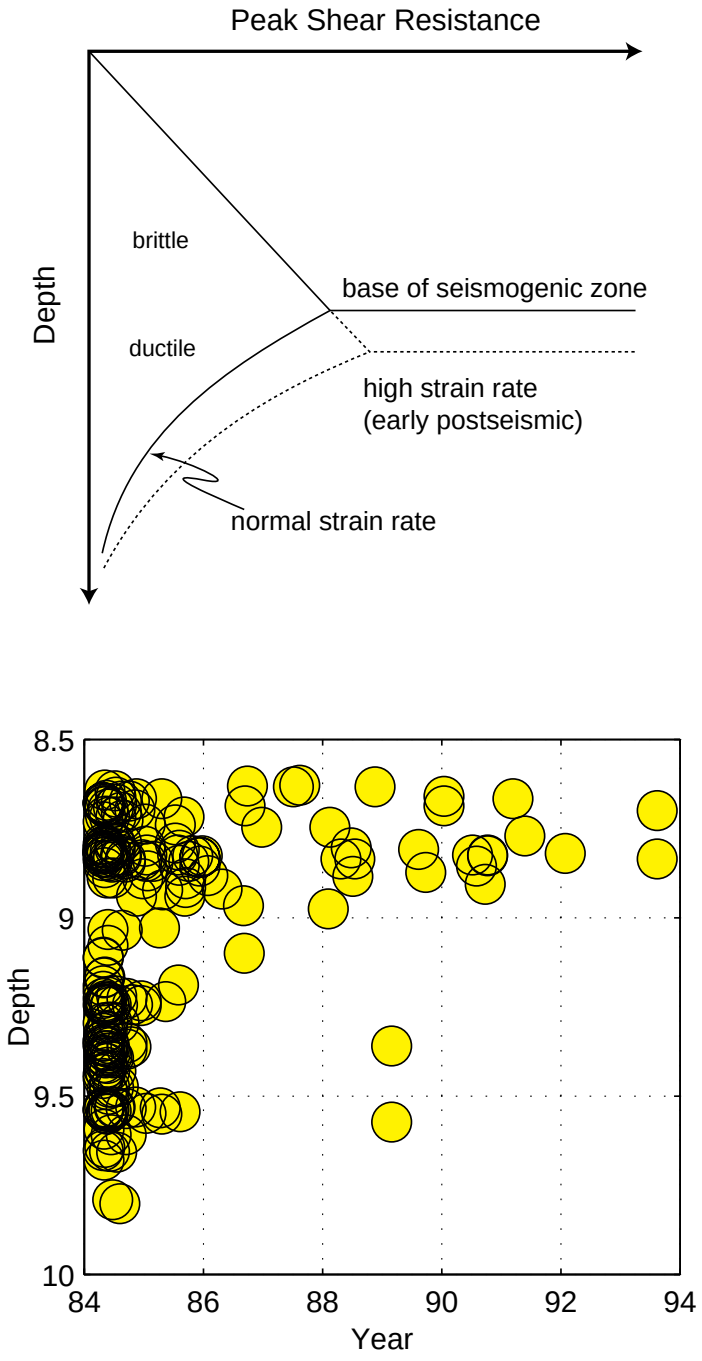

Figure 4.5: (top) Cartoon depicting change of brittle-ductile transition due to higher strain rates right after the mainshock. (bottom) Temporary existence of deeper events is consistent with above mechanism.

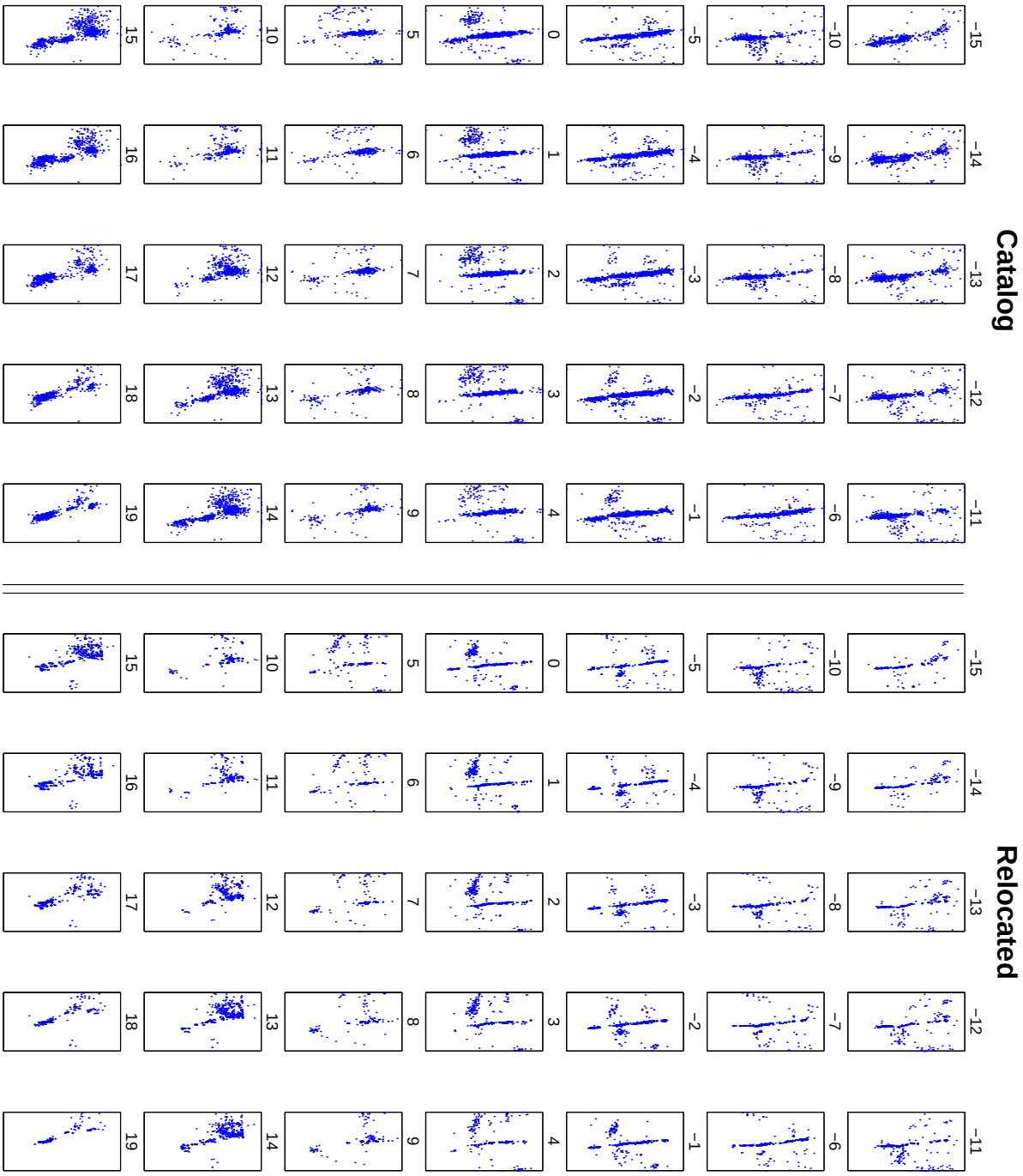

Figure 4.6: Cross-sectional views for (left) catalog locations and (right) correlation relocations. Boxes of seismicity are 6 km across fault and 12 km in depth. Bins span 4 km along the fault centered on numbers corresponding to distance along strike in Figures 4.2 & 4.3.

1994. Thus it is possible that the base of the seismogenic zone normally occurs around 9 km depth in this area, but temporarily increases more than 500 meters deeper due to the increased strain rates after the Morgan Hill mainshock. The interpretation is not conclusive since the phenomenon is only observed on a small portion of the fault and not under other high slip areas.

Figure 4.6 shows latitudinal cross sections of seismicity, i.e. cross sections oriented perpendicular to the strike of the Calaveras fault, before and after relocation. Clearly the Calaveras fault as expressed by seismicity at depth is extremely thin. Parts of the fault that appear in map view to have substantial width, e.g. from 5 to 0 km along strike, are seen in cross section to be an apparent width from the surface projection of a dipping planar fault. Only in areas where the depth extent of seismicity is small or where the fault plane is more vertical, does the fault appear narrow in map view.

Several previously obscured planar distributions of seismicity are now apparent as well. These include several vertical N-S trending faults to the north and east of the Calaveras fault (Figure 4.3). The broad region of seismicity to the west of the Calaveras between 0 and 10 km along strike is seen in cross section to form a blind thrust fault parallel to and southwest of the Calaveras fault that dips $\sim$ 30 degrees to the northeast (Figure 4.6). This seismicity does not appear to match any mapped fault traces when extrapolated to the surface. As will be shown later, the focal mechanisms for events on these off-fault structures are consistent with the alignment of hypocenters and confirm the orientation of these subsidiary faults. Most of the off-fault seismicity appears to be influenced by the Morgan Hill mainshock and is observed to follow Omori's law of aftershock decay.

4.4 Streaks

A number of linear features are apparent in the seismicity plot of Figure 4.3. These streaks of seismicity are predominantly horizontal, which coincide with the right-lateral slip direction on the Calaveras fault. Similar alignments of seismicity have been observed on the San Andreas and Hayward faults and in the southeast rift zone at Kilauea, Hawaii [*Gillard et al.,* 1996; *Rubin et al.,* 1999; *Waldhauser et al.,* 1999]. In each of these cases the streaks appear closely aligned with the slip direction on the fault, suggesting that the streaks arise

due to a slip-controlled process rather than something else such as horizontal layering [*Rubin et al.*, 1999; *Waldhauser et al.*, 1999]. For the Calaveras fault we find that while many of the streaks are nearly horizontal, some appear to have a slight dip (Figures 4.3 & 4.4).

Figure 4.7 shows two of the streaks on the Calaveras fault in detail. The first is a two kilometer sub-horizontal streak that occurs around -10 km along strike distance on Figure 4.3 and is composed of many events of variable magnitude with significant spatial overlap. The four $M \sim 3$'s between 0 and 0.5 km in Figure 4.7 appear to bridge the gap in the streak between the two strands composed of smaller events. The second panel is analogous to plots made by paleoseismologists with the inferred rupture length along strike for each event versus calendar time. This plot shows no clear recurrence pattern other than the tendency for events on adjacent fault segments to be correlated in time. There is significant overlap of seismicity within the streak and the range of observed magnitudes is more or less continuous as demonstrated in the 3rd panel.

The second streak detailed in Figure 4.7 is located at -4 km on Figure 4.3. Events on this streak also have a wide range of magnitudes. Smaller events tend to occur on the periphery of larger earthquakes. In this streak, however, the seismicity is comprised largely of repeating earthquakes. The overlapping circles of similar size indicate that parts of the fault rupture repeatedly in the same sized earthquakes. The 3rd panel in Figure 4.7 shows that there are characteristic magnitudes which correspond to those of the repeating events. In contrast, the magnitude distribution over the entire fault in Figure 4.2 obeys the classic Gutenberg-Richter relation, (100 M 3's, 10 M 4's, 1 M 5). The recurrence interval is also more regular in time and not as strongly correlated with the timing of earthquakes in adjacent segments. These observations suggest that the locked patches of the fault that fail in stick-slip are more isolated on this streak compared with the first streak. The relative isolation of slipping patches could more easily lead to re-establishing the same initial conditions at the onset of earthquakes and hence would lead to re-occurrence of characteristic earthquakes. The relative isolation would also lead to weaker interaction of adjacent earthquakes and hence a more regular recurrence interval.

Many of the events in our study can be considered aftershocks of the 1984 Morgan Hill, California earthquake. The repeating earthquake sequence at 0.5 km in the paleoplot

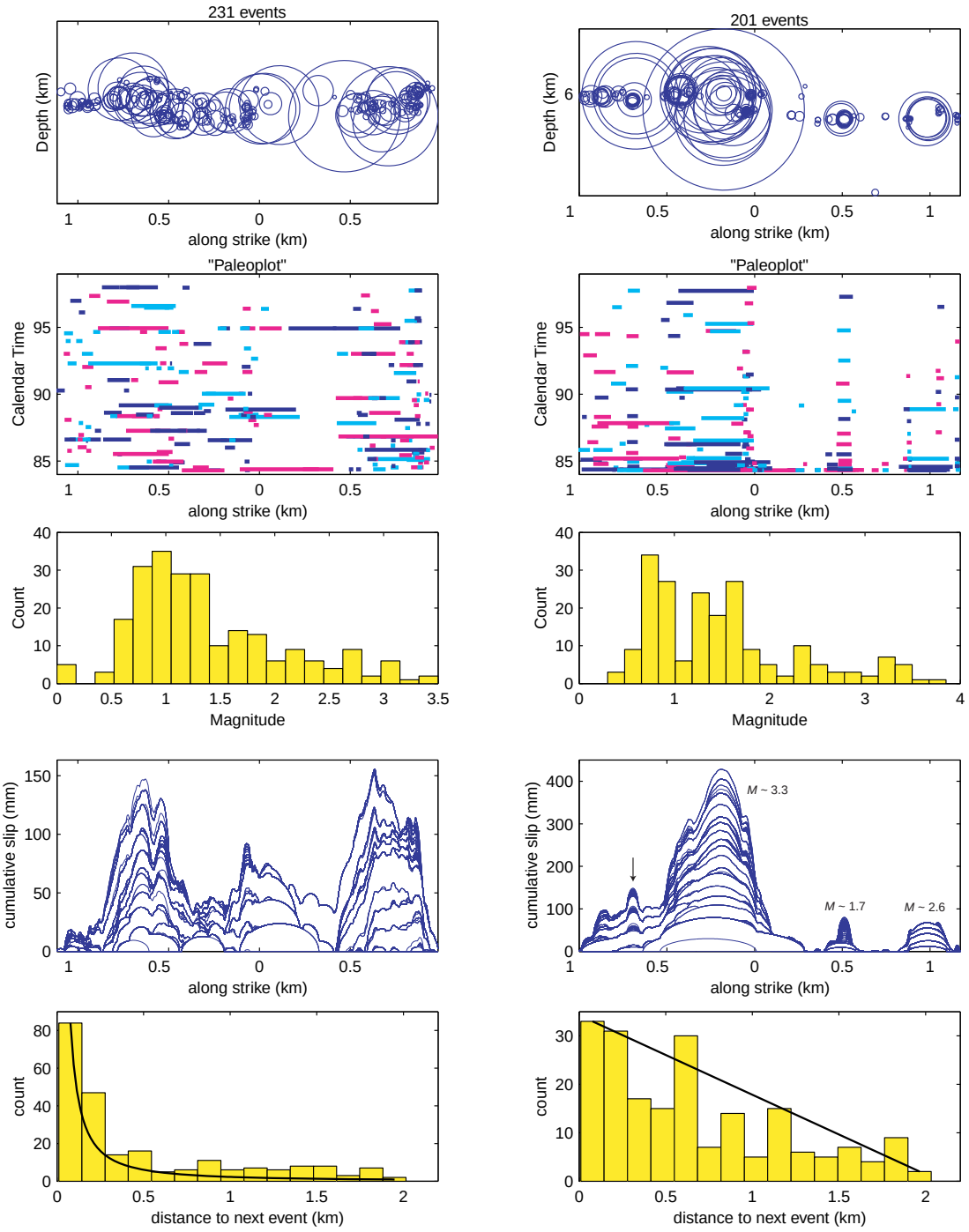

Figure 4.7: Comparison of two linear structures for characteristic-type features in space, time, and size. (left) 2 km long streak consisting of a continuous range of several magnitudes. No clear discernible pattern is observed in time. Evidence of earthquake triggering is present in lowermost panel. (right) Aligned multiplets which contains events of discrete magnitudes, repeatable hypocenters, and many recurrence intervals that can be predicted by an Omori type decay. These recurrence intervals seem largely unaffected by neighboring events and represent minimal earthquake interaction.

panel for the second streak on the right in Figure 4.7 is an example of a repeating earthquake sequence that follows Omori's law of aftershock decay. *Schaff et al.* [1998] showed that repeating aftershocks of the 1989 Loma Prieta also followed Omori's law. They also demonstrated that this observation is consistent with loading of a stuck patch on an otherwise creeping fault in response to a stress step, where the creeping part of the fault obeys a steady-state velocity strengthening friction law. In this case the stress step would have been provided by the 1984 Morgan Hill, California earthquake. It is interesting to note that the occurrence of ~ 13 M 3.3 earthquakes 500 m away from this repeating sequence does not appear to influence the timing of these events.

Assuming a constant stress drop of 3 MPa and a circular crack model, an estimate of the slip for each event can be made. The fourth panels in Figure 4.7 display cumulative slip isochrons plotted for the occurrence of each event within the streak. The characteristic, more predictable behavior, clearly emerges again for the second streak on the right. The two clusters at 0.5 km and 1 km appear to have similar slip rates over the $\sim$15 year interval, despite the difference in magnitudes (1.7 and 2.6 respectively). The cluster of magnitude 3.3's, however, would correspond to over five times this slip rate for the same time period, given the assumption of a constant stress drop. An intriguing feature can be found by the arrow at -0.7 km, where two clusters of different magnitudes rupture the same fault patch with interwoven recurrence intervals. If we assume that the smaller of these events is set up repeatedly with the same initial conditions between large events, then it suggest that much of the area that slips in the larger events may also slip aseismically [*Beeler,* 2001].

Surprisingly, the first streak appears to display some systematic behavior in the accumulation of slip along strike compared to the absence of regular recurrence intervals or repeated hypocentral locations from the first two panels. A somewhat uniform slip rate across this streak results from our assumptions. Applying a linear stress drop with moment relation after [*Nadeau and Johnson,* 1998; *Nadeau and McEvilly,* 1999] produces a more irregular slip distribution and a rather large 2 m of cumulative slip for the M 3.3's in the second streak. It will be difficult for any simple stress drop scaling to satisfy a uniform slip rate. There are approximately the same number of the M 1.7 and M 3.3 events (16 and 13 respectively) and only 5 M 2.6 events. Thus, any constant or monotonically changing stress drop with earthquake size will not result in uniform slip.

If a rectangular source is assumed where the length is greater than the height, it will smooth out the slip distribution compared to that for the circular crack model. With an aspect ratio of 3:1 or larger, the slip is relatively uniform, but many of the fault segments rupture repeatedly both as large and small events. Although, the regular recurrence of the M 1.7 events suggests that this is not occurring.

For seismic slip on circular asperities to keep pace with the surrounding creep rate, unusually high stress drops are implied [*Nadeau and Johnson,* 1998; *Nadeau and McEvilly,* 1999]. A model where repeating earthquakes occur at the border between creeping and locked zones produces the common lower stress drops ($\sim$ 1 MPa), which are constant for all magnitudes [*Sammis and Rice,* 2001]. The distribution of streaks with multiple parallel strands in Figure 4.4, however, seems incompatible with a simple boundary between creeping and locked zones.

From the surface creep rate of 15 mm/yr an estimated 225 mm could have accumulated over this time span — a value approached only at a few places along the streaks. The repeating earthquake models can be divided into two classes based on how they account for total slip across the asperity: either as the sum of aseismic and seismic slip [*Beeler,* 2001] or seismically [*Nadeau and Johnson,* 1998; *Sammis and Rice,* 2001]. On the 2 km scale of these streaks with clusters of repeating events in such close proximity, it may be reasonable to assume a uniform loading rate across the asperities. Yet the choice of a constant or variable stress drop produces fairly irregular cumulative slip distributions with significant gaps. This suggests that a uniform geodetically-determined slip rate can not entirely be accounted for seismically; but that aseismic processes contribute substantially to the deformation as well [*Bakun et al.,* 1986; *Beeler,* 2001].

The lowermost panels in Figure 4.7 display a marked difference in earthquake interaction between the two streaks. For the first streak, a large number of events occur in close proximity to the one that happened just before it, suggesting strong earthquake interaction. In other words, events are tending to trigger rupture on adjacent fault segments. For the second streak the linear fall-off is what would be expected for purely random spatial and temporal behavior in the absence of earthquake interaction. This observation fits cleanly with our idea on the necessary conditions in order for repeating clusters of events to occur — isolated stuck patches, embedded in a sea of creep, whose recurrence intervals aren't

Distance	15 yr	1 day	1min
100 m	5930 (80%)	573 (7.7%)	71 (1.0%)
50 m	5560 (75%)	320 (4.3%)	43 (0.6%)
25 m	4890 (66%)	118 (1.6%)	20 (0.3%)
10 m	3186 (43%)	21 (0.3%)	4 (0.1%)

Table 4.1: Statistics for 7409 relocated events

influenced by surrounding events.

Table 1 attempts to quantify how many of the relocated events are repeats and how many are triggered. The "15 yr" column displays the number and percentage of events that have at least one other event over the 15 year interval that occurs within the corresponding distance for that row. The "1 day" and "1 min" columns indicate the number of those event pairs that occur with much smaller time intervals. Therefore at least two thirds (66%) of the events could most likely be classified as repeats because they have at least one other event which occurs within 25 m in the data set. An estimated source radius for a M 1.5 event is around 30 m. Hypocenters of larger events can be separated by more and still have significant source area overlap. Approximately 8% (573 events in Table 1 of all the relocated events on the Calaveras fault appear to be triggered (occurring within 100 m and 1 day from a prior event). Some of the recurrence intervals are extremely short. For example, one pair of events out of the twenty that are within 25 m and 1 min of each other corresponds to a magnitude 2.5 and 2.7 that occurred only 15 seconds apart in 1988.

4.5 Holes

There are a number of areas on the Calaveras fault that have very little microearthquake activity. The filled areas of all the black circles (excluding Morgan Hill) on Figure 4.8 comprise only about 6% of the total fault area. In other words, 94% of the seismogenic zone in this region has been free of microearthquake activity over the past 15 years. These holes in the seismicity are evident in Figure 4.8: one from -5 to 1 km along strike and 2-6 km depth, and another at 4-7 km along strike and at similar depth. The most prominent is

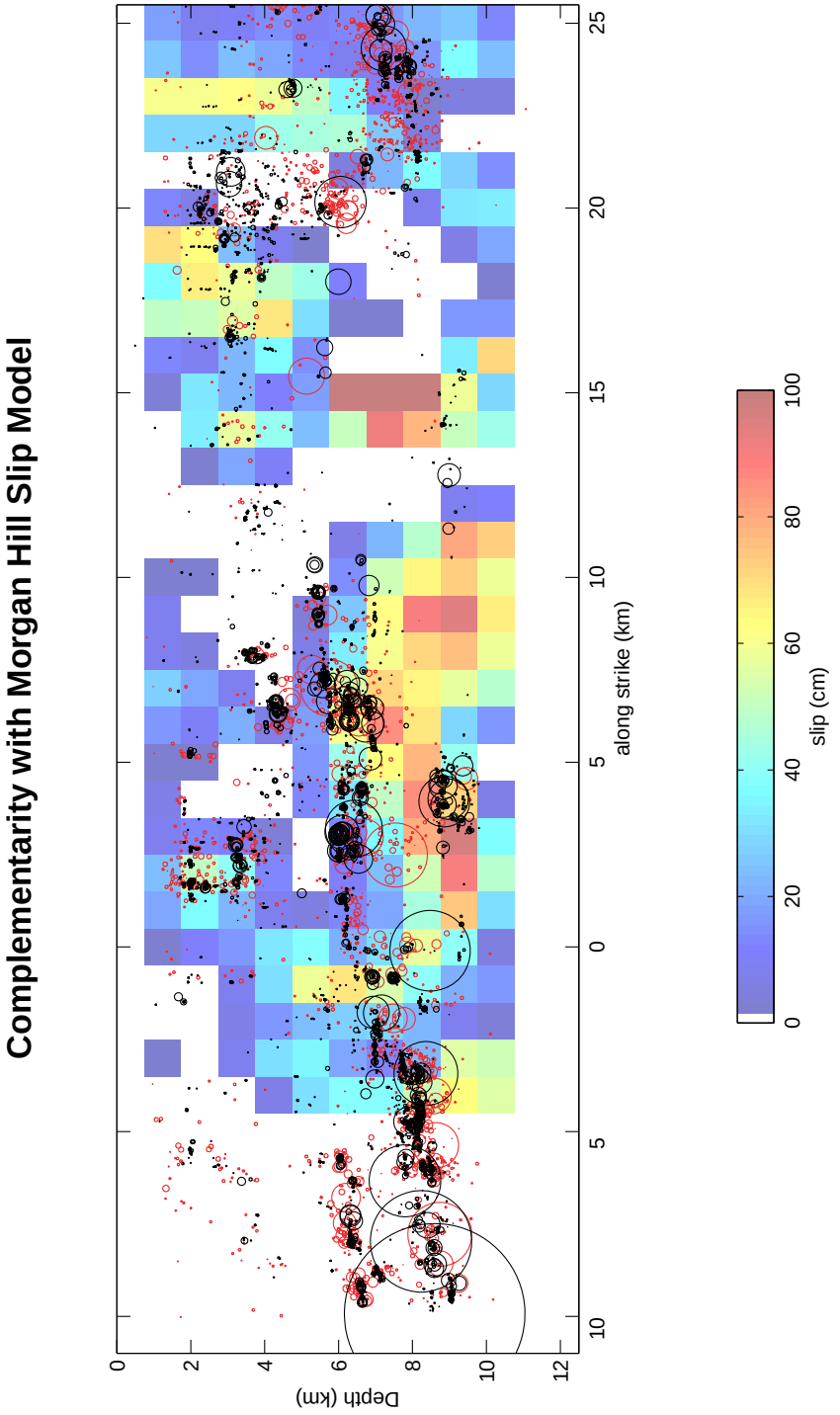

Figure 4.8: The Morgan Hill slip model [*Beroza and Spudich*, 1988] for the M 6.2 event occurring in 1984, compared to the seismicity distribution from 1967 to 1984 (red) and from 1984 through 1997 (black).

the notable absence of seismicity from 10-19 km along strike at depths greater than 5 km. For the time period considered, these areas have remarkably little earthquake activity when compared with the rest of the Calaveras fault. Since the Calaveras fault is known to have both earthquakes as large as M 6.2 and to have a great deal of aseismic creep, it is natural to ask the question of how these holes behave over the long term. Do they slip aseismically or do they slip in moderate earthquakes?

There is direct evidence that at least some of them slip in larger earthquakes. Figure 4.8 also shows a slip model of the 1984 Morgan Hill earthquake derived from waveform modeling of strong motion data [*Beroza and Spudich,* 1988] together with the relocated seismicity. Although the spatial resolution of mainshock slip, particularly the vertical location is poor, it is clear that the area of highest slip in the mainshock at approximately +15 km along strike, is situated within the most prominent hole in micro-earthquake activity. The other area of substantial slip in the earthquake was near the mainshock hypocenter at 0 km along strike and 8 km depth, which is located below one of the holes in microearthquake activity. This anti-correlation of mainshock slip and earthquake activity has been noted previously [*Hartzell and Heaton,* 1986; *Mendoza and Hartzell,* 1988; *Oppenheimer et al.,* 1990]; however, the degree to which areas of slip in moderate earthquakes are devoid of microearthquake activity in the interim is even more striking after relocation.

It has long been recognized that aftershocks are likely to occur in regions of high mainshock-induced stress concentration [e.g., *Beroza and Spudich,* 1988; *Mendoza and Hartzell,* 1988]. It is worth noting, however, that the anti-correlation between microearthquake seismicity and slip in occasional larger earthquakes persists long after aftershock activity has ceased [*Oppenheimer et al.,* 1990]. That is, the seismicity holes are longer-lived features than would be expected if they were simply the byproduct of mainshock-aftershock interaction. It was also a pre-existing condition. Plotted in red on Figure 4.8 are pre-Morgan Hill events since 1967, relocated using only catalog phase data. Although the locations are not as precise, the same general pattern of seismicity persists through the mainshock. This suggests that stress accumulation and release on the Calaveras fault is strongly influenced by spatial variations in fault zone properties.

There is indirect evidence that the holes may behave aseismically as well. Slip in the 1984 Morgan Hill earthquake, although complementary to microearthquake activity, does

not nearly fill all the aseismic areas (Figure 4.8). One should note that microseismicity represents very little total slip relative to the mainshock. A plausible model for how repeating earthquakes occur is that they are stuck asperities surrounded by creep. There are also holes in seismicity that have not yet been filled with larger earthquakes. Finally, there is geodetic evidence for a very large post-mainshock aseismic transient following the 1984 Morgan Hill, California earthquake [*Prescott et al.,* 1984]. Although the slip is not well located, *Prescott et al.* [1984] presented evidence that it was shallower than most of the mainshock slip. Thus, it is possible that some of the holes in seismicity are filled with aseismic slip following the 1984 earthquake.

4.6 A Fault Discontinuity

Maps of the surface trace of the Calaveras fault display substantially more complexity than suggested by the seismicity at depth. Figure 4.9 shows that the simple structure with depth does not closely correlate with mapped surface traces. While Figures 4.3 and 4.6 indicate that the strike of the Calaveras Fault remains essentially constant from -17 to 8 km along strike with minor fluctuations in dip, the surface expression is more complicated and is unmapped over some stretches.

The events between 8 to 20 km along strike in Figure 4.3 correspond to panels 10 to 19 on Figure 4.6. Here the fault structure deviates significantly from a simple planar geometry. In Figure 4.3, it is evident that these events form a prominent left-stepping fault jog. This will act as a restraining feature for right-lateral slip on the Calaveras fault. Thus, it is likely that this fault segmentation acted to terminate rupture of the 1984 Morgan Hill earthquake to the southwest. This possibility had been recognized previously [*Bakun et al.,* 1984; *Beroza and Spudich,* 1988]; however, the fault trace at the surface and at depth do not correspond very closely and it was not necessarily clear from the seismicity what the depth extent of the fault offset was. From the relocated seismicity it is clear that the fault discontinuity extends over the same range as slip in the mainshock.

Both the surface trace and the relocated seismicity at depth indicate a compressional fault offset of the Calaveras fault in the southern reaches of our study area; however, the structure of this feature is quite different in the two cases. The geologically mapped surface

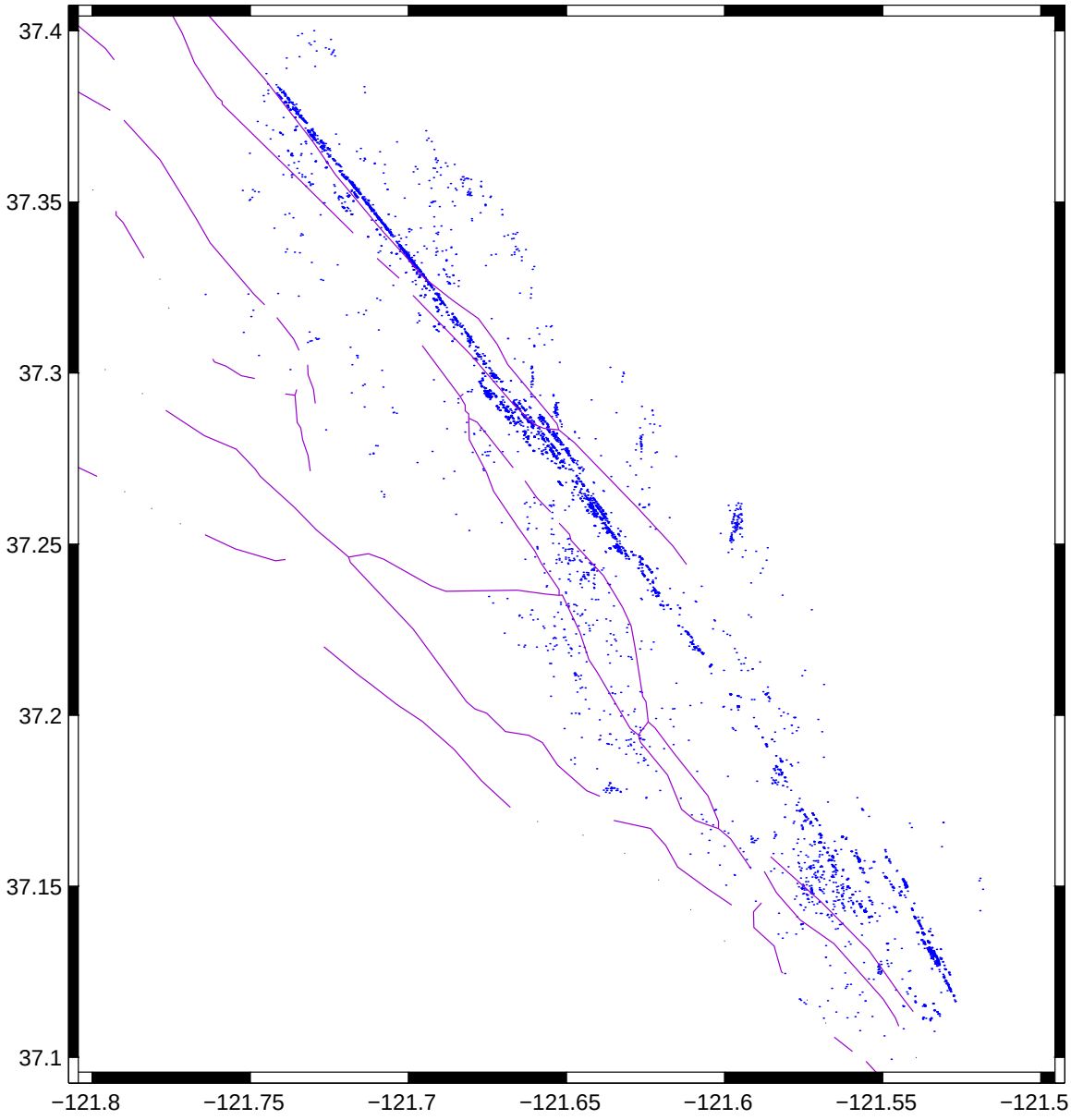

Figure 4.9: Comparison of seismicity in map view with surface faulting.

trace appears quite complicated in the vicinity of the fault offset with multiple parallel strands [*Radbruch-Hall*, 1974]. The fault offset in the surface trace is not located in the same place as the fault offset recorded by microearthquake activity. The seismicity, on the other hand, shows that the offset at depth is on the order of a km, and while there is considerable seismicity off the main fault trace of the Calaveras to the southwest of the jog, most of the seismicity is concentrated on two main fault traces. The western trace appears to dip towards the eastern trace and there is a suggestion that the two meet near the base of the seismogenic zone in the latitudinal cross sections 11-17 of Figure 4.6. In studies of relocated seismicity near a dilational fault offset at Landers, *Felzer and Beroza* [1999], found no evidence that the two fault traces merged at depth.

It is interesting that our technique appears to do well at refining earthquake locations within and surrounding a fault jog. It is easy to understand why it would work well on a simple planar fault, such as the Calaveras fault to the northwest of the fault jog. In that area there are abundant microearthquakes and their mechanisms are likely to be essentially identical. A fault jog, however, is inherently three dimensional and mechanisms will almost certainly be strongly variable. The fact that we get such a clear image of the three dimensional structure of the fault jog in this case suggests that we can apply these relocation techniques to great effect in areas where structure is quite complicated.

4.7 Fault Zone Width

One of the most important parameters for understanding both how faults evolve and the mechanics of earthquake rupture is fault zone width. Some measure of fault-zone width can be extracted from Figure 4.6, which shows cross sections of seismicity oriented perpendicular to the fault strike. With the exception of the aforementioned fault discontinuity, nearly all of the earthquake activity defines a very narrow planar zone following relocation. The orientation varies from nearly vertical in the north from -17 to -9 km along strike, to a dip to the east of about 85 degrees from -5 to 4. Most of the off-fault seismicity clearly falls on other planar structures with different orientations, such as the off-fault blind thrust from 0 to 3 km along strike.

To quantify fault zone width, we divide the fault using a 1 km square grid and measure

distance orthogonal to the fault for each event. We then subtract the mean in each box and take 4 times the standard deviation of the estimate. This means approximately 95% of the relocated earthquakes fall within a planar feature of that width. Figure 4.10 indicates an average 75 m fault zone width for the Calaveras Fault. For comparison, the widths of the two streaks in Figure 4.7 are approximately 25 m. Because the widths we measure are comparable to location errors on these different scales, it is likely that the fault zone is substantially thinner. Our results are consistent with a fault that has zero resolvable width. We also find no evidence for any systematic variation of fault zone width with depth or distance along strike.

Other geophysical estimates of fault width can be obtained by modeling fault zone guided waves. Modeling dispersive wave trains of microearthquakes at Parkfield implies a low-velocity channel 100 to 150 meters wide on the San Andreas fault [*Li et al.,* 1990]. Results for other faults include: 100–200 m for Landers [*Li et al.,* 1994], 30–60 m for Kobe [*Li et al.,* 1998], and 120 m for the San Jacinto fault zone [*Li et al.,* 1997]. Comparision with our estimates may in part represent variations in width for different faults. The two measurements provide complementary information. The distribution of earthquakes indicates the part of the fault zone that is currently active, seismically, whereas wave guides delineate a low velocity zone in comparison with the country rock.

4.8 Stress Orientation

As noted earlier, focal mechanisms of the off-fault seismicity provide independent evidence substantiating the orientation of the structures resolved by the relocation. Figure 11a displays composite focal mechanisms for two N-S trending faults, the blind thrust fault, and events on the Calaveras fault. The N-S trending faults together with the Calaveras fault might appear to form a conjugate set. The focal mechanisms of these events, however, clearly show that these faults are not a conjugate set because the mechanisms of events on the Calaveras fault and on the N-S trending faults are all right-lateral.

The stress tensor orientation based on focal mechanisms and other stress indicators suggests that the San Andreas fault system is weak in the sense that it slips at a low level of resolved shear traction [*Zoback et al.,* 1987; *Townend and Zoback,* 2001]. The focal

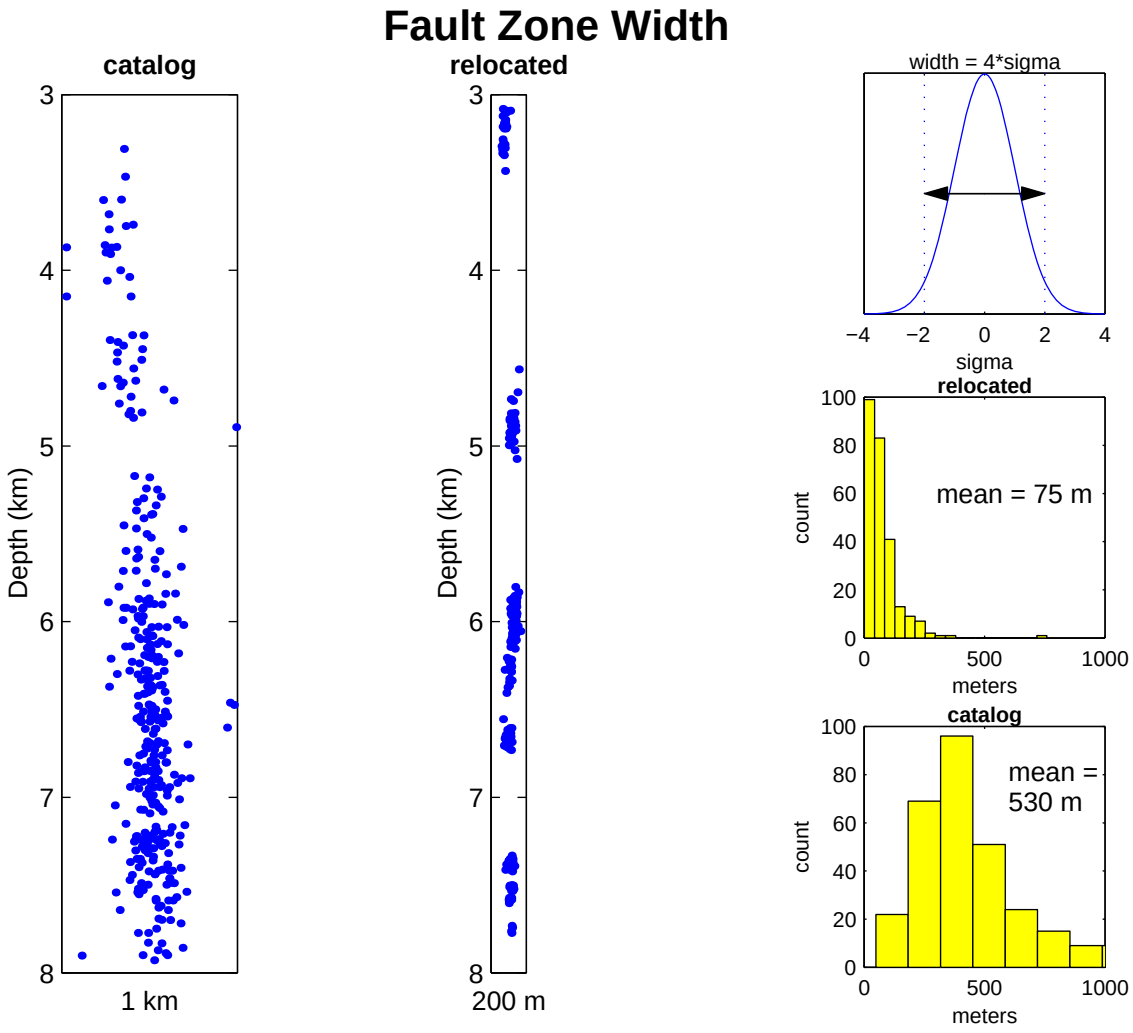

Figure 4.10: Comparison of improved estimates for fault zone width from original catalog locations and relocations.

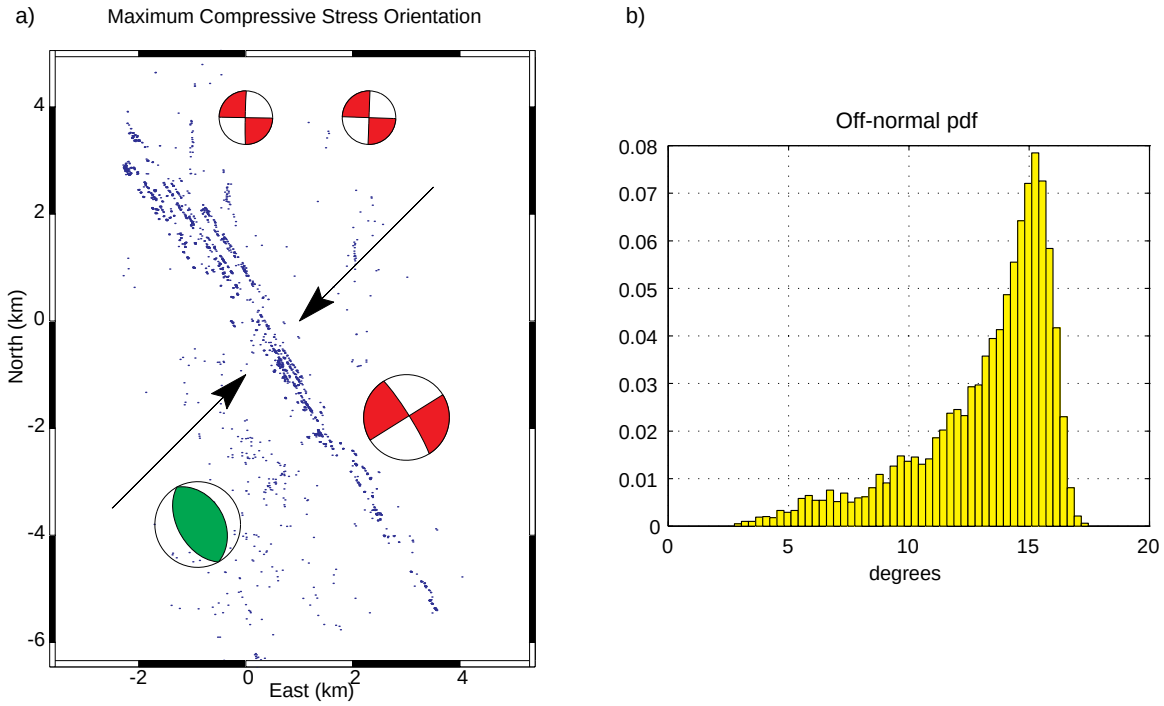

Figure 4.11: (left) Focal mechanisms of Calaveras Fault and off-fault structures. The maximum compressive stress is computed to be at a high angle to the fault. (right) Plane fits to the seismicity used in the stress inversion viewed from different angles.

mechanisms and off-fault seismicity provide an opportunity to estimate the regional stress in the vicinity of the Calaveras fault. There are several particularly fortunate aspects to the location and nature of this seismicity for this purpose. There are both right-lateral, strike-slip, and reverse faulting mechanisms with differing orientation, which in turn have a distinct orientation compared to the right-lateral strike-slip on the Calaveras fault. Moreover, for each of these structures the clearly resolved geometry of the seismicity allows us to differentiate the fault vs. auxiliary plane ambiguity of the focal mechanism. Finally, the active features reach within a few hundred meters of the Calaveras fault itself, allowing us to constrain the stress tensor in very close proximity to this major active fault.

We estimate the stress tensor using a method similar to *Angelier* [1979] in which the slip vector and fault plane are both known. The geometry of the active faults and the orientation of the maximum compressive stress are shown in Figure 4.11. Table 2 shows

Fault	Dip direction	Dip angle	Rake angle
Calaveras	58	84	180
Thrust	61	33	90
N-S1	91	88	180
N-S2	92	89	180

Table 4.2: Fault planes used for stress inversion

the data based on the resolved fault geometry that is used to constrain the stress tensor. The two N-S trending faults reach to within approximately 100 meters and 2 km of the fault respectively. The thrust fault reaches to within less than 1 km of the main Calaveras fault as well.

In order for all of these structures to slip in the observed direction, we find that the expected value for the orientation of the maximum compressive stress is 13 degrees off the normal to the Calaveras fault (Figure 4.11b). The skewed probability density function is obtained by bootstrap analysis perturbing the input data within the errors and over the range of inversion parameters. The 95% confidence interval is [7 16]. This is a very high angle, much higher than would be expected based on laboratory derived values of the coefficient of friction [*Byerlee*, 1978]. An effective coefficient of friction of 0.1, or alternately high pore pressure, was necessary to satisfy the known slip directions and generate traction on the faults sufficient for slip. Our results contrast sharply with those reported for the San Andreas fault in southern California [*Hardebeck and Hauksson*, 1999] and thus have very different implications for the origin of weak faults. In particular, the wide zone of high fluid pressure and low effective normal stress proposed for the southern San Andreas fault, can not apply to our data set for the Calaveras fault.

Previous investigators have obtained similar results for a high-angle, maximum compressive stress orientation in this same region because the areas of the inversion included mechanisms from the secondary faulting structures we have analyzed [*Oppenheimer et al.*, 1988; *Zoback et al.*, 1987]. Our work is distinguished from these earlier studies in that the

precise relative event locations allow us to resolve these secondary faults as active structures that reach nearly to the Calaveras fault itself and hence to constrain the lack of stress rotation in the near field.

4.9 Conclusions

Through applying the double-difference location method to cross-correlation derived differential arrival times, we are able to reduce errors in location for seismicity on and near the Calaveras fault by more than an order of magnitude. This reveals details of fault zone structure and seismicity that were previously unknown. We find that the relocated seismicity is highly organized, which was previously obscured by location errors. The Calaveras fault has many repeating earthquakes and sub-horizontal streaks of earthquakes. Holes in the seismicity appear to be the locus of slip in occasional larger earthquakes. The Calaveras fault at depth is extremely thin, with an average upper bound on fault zone width of 75 meters. The sense of slip on subsidiary fault structures that reach within a few hundred meters of the Calaveras fault indicate that the maximum compressive stress is at a high angle to the Calaveras fault, only 13 degrees from the fault normal vector, supporting previous interpretations that this fault is weak. The relocation technique we have used to study the behavior of the Calaveras fault opens a new window on the earthquake source. By resolving the structure of seismicity at smaller length scales, we can address many important problems in earthquake mechancis.

Acknowledgments. We thank Eva Zanzerkia for her comments on and help with aspects of the relocation work. Helpful discussions and reviews were provided from Andy Michael, Allan Rubin, John Townend, Mark Zoback, Paul Segall, David Pollard, Roland Burgmann, Keith Richards-Dinger, and Jeff McGuire. We thank the NCSN and NCEDC for the ease of retrieving seismograms from their archive and availability of data over the internet. This work was supported by NSF grant EAR-9725238 and EAR-0074084.

4.10 References

Angelier, J., Determination of the mean principal directions of stresses for a given fault population, *Tectonophysics, 56*, T17-T26, 1979.

Bakun, W.H., M.M. Clark, R.S. Cockerham, W.L. Ellsworth, A.G. Lindh, W.H. Prescott, A.F. Shakal, and P. Spudich, The 1984 Morgan Hill, California, earthquake, *Science, 225*, 288-291, 1984.

Bakun, W.H., G.C.P. King, and R.S. Cockerham, Seismic slip, aseisimic slip, and the mechanics of repeating earthquakes on the Calaveras Fault, California, in *Earthquake Source Mechanics, Geophys. Monogr. Ser.*, vol. 37, edited by S. Das, J. Boatright, and C.H. Scholz, pp. 195-207, AGU, Washington, D.C., 1986.

Beeler, N.M., A simple stick-slip and creep-slip model for repeating earthquakes and its implications for micro-earthquakes at Parkfield, *Bull. Seismol. Soc. Am.*, in press.

Beroza, G.C., and P. Spudich, Linearized inversion for fault rupture behavior; application to the 1984 Morgan Hill, California, earthquake, *J. Geophys. Res., 93*, 6,275-6,296, 1988.

Byerlee, J.D., Friction of rocks, *Pure Appl. Geophys., 116*, 615- 629, 1978.

Ellsworth, W.L., Characteristic earthquakes and long-term earthquake forecasts: Implications of central California seismicity., in *Urban Disaster Mitigation*, edited by F.Y.C.a.M.S. Sheu, pp. 1-14, Elsevier, Tarrytown, New York, 1994.

Felzer, K.R., and G.C. Beroza, Deep structure of a fault discontinuity, *Geophys. Res. Let., 26*, 2,121-2,124, 1999.

Fréchet, J. Sismogenè et doublets sismiques, *Thèse d'Etat,* Université Scientifique et Médicale de Grenoble, 206 pp., 1985.

Deichmann, N., and M. Garcia-Fernandez, Rupture geometry from high-precision relative hypocentre locations of microearthquake ruptures, *Geophys. J. Int., 110*, 501-5517, 1992.

Geiger, L., Herdbestimmung bei Erdbeben aus den Ankunftszeiten, *K. Gesell. Wiss. Goett., 4* 331-349, 1910.

Gillard, D., A.M. Rubin, and P. Okubo, Highly concentrated seismicity caused by deformation of Kilauea's deep magma system, *Nature, 384*, 343-346, 1996.

Got, J.-L., J. Fréchet, and F.W. Klein, Deep fault plane geometry inferred from multiplet relative relocation beneath the south flank of Kilauea, *J. Geophys. Res., 99*, 15,375-15,386, 1994.

Hardebeck, J.L., and E. Hauksson, Role of fluids in faulting inferred from stress field signatures, *Science, 285*, 236-239, 1999.

Hartzell, S.H., and T.H. Heaton, Rupture history of the 1984 Morgan Hill, California, earthquake from the inversion of strong motion records, *Bull. Seismol. Soc. Am., 76*, 649-674, 1986.

Li, Y.-G., P.C. Leary, K. Aki, and P. Malin, Seismic trapped modes in the Oroville and San Andreas fault zones, *Science, 249*, 763-766, 1990.

Li, Y.-G., J.E. Vidale, K. Aki, C.J. Marone, and W.H.K. Lee, Fine structure of the Landers fault zone; segmentation and the rupture process, *Science, 265*, 367-370, 1994.

Li, Y.-G., K. Aki, and F.L. Vernon, San Jacinto fault zone guided waves; a discrimination for recently active fault strands near Anza, California, *J. Geophys. Res., 102*, 11,689-11,701, 1997.

Li, Y.-G., K. Aki, J.E. Vidale, and M.G. Alvarez, A delineation of the Nojima Fault ruptured in the M 7.2 Kobe, Japan, earthquake of 1995 using fault zone trapped waves, *J. Geophys. Res.*, it 103, 7,4247-7,263, 1998.

Mendoza, C., and S.H. Hartzell, Aftershock patterns and main shock faulting, *Bull. Seismol. Soc. Am., 78*, 1,438-1,449, 1988.

Nadeau, R.M., and L.R. Johnson, Seismological studies at Parkfield VI; moment release rates and estimates of source parameters for small repeating earthquakes, *Bull. Seismol. Soc. Am., 88*, 790-814, 1998.

Nadeau, R.M., and T.V. McEvilly, Fault slip rates at depth from recurrence intervals of repeating microearthquakes, *Science, 285*, 718-721, 1999.

Oppenheimer, D.H., P.A. Reasenberg, and R.W. Simpson, Fault plane solutions for the 1984 Morgan Hill, California, earthquake sequence; evidence for the state of stress on the Calaveras Fault, *J. Geophys. Res., 93*, 9,007-9,026, 1988.

Oppenheimer, D.H., W.H. Bakun, and A.G. Lindh, Slip partitioning of the Calaveras Fault, California, and prospects for future earthquakes, *J. Geophys. Res., 95*, 8,483-8,498, 1990.

Poupinet, G., W.L. Ellsworth, and J. Fréchet, Monitoring velocity variations in the crust using earthquake doublets: an application to the Calaveras Fault, California, *J. Geophys. Res., 89*, 5719-5731, 1984.

Prescott, W. H., N. E. King, and G. Guohua, Preseismic, coseismic, and postseismic deformation associated with the 1984 Morgan Hill, California, earthquake, in *The 1984*

Morgan Hill, CA earthquake, edited by J. H. Bennett and R. W. Sherburne, pp. 137-148, Cal. Div. Mines and Geo. Spec. Pub. 68, 1984.

Radbruch-Hall, D.H., Map showing recently active breaks along the Hayward fault zone and the southern part of the calaveras fault zone, California, *U.S. Geol. Surf., Misc. Invest.* I-813, 1974.

Rubin, A.M., D. Gillard, and J.-L. Got, Streaks of microearthquakes along creeping faults, *Nature, 400*, 635-641, 1999.

Sammis, C.G., and J.R. Rice, Repeating earthquakes as low-stress drop events at a border between locked and creeping fault pathces, *Bull. Seismol. Soc. Am.*, , submitted.

Schaff, D.P., G.C. Beroza, and B.E. Shaw, Postseismic response of repeating aftershocks, *Geophys. Res. Let., 25*, 4,549-4,552, 1998.

Schaff, D.P., G.H.R. Bokelmann, E. Zanzerkia, F. Waldhauser, G.C. Beroza, and W.L. Ellsworth, Cross correlation arrival time measurements for earthquake location, submitted to *J. Geophys. Res.*, , 2001.

Sibson, R.H., Roughness at the base of the seismogenic zone: contributing factors, *J. Geophys. Res., 89*, 5,791-5,799, 1984.

Townend, J., and M.D. Zoback, Implications of earthquake focal mechanisms for the frictional strength of the San Andreas fault system, *Spec. Pub. Geol. Soc. London*, in press.

Waldhauser, F., W.L. Ellsworth, and A. Cole, Slip-parallel seismic lineations along the northern Hayward fault, California, *Geophys. Res. Let., 26*, 3,525-3,528, 1999.

Waldhauser, F., and W.L. Ellsworth, A double-difference earthquake location algorithm: method and application to the northern Hayward Fault, California, *Bull. Seismol. Soc. Am., 90*, 1,353-1,368, 2000.

Working Group on California Earthquake Probabilities [WGCEP], Earthquake probabilities in the San Francisco Bay region: 2000 to 2030 — a summary of findings, *U.S. Geol. Surv. Open file Rep., 99-517*, Online version 1.0, 60 pp., 1999.

Zoback, M.D., M.L. Zoback, V.S. Mount, J. Suppe, J.P. Eaton, J.H. Healy, D.H. Oppenheimer, P.A. Reasenberg, L.M. Jones, C.B. Raleigh, I.G. Wong, O. Scotti, and C.M. Wentworth, New evidence on the state of stress of the San Andreas fault system, *Science, 238*, 1,105-1,111, 1987.

Chapter 5

Cross correlation arrival time measurements

Abstract. Earthquake location using relative arrival time measurements can lead to dramatically reduced location errors and a view of fault-zone processes with unprecedented detail. There are two main reasons why this approach reduces location errors. The first, not covered in this paper, is that the use of differenced arrival times to solve for the vector separation of earthquakes removes much of the error due to unmodeled velocity structure from the earthquake location problem. The second is that waveform cross correlation can substantially reduce measurement error. While cross correlation has long been used to determine relative arrival times with sub-sample precision, we extend correlation measurements to less similar waveforms and introduce a general quantitative means to assess when correlation data provides an improvement over catalog phase picks. Tests for an example streak of 243 earthquakes on the Calaveras fault demonstrate that relative arrival times with normalized cross correlation coefficients as low as $\sim 70\%$, interevent separation distances as large as to 2 km, and magnitudes up to 3.5 as recorded on the Calnet network are more precise than relative arrival times determined with catalog phase data. Also discussed are improvements made to the correlation technique itself. We find that time domain methods are substantially more robust and recover more observations than frequency domain techniques. Windows 256 samples long also give better results than shorter ones. A comparison is made of the advantages and disadvantages of absolute vs. relative arrival time data for different applications. Finally, it is explained how thresholds and empirical weighting functions may be derived to optimize the location procedure for any given region of interest, taking advantage of the respective strengths of diverse correlation and catalog phase data on different length scales.

5.1 Introduction

The two principal sources of error for most earthquake locations are arrival time measurement error and errors arising from unmodeled velocity structure, subsequently referred to as model error. Progress in reducing both these error sources, most recently using the combined strengths of waveform cross correlation measurements and the double difference location approach [*Waldhauser and Ellsworth,* 2000], has been realized on the Calaveras, Hayward and San Andreas Faults with one to two orders of magnitude reduction in location error at small scale lengths [*Waldhauser et al.,* 1999; *Schaff et al.,* 2001].

Earthquakes have been located using cross correlation measurements and relative location techniques for some time [*Poupinet et al.,* 1984; *Fréchet,* 1985; *Frémont and Malone,* 1987; *Deichmann and Garcia-Fernandez,* 1992; *Got et al.,* 1994; *Ito,* 1995; *Dodge et al.,* 1995]. It is only recently that relative location techniques have been applied to large numbers of events at spatial scales of more than a few km (see Table 5.1) [*Rubin et al.,* 1999; *Waldhauser et al.,* 1999; *Schaff et al.,* 2001]. The reason for this is in part historical. Earlier work concentrated on small clusters of earthquakes such as foreshocks [*Dodge et al.,* 1996] or repeating events [*Poupinet et al.,* 1984] that were certain to have extremely similar waveforms. Moreover, it is only recently that large volumes of waveform data have become readily accessible at earthquake data centers [*Neuhauser et al.,* 1994].

An important step in applying waveform cross correlation to earthquakes at larger spatial scales is the recognition that correlation data can be a significant improvement over catalog data under more general circumstances than was previously appreciated. In this study we use the post-fit relative arrival time residuals from the double difference location algorithm to independently assess the errors in the two data sets. From this quantitative comparison we find that cross correlation measurements can be used with great success to much lower similarity thresholds than have been used previously. For seismicity recorded by Calnet instrumentation and telemetry, we find that cross correlation measurements provide more precise measures of relative arrival time differences than catalog picks at separation distances of up to 2 km.

At larger spatial scales arrival time picks in the catalog provide essential information and without them it would be impossible to relocate all of the seismicity. Thus, combining

Group	Year	Region	Events Relocated
Poupinet et al.	1984	Doublets in Alps and Calaveras Fault	~ 2
Got et al.	1994	South flank fault on Big Island, Hawaii	~ 200
Rubin et al.	1999	Creeping section of San Andreas Fault	$\sim 3,200$ (75%)
USGS/Stanford	2000	Hayward, Calaveras, San Andreas, Landers	$\sim 20,000$ (90%)
USGS/Stanford	current	Entire Northern California catalog	$\sim 250,000$ (99%)

Table 5.1: Progress of correlation-based relative relocation over the years

the two data sets is important. By using post-fit residuals from the location algorithm to develop a rational data weighting for both the catalog and cross correlation arrival time measurements, we obtain locations that take advantage of the strengths of both data sets.

5.2 Residual Analysis and Observation Criteria

Using relative arrival times to determine earthquake locations requires that we have measurements that connect all earthquakes with nearby seismicity. This is straightforward for closely spaced earthquakes with similar waveforms as there are ample nearby earthquakes to connect with. It becomes more problematic as waveforms become less similar, whether due to larger source separation, changes in earthquake mechanism, the effects of earth structure, finiteness of the source, or other effects. For events with less similar waveforms we either have to abandon attempts to locate them within the same framework, or we have to use less precise arrival time information, either cross correlation measurements that have larger errors, or catalog picks of waveform arrival time.

To obtain precise locations for the entire earthquake catalog, we seek to increase the number of quality correlation observations for as many events as possible. This can be achieved in two ways. First the correlation function itself can be made more robust to provide better measurements and to include all relevant data. Second, the parameters that are defined for the observation criteria may be relaxed so as to allow more measurements to be retained. Not every correlation measurement yields useful information for the relocation, especially in exhaustive measurements of all possible event pairs, and less reliable data needs to be excluded somehow. We have used two measures of similarity for this purpose:

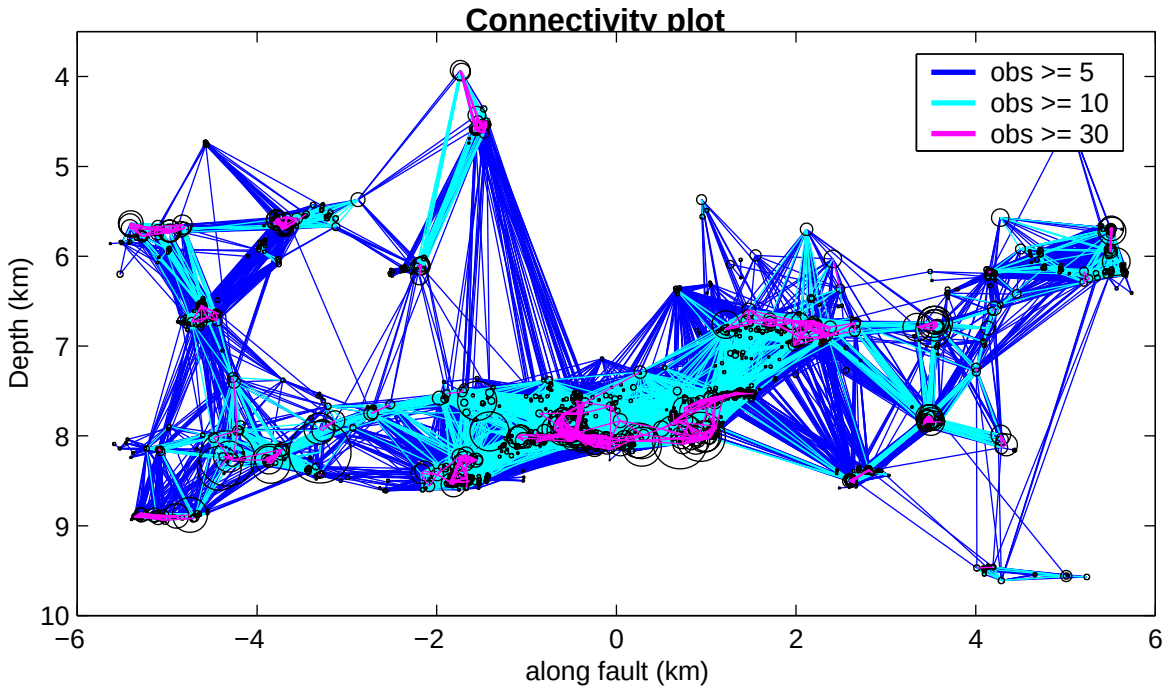

Figure 5.1: Constraint from correlation data with $mcoh > 90\%$ and $CC > 70\%$ for 1494 events on the Calaveras fault. If an event pair has more than 30 observations, it means more than 30 stations match the above criteria.

the normalized cross-correlation coefficient (CC) and the mean coherence ($mcoh$). Once we have iterated the linearized inversion process it is also possible to use the size of the residuals to identify unreliable measurements.

By including more observations and linking all events together, we can avoid the time consuming step of clustering events by waveform similarity. Figure 5.1 displays a connectivity plot for 1494 relocated events on the Calaveras Fault with the observation criteria of $mcoh > 90\%$ and $CC > 70\%$. The connections between earthquakes in this figure demonstrate that many of these events could be located simultaneously with correlation data alone. These events represent about 95% of the seismicity in the catalog for this section of fault. It is not clear, however, how reliable these measurements are compared with the catalog data over these length scales and range of magnitudes.

To address these issues we use the double-difference relocation program [*Waldhauser*

and Ellsworth, 2000] and analyze the residuals of the relative arrival times after relocation. The residuals convey information on how errors vary with the cross-correlation coefficient, mean coherence, inter- event distance, and magnitude. Equating the post-fit residuals with the size of the measurement and/or model error assumes that the model they are based on is the correct model. Whatever model we use, of course, is simply an estimate and hence the residuals may not directly reflect the true error. If repeated measurements can be made then it is possible to estimate the measurement error based on the replicated measurements. For us this can be achieved only for sequences of repeating earthquakes. More useful to us is the total error due to both measurement error and unmodeled velocity structure, which we approximate with the post-fit residuals for this over-determined problem.

Figure 5.2 illustrates the procedure for the 1494 events on the Calaveras Fault, comprising $\sim$ 300,000 S-wave residuals as a function of cross-correlation coefficient, CC. We observe more scatter for lower values of the cross correlation coefficient, which is apparent from the residual distribution for finite bins of CC shown in Figure 5.2a. Three probability distributions are fit to each case. The standard deviation of the Gaussian distribution, σ, is seen to decrease with increasing CC. In Figure 5.2b and 5.2c, quantile plots are displayed to compare how well each distribution describes the data for the $CC = 70\%$ and $CC = 99\%$ cases. The Weibull probability density function with two adjustable parameters explains both cases the best. The Gaussian distribution does an adequate job representing the 70% bin but for the 99% bin the histogram is best described by the exponential pdf. The strong energy in the tails suggests that minimizing the L1 norm may be more appropriate than least-squares at least for some data [*Shearer,* 1997]. We can evaluate the cross correlation data for a given value of CC relative to the catalog data using the standard deviation of the residuals. These standard deviations are also used to derive empirical weighting functions described in the last section.

An extremely nice feature of residual analysis is that it maps a variety of parameters each with different units or quantities being measured to a common system in which they can be compared directly. For instance the nominal cutoff of 90% often employed for CC and $mcoh$ has no direct meaning in terms of location. Residuals in units of milliseconds do. The two parameters measure different things and so the value of 90% is not expected to mean the same thing for both. The value also depends on our choice of frequency band

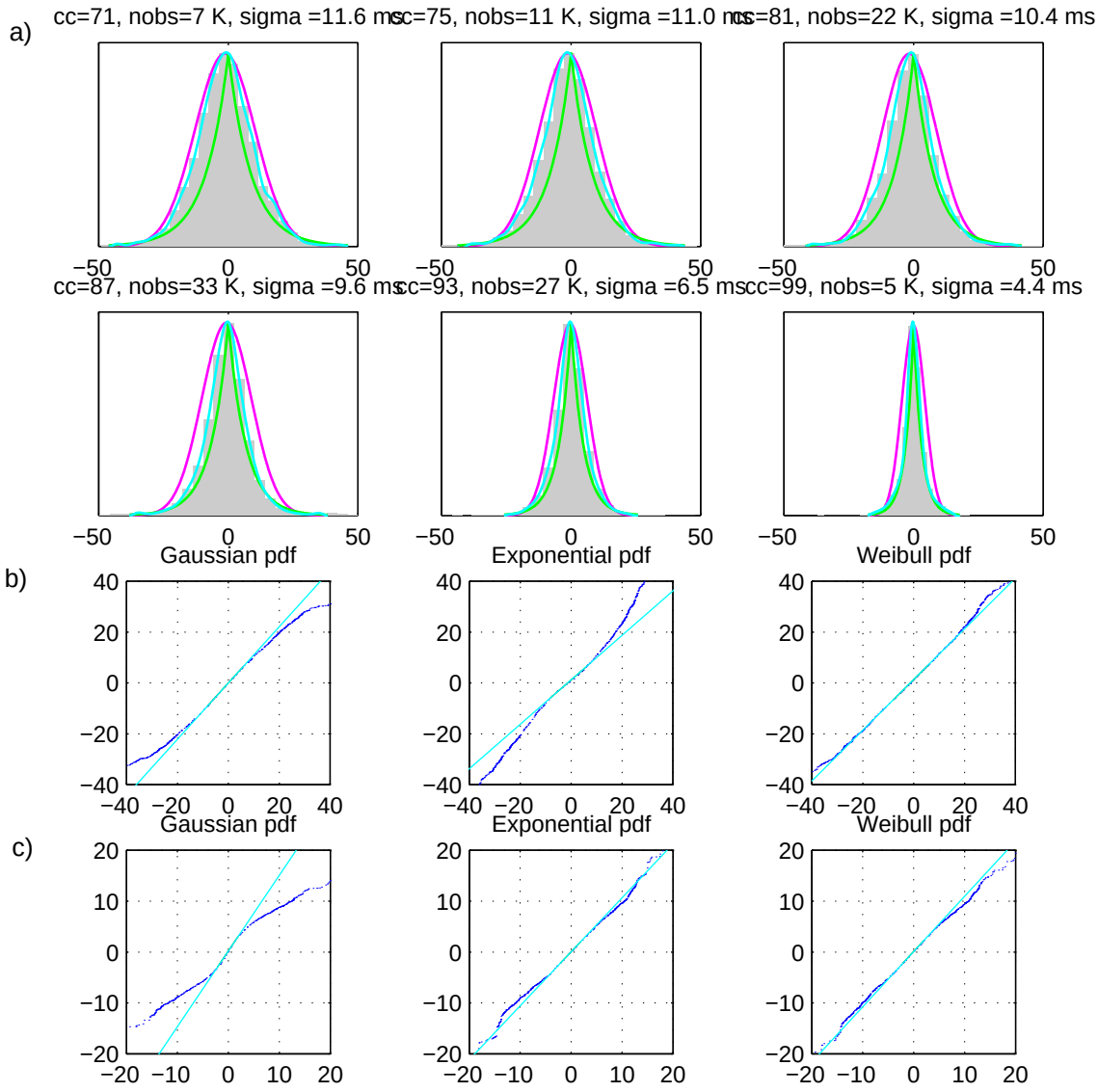

Figure 5.2: Analysis of $\sim$ 300,000 S-wave residuals from the Calaveras fault as a function of correlation coefficient. a) Histograms for finite bins of CC with Gaussian, exponential, and Weibull pdf fits for comparison. b) Quantile plots showing how well each distribution (y-axis) describes the data (x-axis) in ms for the $CC = 70\%$ bin. c) Same for $CC = 99\%$ bin.

and smoothing applied to the coherence.

Figure 5.3 shows the residuals and the number of observations as a function of both CC and $mcoh$. In figure 3b, the maximum ridge of the surface is shifted to the right of the diagonal line $CC = mcoh$. If the observations clustered around the diagonal, it would mean the two parameters are more or less equivalent measures of the quality of an arrival time measurement. The shift indicates that $mcoh$ is a less stringent parameter for quality control since the threshold value of 90% would accept 275,000 measurements as observations for $mcoh$ whereas CC would allow only 160,000. The residuals in Figure 5.3c are also lower than those in Figure 5.3d for the same values of the two parameters.

Figure 5.3 also shows that neither similarity measure captures only the most useful observations. We expect our most reliable measurements to have both high CC and $mcoh$, which is substantiated by the location residuals (Figure 5.3a). Many observations with 90% $mcoh$ also have 70% CC and therefore are somewhat suspect, which is reinforced by their higher post-fit residuals. We choose to employ a double selection criteria, $CC + mcoh = 170$, for winnowing the data in this case. If only a single parameter is desired, Figure 5.3c and 5.3d show that CC does a better job of discriminating quality observations. For example, at the 95% level, the standard deviations of the residuals are below 5 ms for CC, whereas for $mcoh$, they range from 2 to 16 ms. Applying both criteria, we obtain many more observations (600,000) than by applying either one alone. Previous studies have used more strict cut offs [e.g. *Got et al.*, 1994; *Dodge et al.*, 1995]. We find that those selection criteria are overly conservative and concentrate on the question of when the correlation measurements are better than the catalog phase data. We find that much lower thresholds may be applied for the purposes of earthquake location provided weighting of the observations is carefully done.

5.3 Inter-Event Distance

Correlation measurements, unlike measurements used in catalog locations, are known to degrade with inter-event separation distance. This is because waveform similarity breaks down due to increasingly different earth structure sensed by waves from more widely separated events. A Fresnel zone argument suggests that waveform similarity should hold at

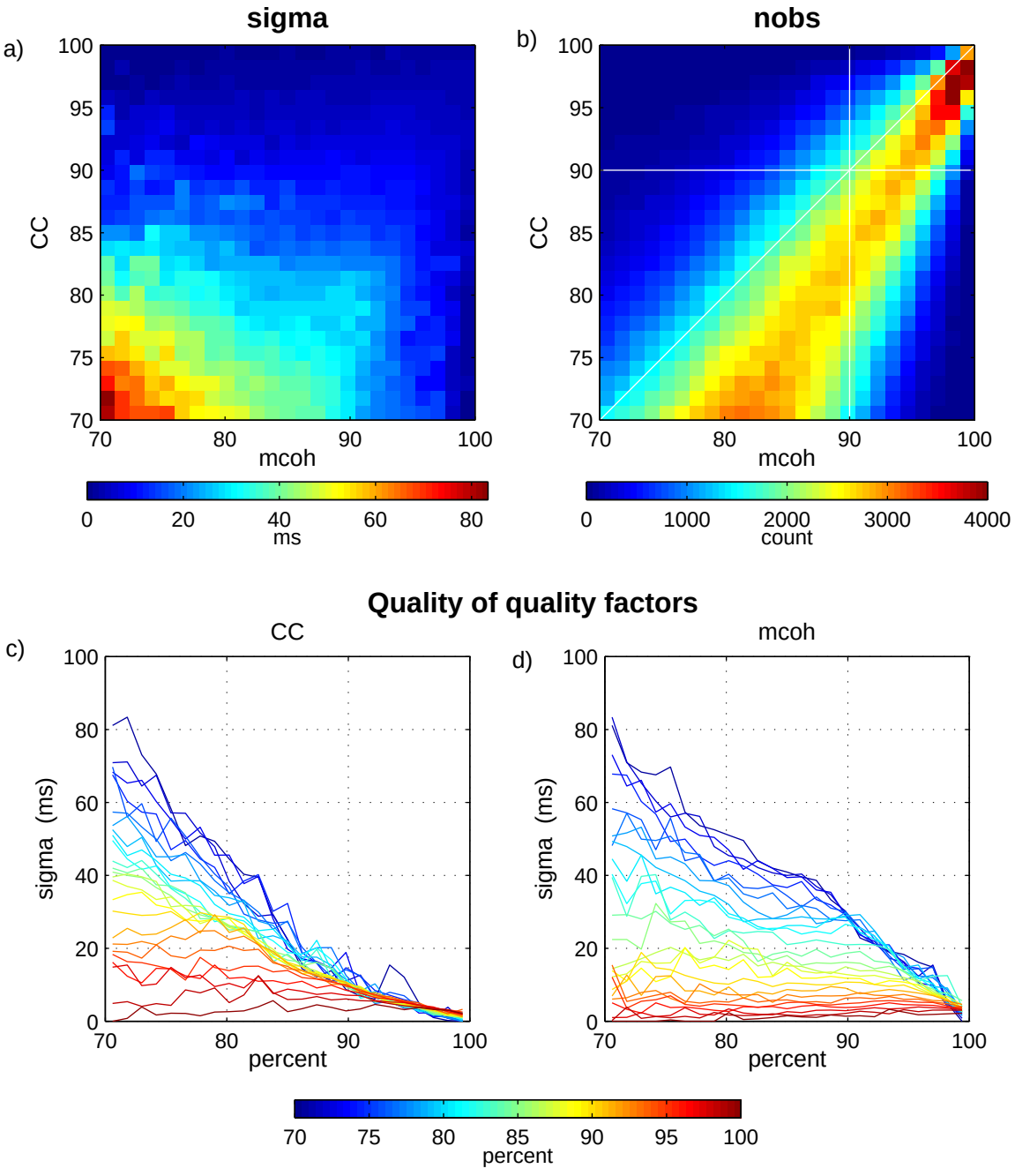

Figure 5.3: a) Standard deviation of residuals as a function of similarity parameters. b) Number of data measurements with corresponding similarity measurements. Several reference lines are shown to evaluate different observation criteria. c) and d) Same residual data represented with lines to show detail. Color scale represents the variation of the other similarity parameter (i.e. on the CC plot the colors reflect $mcoh$).

separation distances of up to a quarter of a wavelength [*Geller and Mueller,* 1980]. More uncertain is the reliability of correlation measurements for kilometer scale separation distances as seen on Figure 5.1.

To examine this question we consider the sub-horizontal streak of earthquakes from -1 to 1 km along-strike at 8 km depth. Figure 5.4 shows the location results for the streak using 299,642 identical observations (same event pairs and stations) with catalog phase data only (top) and correlation measurements only (bottom), where the effect of differing measurement error between the two data types is isolated by keeping other inversion parameters fixed. To ensure matching observations for the catalog data, we used correlations with $CC > 0$ and a relatively long window length of 256 samples (2.56 s). Qualitatively, the correlation data yields better results over these length scales (0-2 km) and for this range of magnitudes, 0 to 3.5. This is based on our intuition that it would be more unlikely for the location program to collapse small and large events alike onto a thin, linear feature and that more error in the data will increase the scatter in locations, especially depth. Part of the better apparent performance of the correlation measurements, however, may be attributable to the fact that while the overall dimension is up to 2 km, the events are connected to others with measurements taken over much smaller separation distances. Thus, many of the measurements are taken at much smaller inter-event distances where cross correlation measurements should work well.

Figure 5.5 examines the effect of event separation on the measurement error more quantitatively by plotting the median and standard deviation of the residuals as a function of separation distance. Each data point is computed for an equal number of residuals and extreme outliers are removed using ten times the median absolute residual as a cutoff. At zero separation distance the residuals reflect only measurement error for the two data types in the ideal case, which amounts to approximately 3 milliseconds for the correlation measurements and approximatly 11 milliseconds, or just over a sample, for the catalog measurements. The increase in residuals with distance for the catalog data is due to model error, i.e., uncertainty in the travel time predictions from the earth model. For the correlation data it is a combination of both increased measurement and increased model error with separation distance. Note, however, that the increase in residuals for the cross correlation data occurs very slowly with increasing event separation, at a rate comparable to the increase

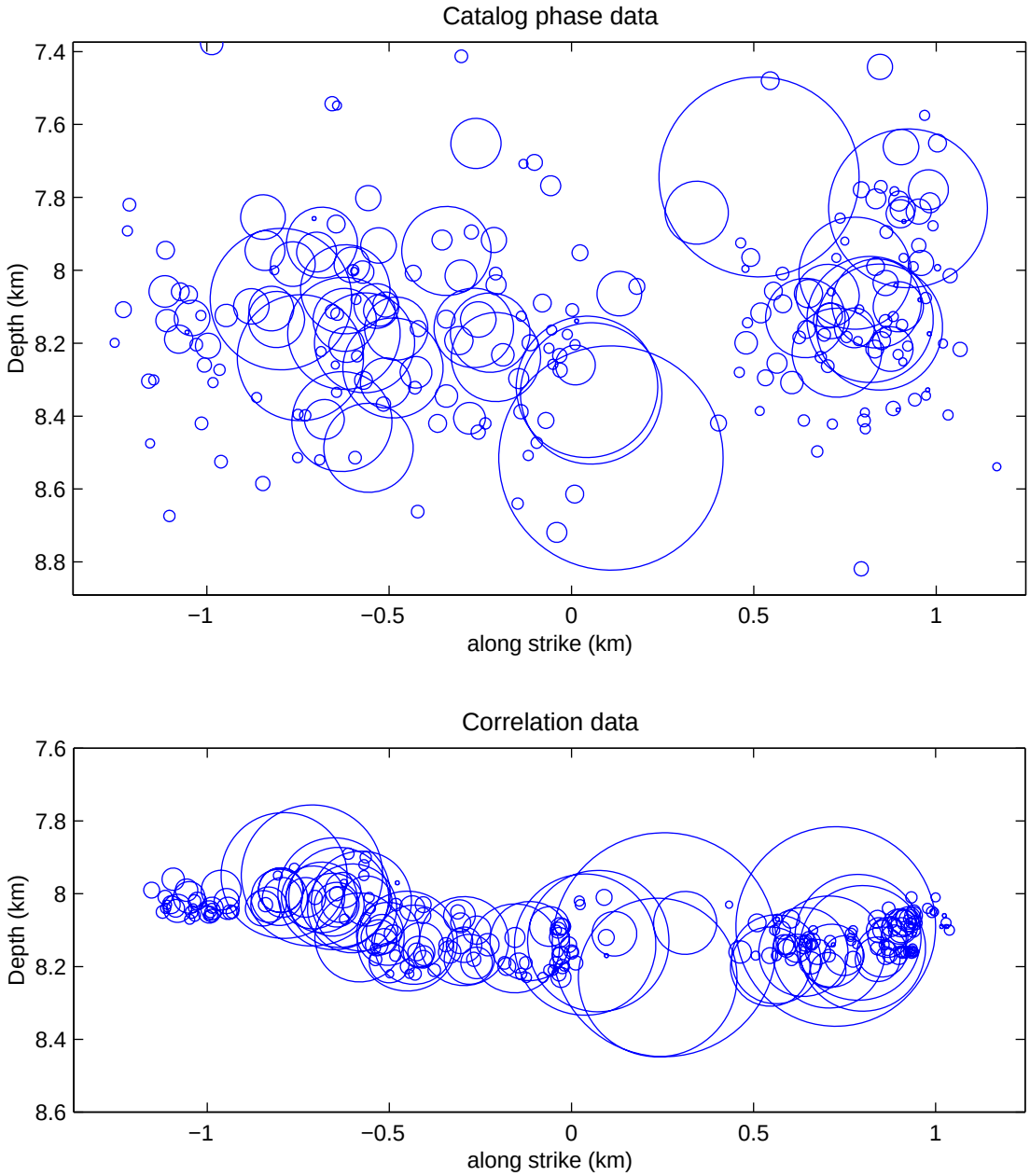

Figure 5.4: Comparison of measurement error between (top) catalog only and (bottom) correlation only data consisting of 299,642 identical observations (model error fixed) for the relocation of a 243 event streak.

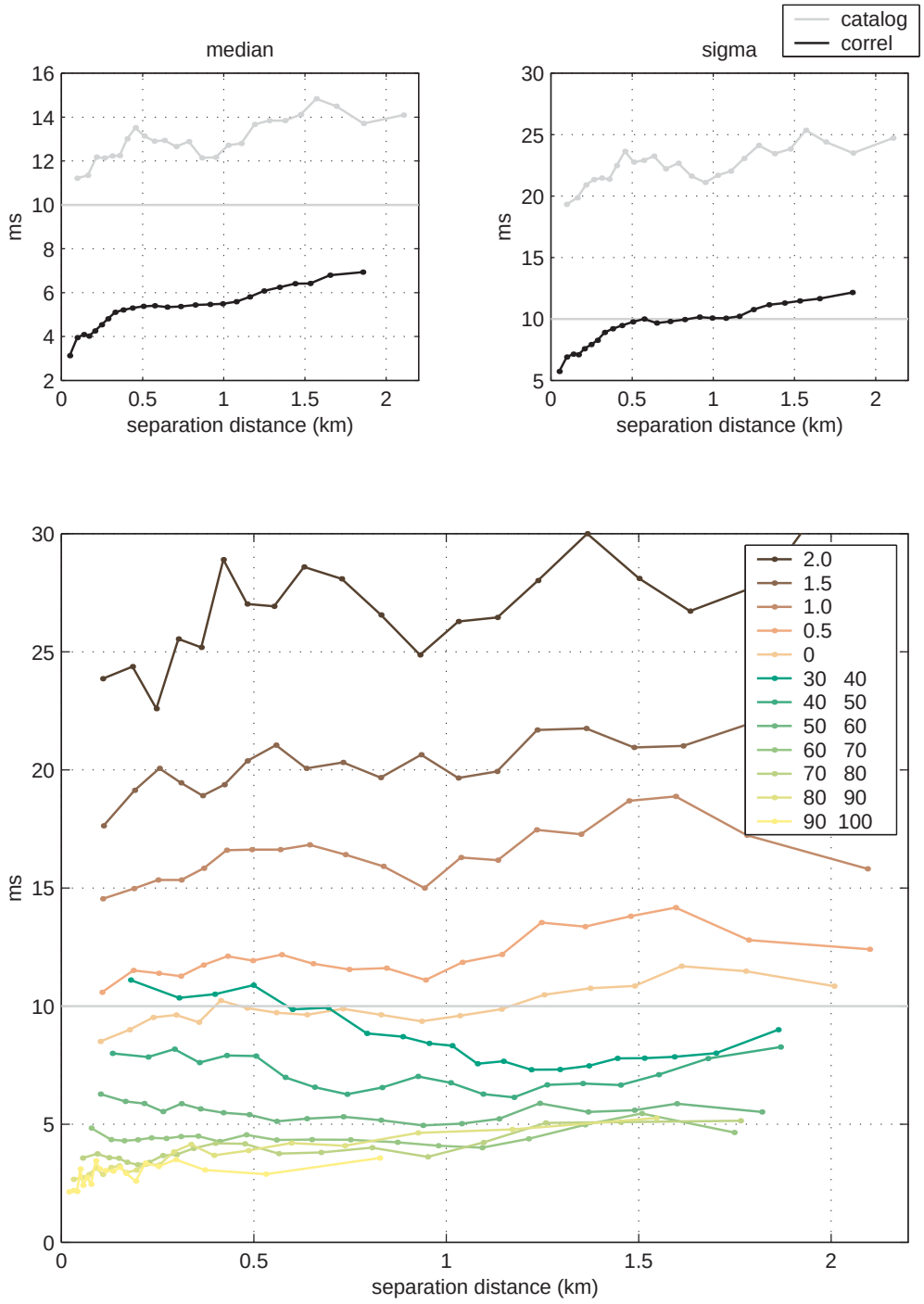

Figure 5.5: Statistics for 299,642 differential travel time residuals. a) Catalog and correlation median residuals shown as a function of interevent separation distance for 25 bins each containing 12 K obs. b) Same but for standard deviation. c) Median residuals separated according to quality. $CC > 0$ and catalog weights [0 3] were used in the inversion.

for the catalog data. This indicates that the increase in residuals for the cross correlation measurements is due primarily to unmodeled velocity structure rather than measurement error. The residuals from the correlation measurements for this streak are at least a factor of two smaller than the catalog data all the way out to 2 km separation distances. In fact as long as the correlation measurements remain below 10 ms, they will be better because precision of the catalog measurements is limited by the 10 ms sampling interval.

We also have some independent information on the quality of each observation for both the catalog and correlation data. For the catalog observations this information consists of a subjective quality measure ranging from good, 0, to poor, 3. For the differential measurements we are using, the average weight can assume half-integer values. For the correlation measurements we use the cross correlation coefficient as a measure of measurement quality. Figure 5.5c shows that this prior information largely predicts the level of error as expressed by the median residuals. At zero separation distance, the residuals reflect measurement error alone and indicate why the best correlation data ($90\% < CC < 100\%$, $\sim$ 2 ms) results in nearly an order of magnitude improvement over average catalog data (weight 1.5, $\sim$18 ms). It is surprising, however, that correlation measurements with CC's as low as 40% still appear better than the best catalog data for this streak.

The catalog residuals are computed from the locations obtained from Figure 5.4a and thus are the minimum possible from the least-squares estimate of locations for this data set. Ideally the residual analysis should be performed once one has obtained locations believed to be closer to the truer picture. The catalog residuals would therefore increase over those shown in figure 5 if computed from the more precise correlation-derived locations.

5.4 Magnitude

The same approach may be used to compare the errors in correlation and catalog data as a function of magnitude. In Figure 5.6a, correlation measurement quality decreases with increasing magnitude most likely due to clipping and possibly source-finiteness effects on the seismograms. For the catalog data, however, measurement quality increases slightly for the larger events because of a better signal to noise ratio. Still, the correlation data achieve subsample precision and thus outperform the catalog data for this range of magnitudes (0

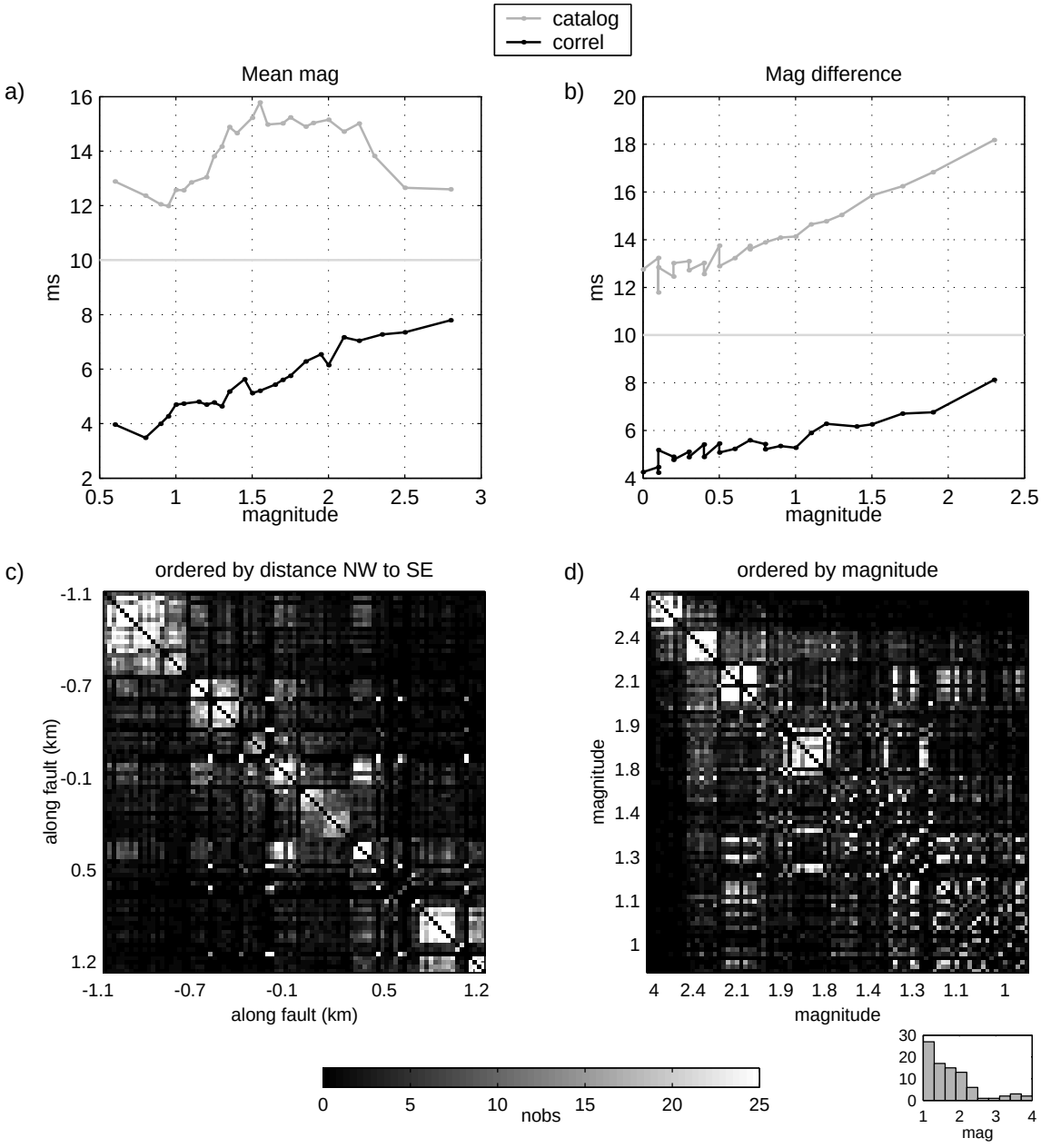

Figure 5.6: a) Median residuals for 25 bins each containing 12 K obs as a function of mean magnitude for the 299,642 event pairs. b) Median residuals as a function of magnitude difference. c) Observation matrix for 88 events at Bear valley ordered by distance along strike. d) Same matrix ordered by magnitude. The observation matrix is related to the correlation matrix, but refers to the number of stations that meet the observation criteria for each event pair.

to 3.5). Moreover, the correlation measurements are able to recover many small magnitude events for which catalog measurements were minimal. Although cross-correlation measurements remain precise for the larger events, the cross-correlation coefficient, which we use to assess measurement quality, decreases with increasing magnitude. This is primarily a result of waveform clipping. The measurements remain precise in part because clipping at these levels of ground motion is due to the limitations of the telemetry system, rather than true clipping of the sensor [*Ellsworth,* 1998]. Thus, some aspects of the true ground motion, such as the zero crossings, should be preserved with fidelity and hence may continue to give reliable measurements. The lower waveform similarity explains why we are able to use waveform cross correlation for larger events, while other studies have not. If quality thresholds are set too high, many useful observations will be discarded.

Figure 5.6b displays median residuals as a function of the difference in magnitude for the event pairs. We expect large events to not correlate as well with small events, which the trend reflects. The catalog residuals also increase with magnitude difference, suggesting that the different signal to noise ratios between the two events introduces error comparable, in a relative sense, to that introduced into the correlation measurements by waveform differences. We find that large events correlate well with other large events despite differences in location, clipping, and finite-fault effects. Evidence to this effect is also shown in Figure 5.6c, which shows observation matrices for a 2 km long streak of earthquakes at Bear Valley (Figure 5.10). The 88 events are ordered on both axes in 6c as function of distance along strike and in 6d as a function of magnitude. Over this distance scale, events larger than magnitude 1.8 seem to correlate best with other events of like magnitude rather than with smaller events in closer proximity. In fact, the large events often do not even have overlapping source areas. For smaller events, interevent distance seems to be the controlling factor (Figure 5.6d).

We've presented two lines of evidence: the sharpness of the relocation results and the lower residuals for correlation measurements, that indicate correlation data can be significantly better than catalog data over greater distance and magnitude ranges than previously assumed. The waveforms themselves support this conclusion. The top panel in Figure 5.7 shows the waveforms for the streak shown in Figure 5.4 at a nearby station (CCO) aligned according to the P-wave picks from the catalog. The bottom panel of Figure 5.7 shows the

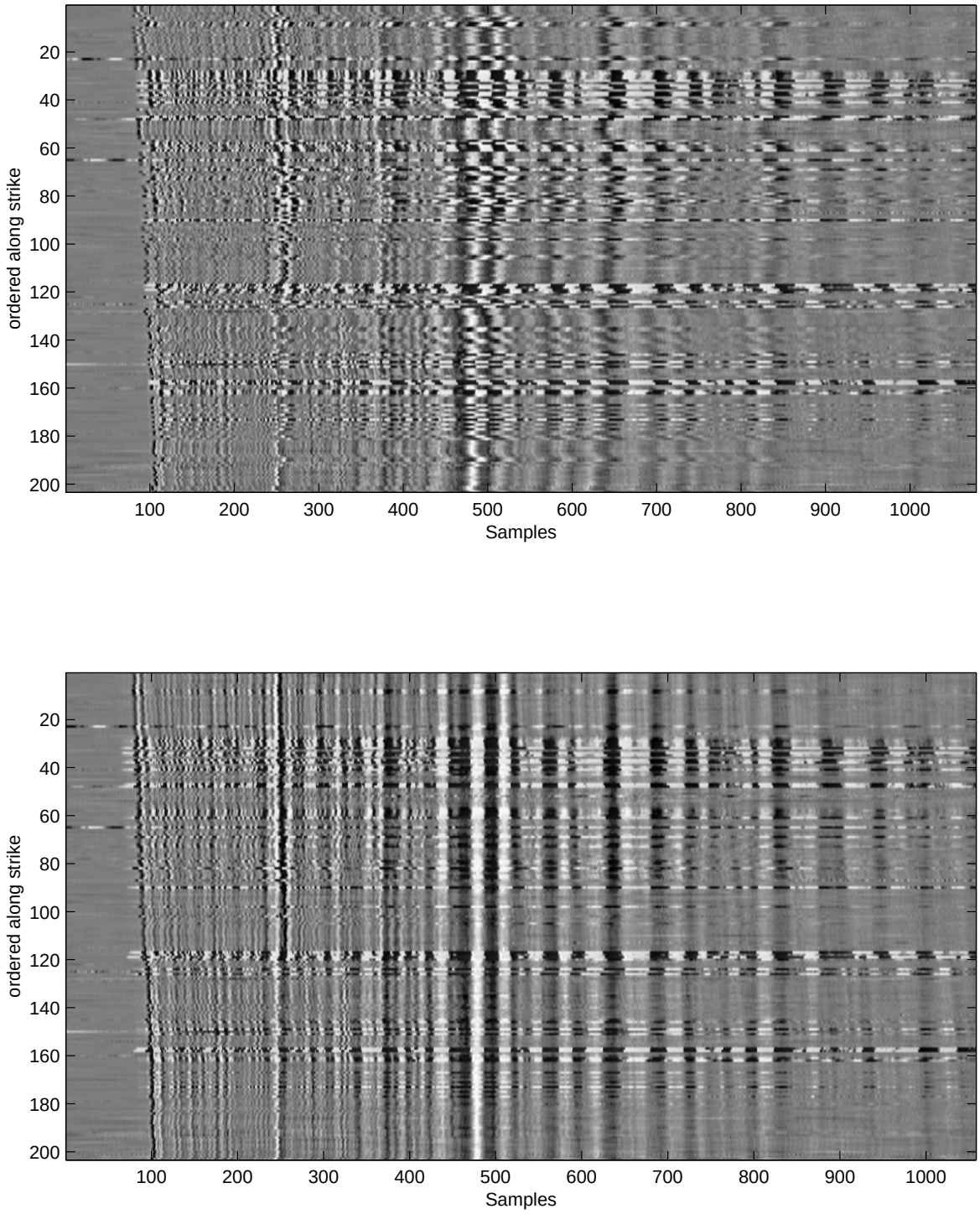

Figure 5.7: Unfiltered seismograms at station CCO for 2 km streak ordered by distance along strike in (top) aligned according catalog P-wave picks and in (bottom) aligned by cross-correlation.

same seismograms aligned by cross correlation on the high energy S-wave arrival between 450 to 520 samples. In Figure 5.7 the events are ordered along strike from NW to SE. This is essentially a receiver gather of the kind commonly used in controlled source seismology. The move-out for the P-wave coming in around 100 samples is consistent with the 2 km length of the streak. Several features are interesting to note. Visually, the similarity extends over the 2 km range for the correlation case and it is a clear improvement over the catalog data. The largest events appear as black and white horizontal bands because they are clipped, but since the phase is preserved even when clipped, the zero crossings allow the cross correlation to successfully align these events. The magnitude 3.5 event corresponds to trace 117. The seismograms from 30 to 42 correspond nicely and show magnitude 3's and 1's interspersed. Here is evidence that even events of substantially different magnitude correlate sufficiently well to align them properly. These same events on the catalog data plot (Fig. 5.7a) appear to have interchanging polarities from 450 to 520 samples because they are shifted by up to half a cycle, which is approximatly a 20 sample error. Because the correlation data is aligned to the nearest sample or even subsample precision, this translates to greater than an order of magnitude improvement in the measurement error.

5.5 Window Alignment

Our results were all computed with a fast, robust correlation program called CORREL designed to input directly into the HYPODD double-difference relocation code [*Waldhauser and Ellsworth*, 2000]; both freely available by request from the authors. In this and the next section we examine some details of our processing as compared to other methods. We also address some aspects of the relative merits of time domain vs. frequency domain techniques, optimal window lengths, and the need for clustering of waveforms by similarity. While the prior discussion will appeal to a more general audience interested in the relative quality of correlation vs. catalog data, below is more technically inclined intended for those who will actually implement these methods in their research in order that they may learn some of our success and avoid a few of the pitfalls that we encountered.

Typical standard errors for catalog hypocentral locations in Northern California range from hundreds of meters to a kilometer in the horizontal and about twice that in the vertical.

The largest error source is unmodeled earth structure, but errors in individual arrival time measurements are also important. Errors in the P-wave arrival time range from a sample up to as much as a second (100 samples). Ordinarily S-wave picks are not recorded, and thus the additional constraint on hypocentral locations they would provide, particularly in depth, is not realized. Since correlation techniques operate on a window of S-wave energy, it is not necessary for a discernible first break to be present. Thus, we are able to include many S-wave observations in our analysis.

Sub-sample precision for relative arrival time measurements for earthquakes with similar waveforms is by now well documented for both time domain and frequency domain methods [*Poupinet et al.,* 1984; *Frémont and Malone,* 1987; *Deichmann and Garcia-Fernandez,* 1992; *Got et al.,* 1994; *Aster and Rowe,* 2000]. Since this is so much smaller than catalog measurement errors, alignment to the nearest sample provides most of the benefit for improving earthquake locations. With subsample precision we would expect further adjustments only on the scale of meters to tens of meters (e.g. 10 ms $\times$ 6 km/sec = 60 m).

To make the correlation measurement we choose a window around the arrival times for a pair of events. Since these windows are most often referenced to the catalog pick or a theoretical arrival time, they can be grossly misaligned and contain only a fraction of the true similar waveform needed for a useful comparison. We have encountered this problem even for the nearly identical waveforms of repeating events, where a particularly noisy day at a station may obscure the first arrival for one of the events. For this reason, we need to be able to recover initial window offsets as large as approximately 1 sec. to maximize the total number of observations.

Figure 5.8 demonstrates how well three different correlation techniques recover lags up to 1 sec. The correlations are performed on identical seismograms (noise-free) using 256 sample windows for a variety of offsets. Figure 5.8a is computed from the cross-correlation function in the time domain obtained by the inverse Fourier transform of the cross spectrum. Figure 5.8b is the direct time domain cross-correlation function calculated by shifting and summing the seismograms one sample at a time. Figure 5.8c is the cross spectral phase technique introduced by *Poupinet et al.,* [1984]. The lag, dt, should be the diagonal line $y = x$, and the similarity measure should equal 100 percent for each run. The similarity measure used in the time domain is the correlation coefficient, CC, and in the

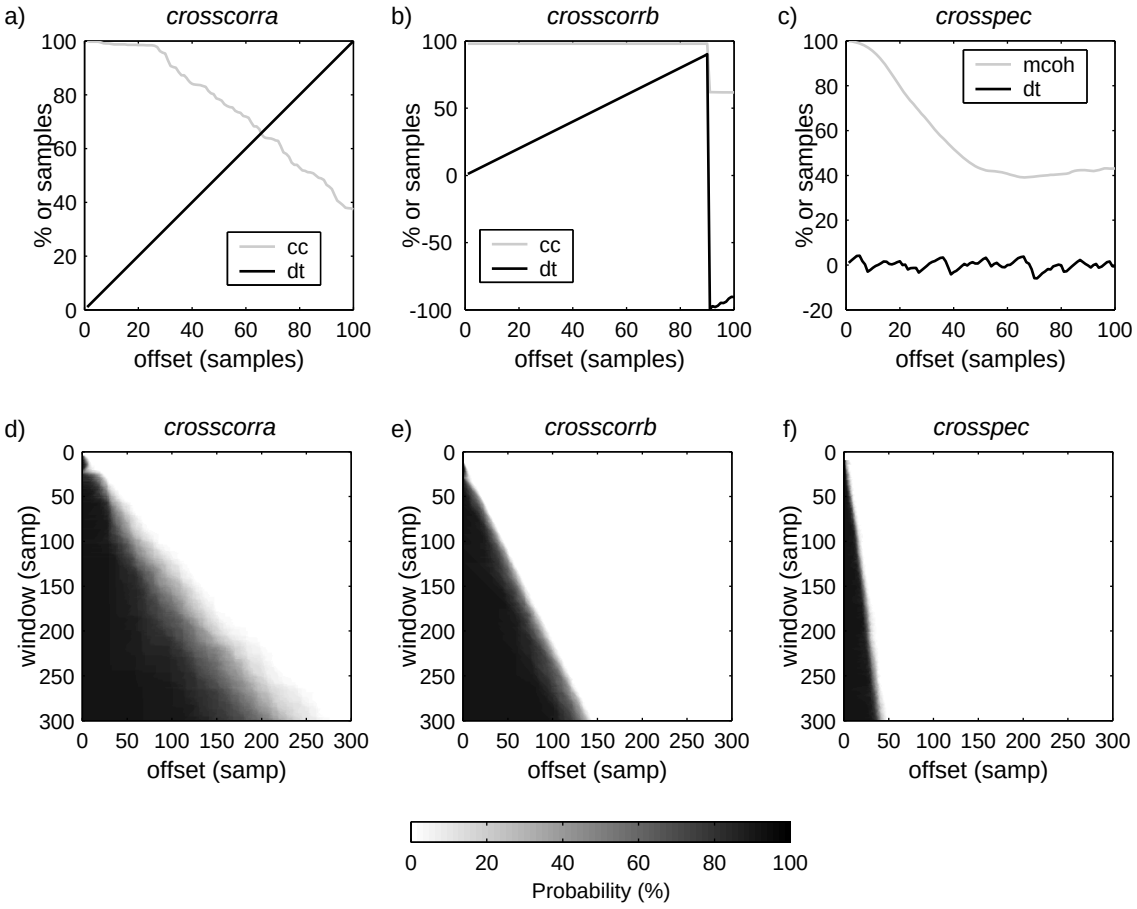

Figure 5.8: a) through c) Comparison of the performance for three different correlation methods as a function of offset (window is 256 samples). d) through f) show the probability of recovering window misalignments for various window lengths.

frequency domain is mean coherence, $mcoh$, over a limited frequency band from 2.5 to 12 Hz.

Figure 5.8a demonstrates that the first approach is the most robust and reliable for recovering lags up to one second. The other time domain function, $crosscorrb$, shown in Figure 5.8b performs well also, but breaks down after 90 samples. The frequency domain method in Figure 5.8c only recovers misalignments in this case up to 8 samples. Based on these tests we chose $crosscorra$ to align seismograms to the nearest sample. For large-scale relocations such as the Calaveras fault that involved $\sim$ 8000 events and 108 million correlation measurements, computational speed can be an issue [*Schaff et al.*, 2001]. The

direct time-domain calculation is faster for shorter windows because it does not involve taking the Fourier transform as in the other two methods. $Crosscorrb$, however, is sensitive to another parameter — the maximum lag to search over, which tends to degrade performance and is not as robust. $Crosscorra$ can do in one iteration what the other techniques may need to do in several steps requiring more complex coding. For the sake of simplicity, reliability, and the potential to recover the largest offsets, the technique in $crosscorra$ offers the best solution and the most observations.

Our cross correlation measurement algorithm is able to perform about one million correlations per hour on our somewhat dated Sun Ultra 1, which for the Calaveras fault translated to around four and a half days of continous processing. If we wanted to correlate all $\sim 250,000$ events in Northern California with reasonable distance thresholds, it would require only about ten times as much time or about 45 days. The correlation problem is easily parallelized by dividing into groups of events and stations. Therefore building a complete correlation database is manageable in a few weeks with currrent technology provided the data is available locally. The main bottleneck in our processing is in acquiring the waveform data.

The above tests are shown only for a single seismogram and for a window length of 256 samples. The maximum offset that can be recovered is a function of window length. To determine this we measure the breakdown point over a range of window lengths for a hundred different seismograms. Figures 5.8d, 5.8e, and 5.8f show these results for each method displayed as the probability of recovering the correct lag time as a function of window length. Again, we see that $crosscorra$ outperforms the others. To obtain the best measure in the frequency domain it is important for the seismograms to already be aligned close to the nearest samples. As an example, for the two time domain techniques we have a 90% probability of recovering all offsets up to in 5.8d) 50% and in 5.8e) 40% as large as the window length while for the frequency domain technique in 5.8f) the offsets could not be much larger than 13% of the window length. Depending on the expected errors in the catalog picks, these relations can be used to determine the minimum window length required. We've chosen to use window lengths of 256 samples for the window alignment portion of the correlation code in order to retrieve as many offsets as possible and therefore obtain the most observations for the relocation. Longer windows have the added benefit

that they have a greater chance of capturing coherent energy if the waveforms are initially misaligned or if the signal to noise ratio is low.

As described earlier, cross correlation-coefficients and mean coherence above 90% mean the seismograms are extremely similar and the delay measurements are usually reliable. Note, however, that CC for $crosscorra$ degrades much sooner than the delay measurement even though the seismograms are identical. $Crosscorrb$, on the other hand, remains at the correct value of 100% until the break down point for the delay. While the delay computed by $crosscorra$ may be correct even up to large offsets, the corresponding measure of quality could be lower than some set threshold (90% for example) and subsequently be rejected as an observation for the relocation. To ensure all good observations are retained, we perform an additional correlation to get a more reliable measure of waveform similarity. Since the windows are aligned to the nearest sample, we use the faster $crosscorrb$ and search over a small range of lags ($\pm$ 5 samples). At this stage we also fit a parabola near the peak cross-correlation function to achieve final subsample precision.

5.6 Subsample Precision

Very small scale features of seismicity such as repeating events and streaks have been resolved by applying subsample measurement techniques to waveform data [*Poupinet et al.*, 1984; *Deichmann and Garcia-Fernandez,* 1992; *Schaff et al.*, 1998; *Rubin et al.*, 1999; *Waldhauser et al.,* 1999]. Fitting a line to the phase of the cross spectrum allows subsample precision in that the slope of the line is not constrained to give a slope that corresponds to an integer offset of samples. In the time domain, we achieve sub-sample precision by fitting a parabola to 5 points around the peak of the cross-correlation function and use the analytic expression for its peak and center to obtain the inter-sample lag and correlation coefficient [*Deichmann and Garcia-Fernandez,* 1992; *Dodge et al.*, 1995].

An advantage of the frequency domain technique is that the line fit to the phase of the cross spectrum can be weighted by the coherence so that the slope measurement is influenced by the freqency components that have the greatest similarity [*Poupinet et al.*, 1984]. This may be a useful feature for events that are separated by larger distances, which are most likely dissimilar at high frequencies, but might be coherent at low frequencies.

Another advantage of the frequency domain technique is that error estimates are easily obtained for the delay measurement [*Got et al.,* 1994; *Aster and Rowe,* 2000]. A disadvantage is that for short window lengths the frequency resolution is limited since there are fewer points in the cross spectrum. To extract more information for short windows, a multi-taper approach can be implemented [*Aster and Rowe,* 2000].

A significant drawback of the cross spectral approach is the need to unwrap phase for large offsets. Figure 5.9 illustrates the difficulty with an example. The top panel depicts two waveforms from a cluster of repeating events aligned to the nearest sample. Because they are co-located and have nearly identical waveforms at many other stations, the differences are primarily due to noise in the data. Figure 5.9b displays the coherence, which is high between 3 and 6 Hz, but takes a large dip around 1.5 Hz. Figure 5.9c shows the phase of the cross spectrum along with the line fit constrained to go through the origin according to equation $\phi(f) = 2\pi dtf$. The slope then gives us an appropriate subsample lag, dt. If we had chosen to unwrap the phase first, as in Figure 5.9d, a very different result is obtained because the erratic behavior at 1.5 Hz is interpreted as a 2π jump. The line fit through the origin then returns a slope that is grossly in error.

It is known that low frequencies are likely to be unreliable for small earthquake recordings. We tried fitting the slope without the constraint on the intercept (since we only need to recover the slope for our measurement). This approach provides a better result in this case (1.5 samples) as shown in Figure 5.9d. The above scenarios were created for a window length of 220 samples. If we repeat the procedure for a window length of 226 and unwrap the phase, the result changes. Not fixing the intercept, in this case, results in a negative slope and a delay estimate with significant error (-9.7 samples).

In summary, unwrapping the phase can be problematic. If the seismograms are aligned to the nearest sample, however, unwrapping is not needed and excellent results can be obtained whether or not the line fit is constrained through the origin. It is only when the frequency domain method is used to recover large lags that the problem arises.

The need to unwrap the phase is one reason the frequency domain technique breaks down for misalignments greater than a few samples. The results in Figure 5.8c, however, were carried out for a noise-free case, and most likely fail due to the smoothing of complex

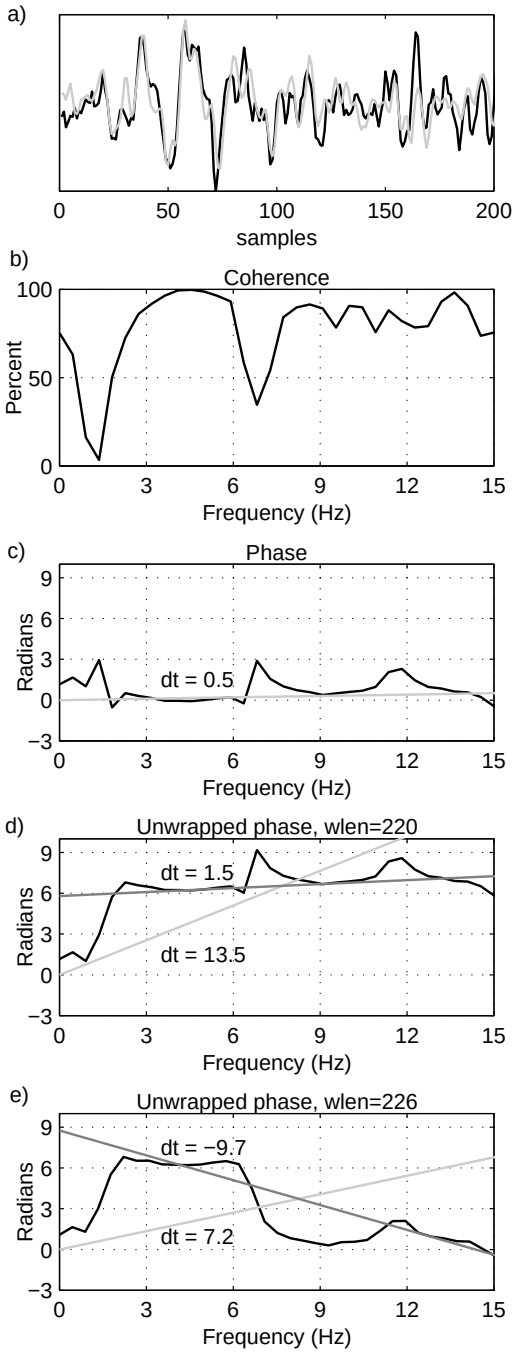

Figure 5.9: Illustrating with the waveforms of two repeats at a noisy station the dilemma whether to unwrap the phase and/or to force the line fit through the origin.

numbers over the frequency range [*Jenkins and Watts,* 1968]. In the complex plane, the average of several numbers with rapidly increasing phase will tend toward zero and therefore will not reflect the appropriate higher phase values for greater offsets.

The time domain function, $crosscorrb$, has several advantages for the second stage in our processing where we try to obtain sub-sample precision. A cosine taper is not necessary and therefore short windows are more easily handled. It is faster especially for windows lengths other than powers of 2. Negative correlations are also easily distinguished from positive, which occurs on occasion when station polarities are reversed, inadvertently. Disadvantages are that some assumptions are made as to the shape of the cross-correlation function around the maximum when a parabola or sinc function is used. Another disadvantage is that error estimates are less easily obtained. *Bokelmann* [1992] has devised a sum-of-squares approach, however, to estimate errors for the time domain measurement.

Figure 5.10 compares locations derived from time and frequency domain measurements for the final subsample measurement. The 88 events shown are seismicity at Bear Valley on the creeping section of the central San Andreas fault. Identical observations are used for each set of locations. The results are quite similar. Histograms of time differences and location differences are shown in Figure 5.10c and 5.10d. The rms misfit of the residuals from the time domain location (.0109 s) is slightly smaller than that for the frequency domain (.0115 s). We have found a similar trend for other data. At the subsample level, then, interpolation of the cross-correlation function and the cross spectral approach appear to perform approximately equally well in terms of location.

For regions with large inter-event separation distances we do not notice a substantial difference in the locations obtained by the two measurement methods suggesting that the benefits of coherence weighting at low frequencies are not realized. The time domain techniques are our preferred method overall because of the speed and robustness considerations summarized in Table 5.2. The basic algorithm we use applies a simple 2-step procedure: aligns to the nearest sample with $crosscorra$ and then measure to subsample precision and calculate a more accurate cross correlation coefficient with $crosscorrb$.

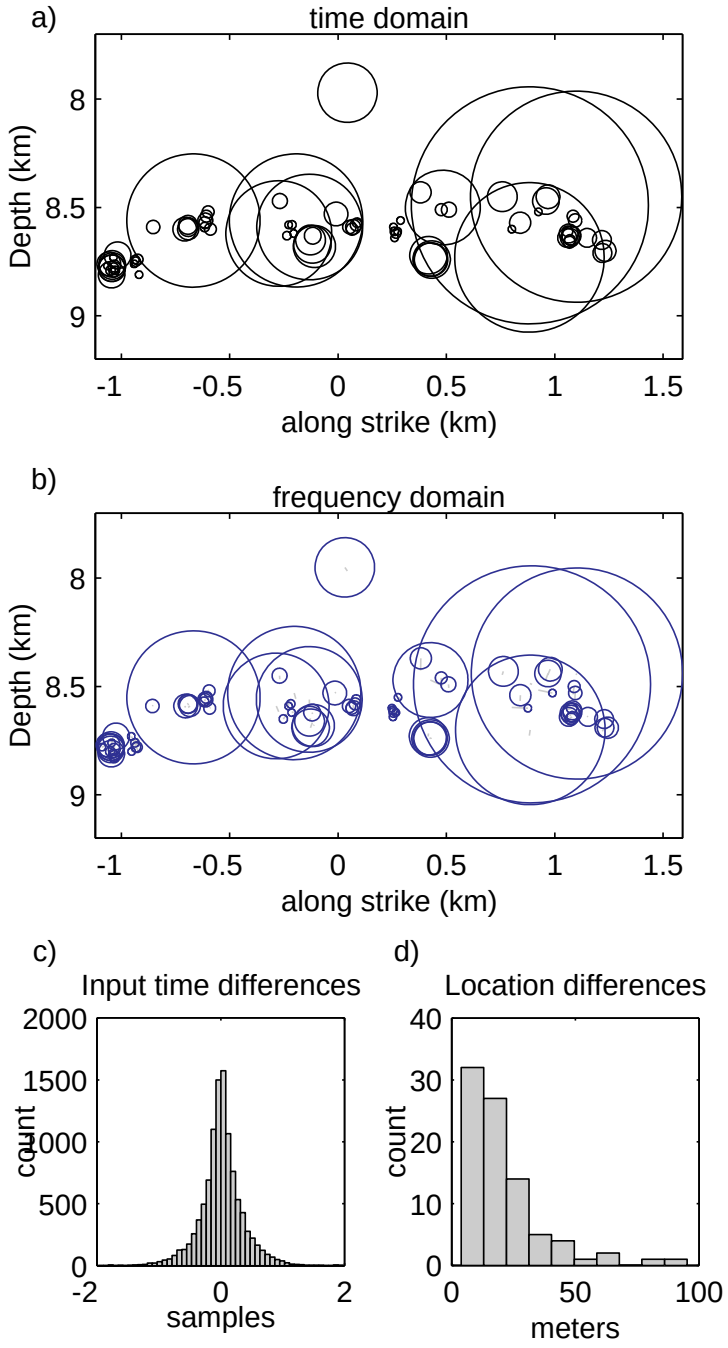

Figure 5.10: Streak of 88 events at Bear valley located to final subsample precision with a) $crosscorrb$ and b) $crosspec$. Barely visible gray lines denote vector changes in hypocenter locations. c) Input differential travel times largely agree within a sample. d) Location differences on the order of 10's of meters.

Test	$crosscorra$	$crosscorrb$	$crosspec$
Large offsets	best	good	nearest samples
$CC/mcoh$	fair	best	nearest samples
Speed	slow (one-step)	fastest	slowest (many steps)
Robustness	best	fair	least
Error estimate	yes	yes	yes
Subsample	good	good	good

Table 5.2: Three correlation functions rated

5.7 Absolute vs. Differential Travel Times

Most earthquake location algorithms use absolute arrival time data because that is the natural measurement for locating a single earthquake and seismic network operations usually locate one event at a time; however, there are advantages to considering more than one earthquake at a time and these advantages have been exploited, for example, by joint hypocentral determination [e.g. *Pujol*, 1988]. More recently earthquake location programs have used relative arrival time data [*Fréchet,* 1985; *Got et al.,* 1994; *Waldhauser and Ellsworth,* 2000]. Differential arrival times are the natural output of cross correlation measurements that compare pairs of events and it is possible to measure relative arrival times much more accurately than absolute arrival times.

The double-difference method [*Waldhauser and Ellsworth*, 2000] is the most recently developed location technique based on arrival time differences. Several advantages are apparent with the double difference approach. Forming arrival time differences removes much of the model error for similar ray paths. Each observation can be thought of as having, in a sense, its own station correction to account for unknown earth structure. This approach is much better at removing the effect of unmodeled velocity structure over a large source volume than a single station correction and achieves a similar effect to source-specific station corrections [*Richards-Dinger and Shearer,* 2000]. By itself this approach can account for an order of magnitude reduction in location errors.

For purposes of earthquake location, inverting the correlation data output directly appears superior to having an intermediate inversion to convert to absolute arrival times. Absolute arrival times adjusted by correlation, however, still have their utility for many other

areas of investigation, travel time tomography for instance. They also facilitate plotting the aligned seismograms for visual inspection of how well correlation is improving things as in Figure 5.7 [*Dodge et al.,* 1995; *Aster and Rowe,* 2000].

Relative delay times obtained by correlation for a set of similar waveforms are never perfectly consistent (i.e., $\Delta t_{12} + \Delta t_{23} = \Delta t_{13}$). However, linear least-squares can be used to invert for the best fitting absolute time adjustments, T_i [*VanDecar and Crosson,* 1990].

$$\begin{pmatrix} 1 & -1 & 0 & 0 \\ 1 & 0 & -1 & 0 \\ 1 & 0 & 0 & -1 \\ 0 & 1 & -1 & 0 \\ 0 & 1 & 0 & -1 \\ 0 & 0 & 1 & -1 \\ 1 & 1 & 1 & 1 \end{pmatrix} \begin{pmatrix} T_1 \\ T_2 \\ T_3 \\ T_4 \end{pmatrix} = \begin{pmatrix} \Delta t_{12} \\ \Delta t_{13} \\ \Delta t_{14} \\ \Delta t_{23} \\ \Delta t_{24} \\ \Delta t_{34} \\ 0 \end{pmatrix} \tag{5.1}$$

Variations on this technique have been used to incorporate relative arrival time measurements into earthquake location techniques that use absolute arrival times [*Deichmann and Garcia-Fernandez,* 1992; *Dodge et al.,* 1995; *Shearer,* 1997; *Aster and Rowe,* 2000]. This approach has been successful in relocating groups of earthquakes that are close to each other and have similar waveforms. Figure 5.11 illustrates some of the drawbacks, however, even for clusters of repeating events. The middle panel shows the cross-correlation matrix for a multiplet composed of thirteen events and the bottom panel displays the same matrix, but with a cut-off of $CC < 90\%$ as an observation criteria. The absolute travel time inversion now becomes singular because the last 3 events are not tied to any of the other events by observations. Therefore all the observations from this station must be discarded, unless smaller clusters could be defined. We know from other stations that the waveforms are very similar and in fact have enough observations to determine that these earthquakes are co-located. A major advantage of the double difference technique is that no clustering is needed and hence all the observations can be included.

The identification of appropriate clusters and finding a way of tying them together has been one of the most challenging aspects of using cross correlation data for large-scale earthquake relocation. Once clusters are defined, there must be some means of connecting them to one another in order to recover the whole picture of seismicity. Two possible approaches are: dividing the seismicity into similar groups on a station by station basis

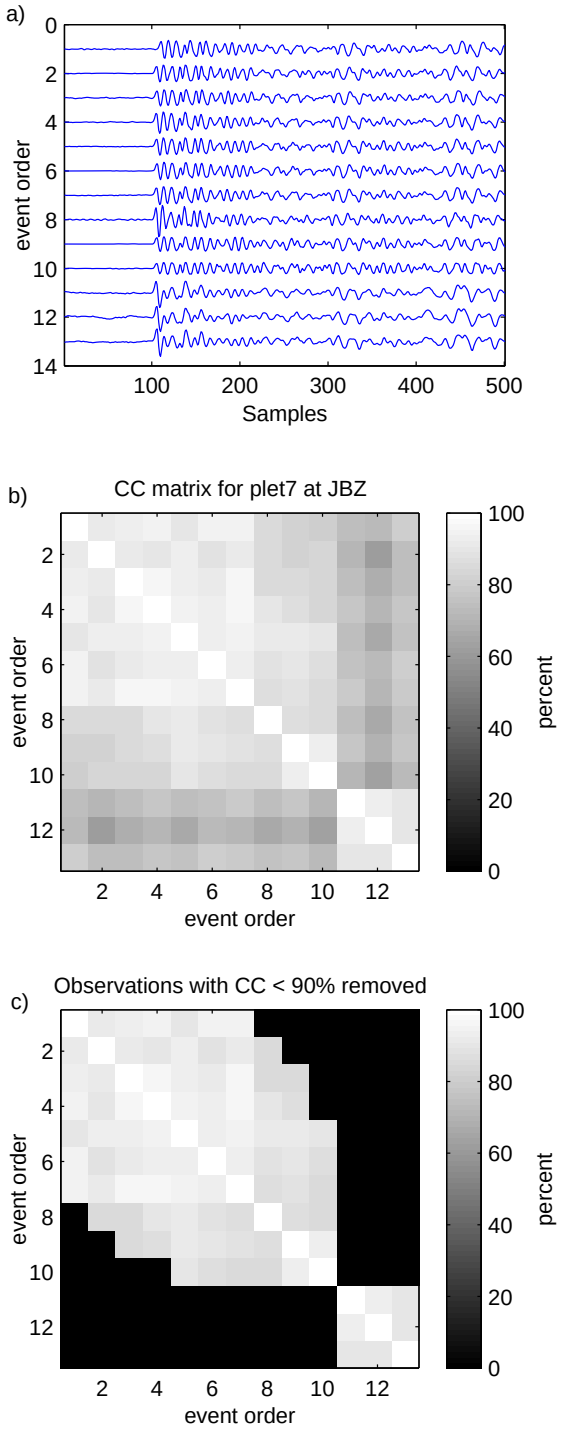

Figure 5.11: a) 13 repeating events at station JBZ b) Cross-correlation matrix c) Same matrix with $CC < 90\%$ removed which becomes singular in the absolute arrival time inversion.

[*Aster and Scott,* 1993; *Dodge et al.,* 1995; *Shearer,* 1997; *Aster and Rowe,* 2000] and isolating clusters of events for all stations [*Poupinet et al.,* 1984; *Got et al.,* 1994; *Rubin et al.,* 1999]. For the latter method, only relative arrival times are used and so the problems of singularity are avoided. All that remains is determining the relative locations of the clusters with respect to each other. This is usually done by fixing them at the barycenter of their catalog locations, which has the potential for inaccuracies. If absolute arrival time data is required by the location program, the first option is usually used. The clusters will vary significantly from station to station because waveform similarity is site specific (Figure 5.12) and any set threshold based on a measure of coherence will break things into groups differently.

A shortcoming of defining clusters at each station is that while the relative times will be precise within each cluster, the reference picks that define the absolute time for each clusters might not be. Reference picks are those from which all the relative times are measured (see Figure 5.14a). In the location process the reference picks will control the relative positions between clusters and tie them together in the inversion. This creates biased inconsistencies in the measurements, which are evident as a multi-modal distribution of residuals for a station (Figure 5.13a). Since the least-squares estimate assumes the statistics are Gaussian, this has the effect of degrading the precision of the locations (Figure 5.13b). The median of each mode more or less represents the misfit of each reference pick. Several approaches have been used to deal with this problem including: manual picking of the reference time, taking the median of absolute travel times, a group correction for each cluster, and picking the time on stacked traces. Nevertheless, whatever error remains in determining the reference picks will map into the final locations in an undesireable way.

Aside from determining reliable reference picks, defining the clusters themselves is a difficult problem. Various clustering algorithms that have been used for this include: nearest neighbor, dendograms, and self-defined criteria [*Aster and Scott,* 1993; *Got et al.,* 1994; *Dodge et al.,* 1995; *Aster and Rowe,* 2000; *Waldhauser and Ellsworth,* 2000]. Clustering is non-trivial because the degree of waveform similarity and distribution of seismicity often do not separate into distinct groups in an obvious way. Indeed, clustering has even proven challenging when working with repeating events — the simplest of all clusters.

We experimented with one idea to avoid clustering when absolute travel time data was

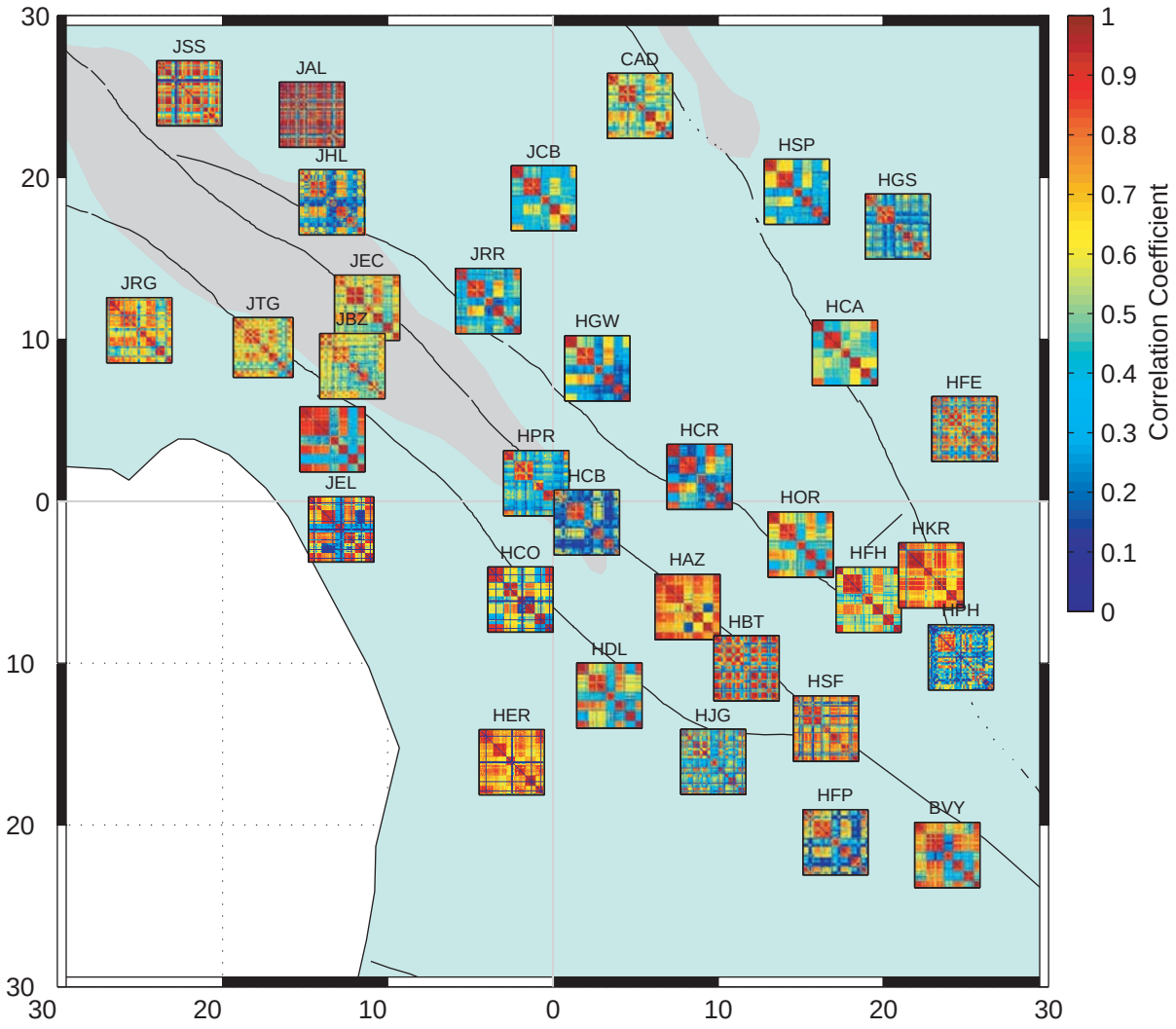

Figure 5.12: Spatial variability for the CC matrix of 7 multiplet clusters located at the origin. Multiplets can be discerned as highly similar blocks along the diagonal, at HGW for example. This variation poses a challenge in determining a fixed threshold for the observation criteria applied across all stations. Axes in km.

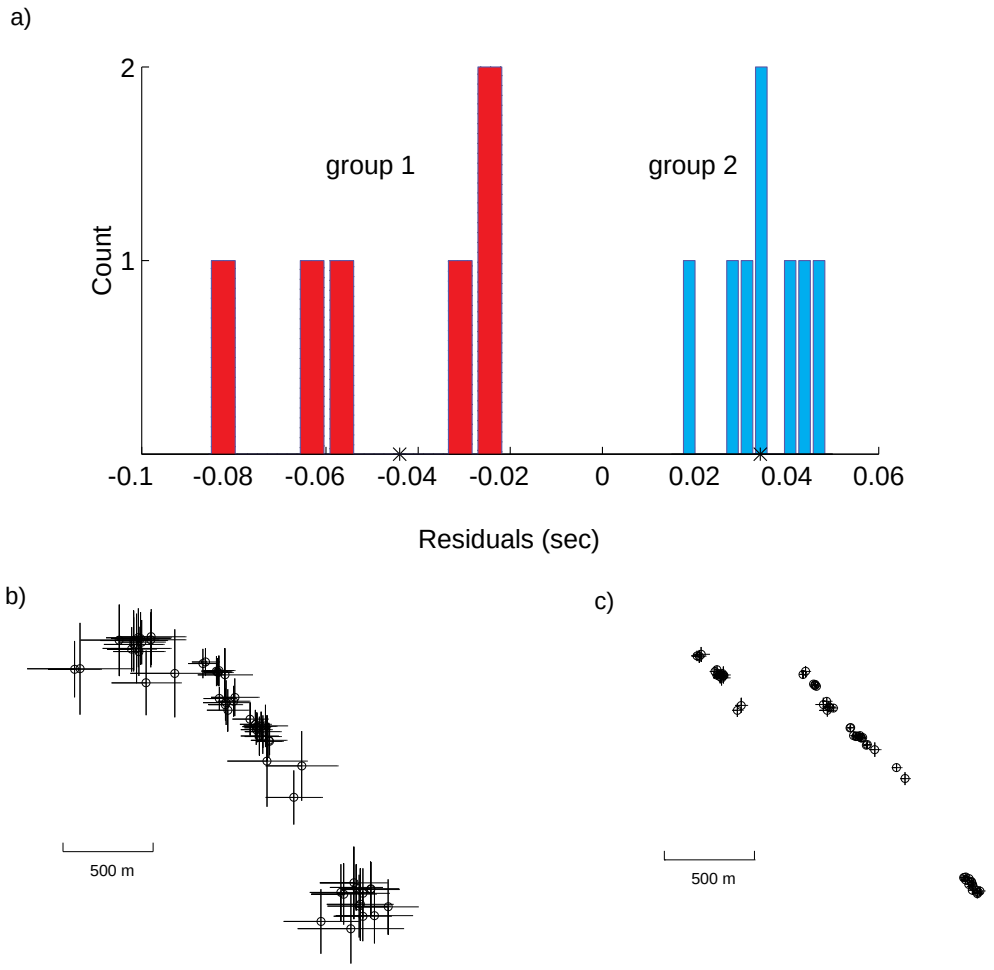

Figure 5.13: a) Clusters defined at stations often become manifested as a separation of absolute travel time residuals after relocation. The error in the reference pick can be approximated as the median of the residuals (asterisk) for each group. b) The deviance of this multi-modal distribution from Gaussian statistics and forced inconsistencies due to the reference pick can cause the least-squares inversion to perform even worse than if clustering had not been applied. c) Implementation of a group correction (separate station correction for each group) improves the fine-scale location but also introduces the usual ambiguity of station corrections not knowing the relative position of groups with respect to each other.

required. The thought was to just use all the data at a station for the absolute travel time inversion and to allow weighting by similarity to account for erroneous measurements. Figure 5.14 displays the scenario. Suppose two multiplets are recorded at a station shown in the top panel. The correlation matrix for all the events is shown in Figure 5.14b which reveals high similarity within clusters, but low correlation between clusters. Our theory was to weight by cross-correlation coefficient so that the most similar events are most heavily adjusted and the less coherent measurements the least. However, looking at the delay matrix, we discover that all the delays which correspond to the low coherence areas ($CC \sim 50\%$) are consistent and even though the weight is low, the delays can all be fit well since the waveforms are so similar. In other words, biases are introduced with very little error. Figure 5.14a was adjusted by equation. 5.1 using a 50 sample window. Because of the opposite polarities, the two troughs become aligned causing the first breaks to be offset by almost 10 samples in accordance with the delay matrix. The relative times within the multiplets are precise, but the effect is similar to creating clusters, anyway, only with a more severe misalignment in the reference picks.

One additional drawback to the absolute arrival time inversion (eq. 5.1) is that it assumes closure. In other words, for 3 events the lags behave according to $\Delta t_{12} + \Delta t_{23} = \Delta t_{13}$. This relation may not be valid for events arranged linearly on a long streak. For example, the first event may not correlate well with the last event 2 km away. Similarly it may not be true even for repeating events if the waveforms change over time, due to a velocity change, coherence break down, or attenuation [*Schaff and Beroza.*, 2001; *Baisch and Bokelmann*, 2001]. Figure 5.15a displays the effects of the M 7.1 Loma Prieta earthquake on the waveforms of a repeating event sequence on the San Andreas Fault ordered in time. Note that the pre-Loma Prieta event is most similar to event number 14, the last event in the sequence and is least similar to the event that immediately follows it. This is an effect of time-dependent velocity structure distorting the waveform due to the effects of the 1989 Loma Prieta earthquake [*Schaff and Beroza.*, 2001]. A similar problem exists for streaks except the time order axis would reflect distance instead. Weighting by the correlation matrix in Figure 5.15b will suppress the effect somewhat, but the assumption upon which equation 5.1 is built is still invalid. With the double difference technique, no closure is assumed so poor or inconsistent measurements can easily be removed.

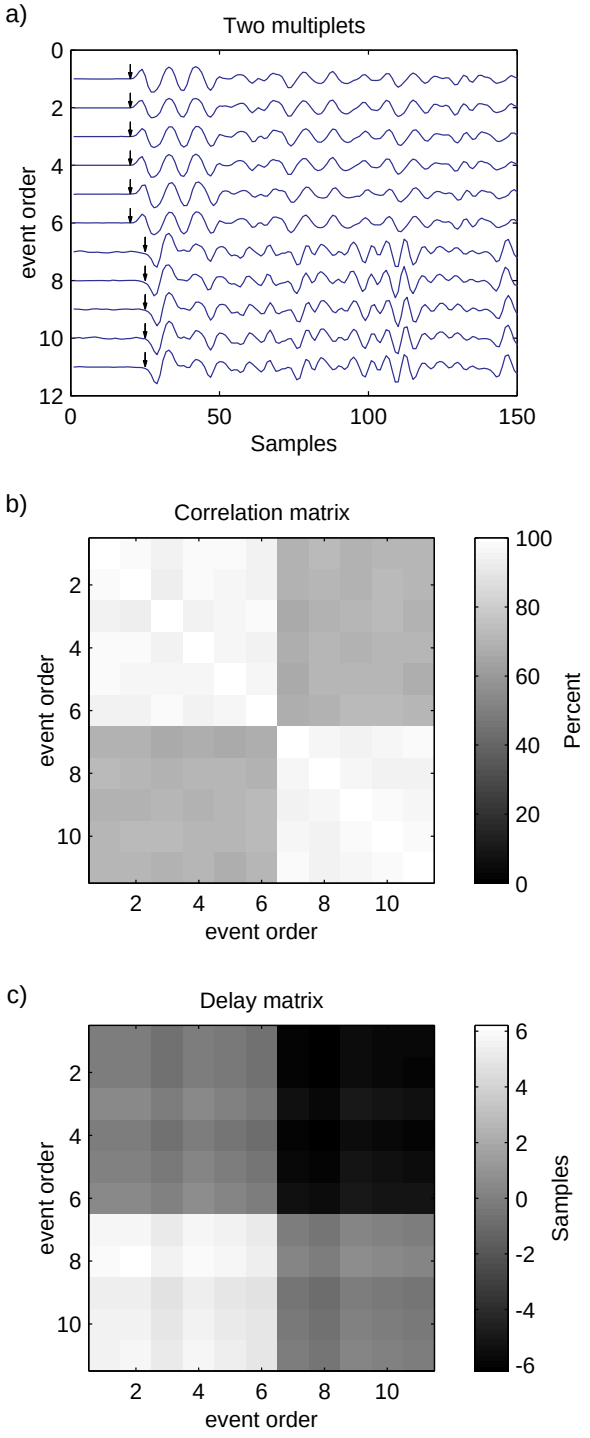

Figure 5.14: a) Two multiplet clusters aligned by correlation, true arrival times reflected by arrows. b) Corresponding CC matrix and c) delay matrix. Similarity between clusters is low but delays are all consistent. The peaks and troughs from the opposite polarities have become aligned causing a biased half-cycle offset between the two clusters.

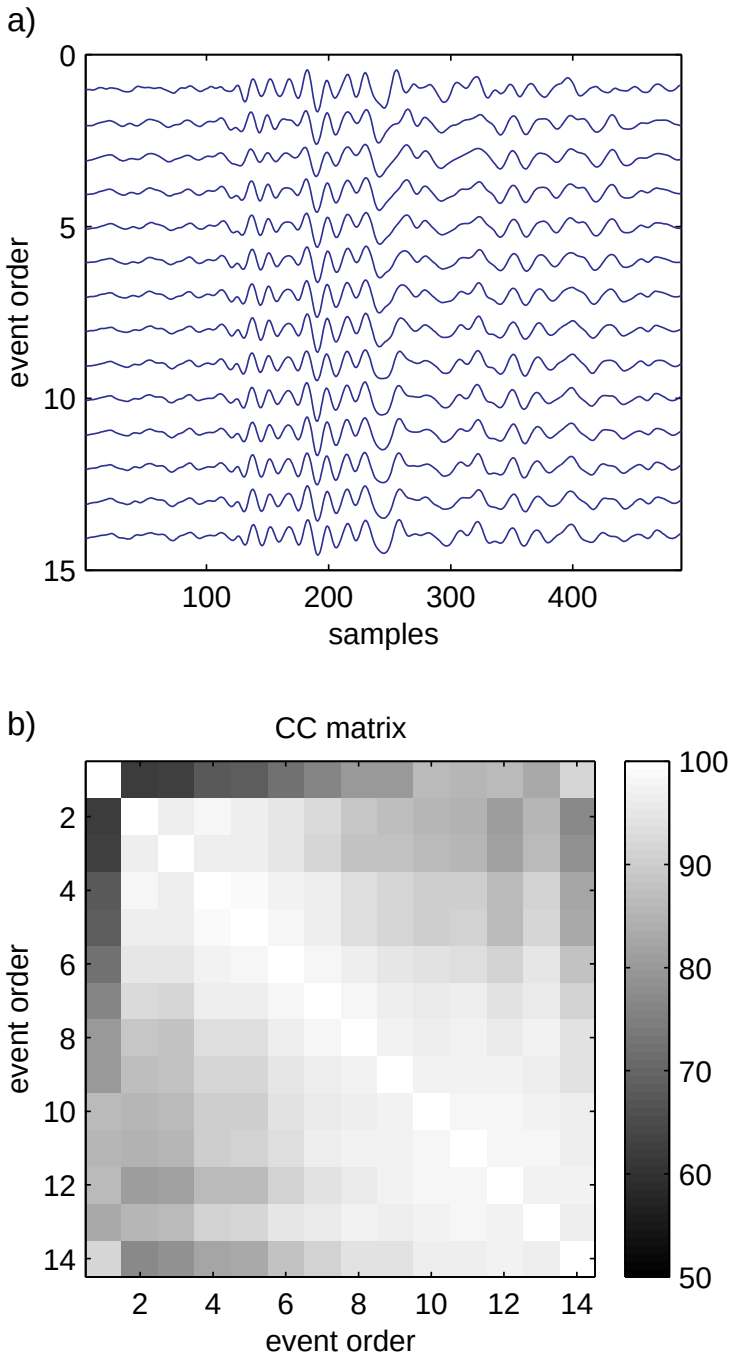

Figure 5.15: Absolute arrival time inversion implies closure. a) Waveforms for a repeating event cluster that have been altered by the 1989 Loma Prieta earthquake. b) CC matrix reveals the first event (pre-Loma Prieta) is more similar to the last events. Events 2-5 after Loma Prieta, conversely, are more similar to each other.

Absolute	Differential
advantages	*disadvantages*
plotting waveforms	too cumbersome to plot
existing routines (i.e. tomography)	new routines to create
less memory	lots of memory required
———	———
disadvantages	*advantages*
clustering necessary	no clustering required
intermediate inversion	native format for correlation data
correlated errors	more Gaussian-type statistics
singular matricies	better conditioned problem
loss of redundancy	best multiplets favored because more obs
closure implied	closure not necessary
affected by model error	eliminates more model error

Table 5.3: Comparisons on the implementation of correlation data for location purposes

A variety of issues have been addressed regarding the use of correlation data to obtain absolute arrival times. These have been explored with relocation purposes in mind, but would apply to other fields of study as well. For instance, devising a relative arrival time tomography code to accept the native format for correlation data would most likely provide superior results, as well, since it would avoid the same difficulties of clustering, ill-conditioned inversions, and closure assumptions described here. To date, whenever absolute arrival times have been required from correlation measurements, clustering has been performed [*Deichmann and Garcia-Fernandez,* 1992; *Dodge et al.,* 1995; *Shearer,* 1997; *Schaff et al.,* 1998; *Aster and Rowe,* 2000].

An important consideration is that converting differential times to absolute eliminates much of the data redundancy which the inversion relies on for success. The number of possible correlation measurements for n events goes as $n(n-1)/2$. To simultaneously locate two multiplets with the double difference technique, one containing 20 events and the other 3 events, the first cluster may have as many as 190 observations per station, whereas the second cluster can have at most 3 observations per station. Therefore assuming equal weights, the inversion will give greater preference to larger, presumably more important clusters due solely to the amount of data reflected by the 190:3 ratio. If absolute arrival

times are used, this observation ratio would only be 20:3 and so smaller structures will have greater influence on the solution. Table 5.3 summarizes our findings on the pros and cons of absolute vs. differential travel times from how correlation data has commonly been applied for the purposes of location.

If the end result desired is improved earthquake locations, the main focus of this paper, we find it best to directly invert the data with no intermediate steps. Accurate absolute arrival times are an end in themselves, however, having many uses for plotting and aligning waveforms for subsequent calculations such as magnitude, duration, etc. For these cases it would be nice to have a robust absolute arrival time inversion as well.

To accomplish this, we may follow the location approach and simultaneously invert both correlation and catalog phase data by modifying equation 5.1,

$$\begin{pmatrix} 1 & 0 & 0 & 0 \\ 0 & 1 & 0 & 0 \\ 0 & 0 & 1 & 0 \\ 0 & 0 & 0 & 1 \\ 1 & -1 & 0 & 0 \\ 1 & 0 & -1 & 0 \\ 1 & 0 & 0 & -1 \\ 0 & 1 & -1 & 0 \\ 0 & 1 & 0 & -1 \\ 0 & 0 & 1 & -1 \\ 1 & 1 & 1 & 1 \end{pmatrix} \begin{pmatrix} T_1 \\ T_2 \\ T_3 \\ T_4 \end{pmatrix} = \begin{pmatrix} t_1 \\ t_2 \\ t_3 \\ t_4 \\ \Delta t_{12} \\ \Delta t_{13} \\ \Delta t_{14} \\ \Delta t_{23} \\ \Delta t_{24} \\ \Delta t_{34} \\ 0 \end{pmatrix} \tag{5.2}$$

where the appended t_i data points are catalog arrival times with the mean removed. This formulation has been presented before [*Deichmann and Garcia-Fernandez,* 1992; *Shearer,* 1997] and reduces the need for clustering; although it was still applied in practice. *Shearer* [1997] noted this set-up will tend to be dominated by correlation data, even if weighted equally to the catalog data, simply due to the sheer number of observations. If consistent biases exist as in Figure 5.14, this will be a problem because the catalog data will have little influence.

We propose that the optimal solution may be to use the original form in equation 5.1 and compute catalog travel time differences in addition to the correlation measurements. This will reduce the observation ratio bias and make relative weighting between the two data types more straight forward as described in section 5.9. The inversion will be better conditioned — another limitation in Table 5.3. Because catalog measurements are unaffected by

large interevent separations, the closure assumption is also now valid.

A point worth emphasizing is that all correlation techniques will inherently introduce unwanted correlated errors. This is the main message of Figure 5.14. Groups of similar events will have biased delay measurements with respect to other groups of similar events. If one interconnecting event pair measurement is high they will all be high, even if the associated coherences are low. The reason is because of the high degree of similarity within the groups. The larger the groups, the stronger and more consistent the biases controlling the relative position of the clusters. If the coherence is low, the corresponding lags, dt, should have more error and be randomly distributed about the true measurement for the inversion to work well. Instead the measurements have few inconsistencies and may have a strong bias depending on the shape of the waveforms. Correlated errors will always be present when considering large location problems such as in Figure 5.1. It will never be possible to design perfect thresholds for clustering to eliminate all these effects. Increased redundancy by including more stations will tend to counteract individual station biases. These statements are universal considerations for all inversions that desire to use correlation data — earthquake location, absolute arrival time, tomography, etc.

5.8 Window length

Cross correlation measurements are fundamentally different from first-break measurements of arrival time in that they align a packet of energy of some duration. Thus, an important parameter in measuring arrival times using cross correlation is the window length over which the seismograms are aligned. For earthquake location, it is desirable to have more observations for better constraint and redundancy. It is commonly seen that the number of observations increases with decreasing window length for a set observation threshold. Figure 5.16 compares 869,345 identical observations for different window lengths for the streak in Figure 5.4. There is a strong tendency towards higher CC's for shorter window lengths.

The arrival times for all the window lengths shown are very similar, to within one or two samples. In terms of residuals and the sharpness of the relocations, the longest window length of 256 samples gives the best results for the streak. It implies that the slowness

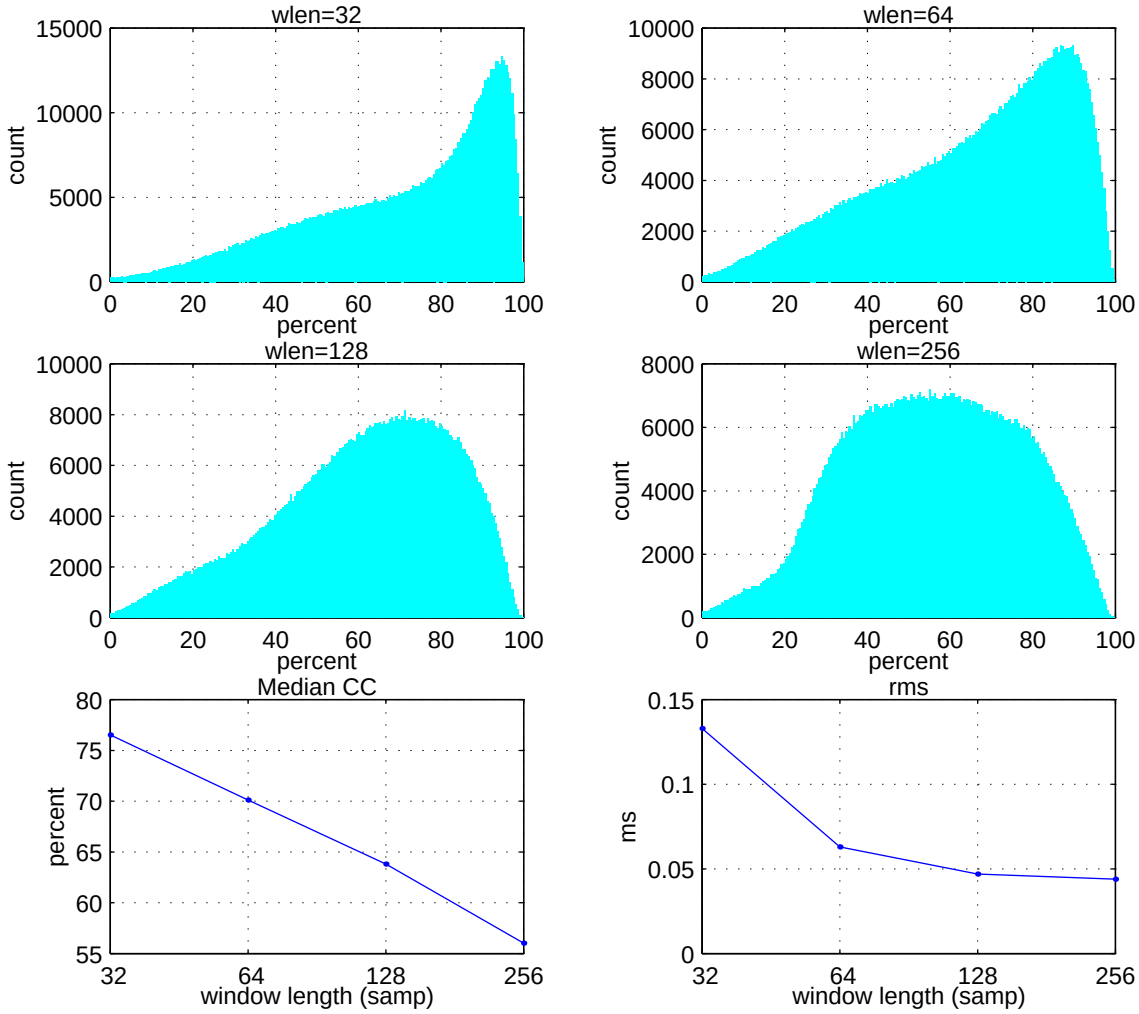

Figure 5.16: 869,345 identical observations for different window lengths. Longest windows (256 samples) have lower CC's but produce sharper locations and better rms misfit for the streak.

of the arrivals at the source are similar to that of the direct arrival over the entire window considered. This was previously observed for a similar data set and suggests that much of the early coda is generated near the site rather than over a larger scattering volume [*Dodge*, 1997]. If the observation criteria thresholds are too high many of these better measurements may be discarded. Longer windows seem to work best overall for the regions we've looked at, although this may be biased because of the abundance of repeats and streaks for these

areas. A more detailed residual analysis, as presented earlier, could help to determine if longer windows are valuable for greater separation distances as well.

5.9 Empirical Weighting Functions

Residual analysis has provided useful guidance in choosing appropriate thresholds from the similarity measures, CC and $mcoh$, and helped to justify the application of correlation data out to larger separation distances and higher magnitudes. The residuals can also be used to develop empirical weighting functions for the location algorithm. Standard deviations of the residuals are a natural choice for weighted least-squares. There are two types of weightings currently used in the double-difference location algorithm: a priori and dynamic [*Waldhauser and Ellsworth,* 2000]. We use the similarity measurement as prior information on data quality and convert it to a weighting factor. The standard deviations obtained as a function of CC in Figure 5.2b may be used for this purpose (Figure 5.17a). Figure 5.17c compares an empirical weighting function calculated from Figure 5.17a as σ^{-2} (normalized from 0 to 1) with a linear and the commonly used Hannan-Thomson weighting function. Since this function is likely to vary from region to region, a new one may be derived by first iterating on the locations, performing the residual analysis, and then relocating with a more apropriate weighting for that area.

The second type of weighting is dynamically applied during the inversion. Perhaps the most important is the inverse weighting with interevent distance. For catalog phase data, this is essential to accommodate model error over larger separations. It is also important, however, for correlation data since the delay measurement itself becomes less accurate with distance. Figures 5.17b and 5.17d illustrate the conversion of residuals for both catalog and correlation data to distance weighting functions for the events in Figure 5.1. As noted earlier, residual analysis has the nice feature that it can compare very different things in a common frame of reference. Mapping everything to the units of time allows for direct, quantitative comparisons. For example, Figure 5.17b suggests that catalog weight zero and correlation data should probably be given equal weight at about 500 meters separation distance. At zero separation, the correlation measurements should have 5 times higher weight than the best catalog measurements. Beyond 2 kilometers the correlation data is

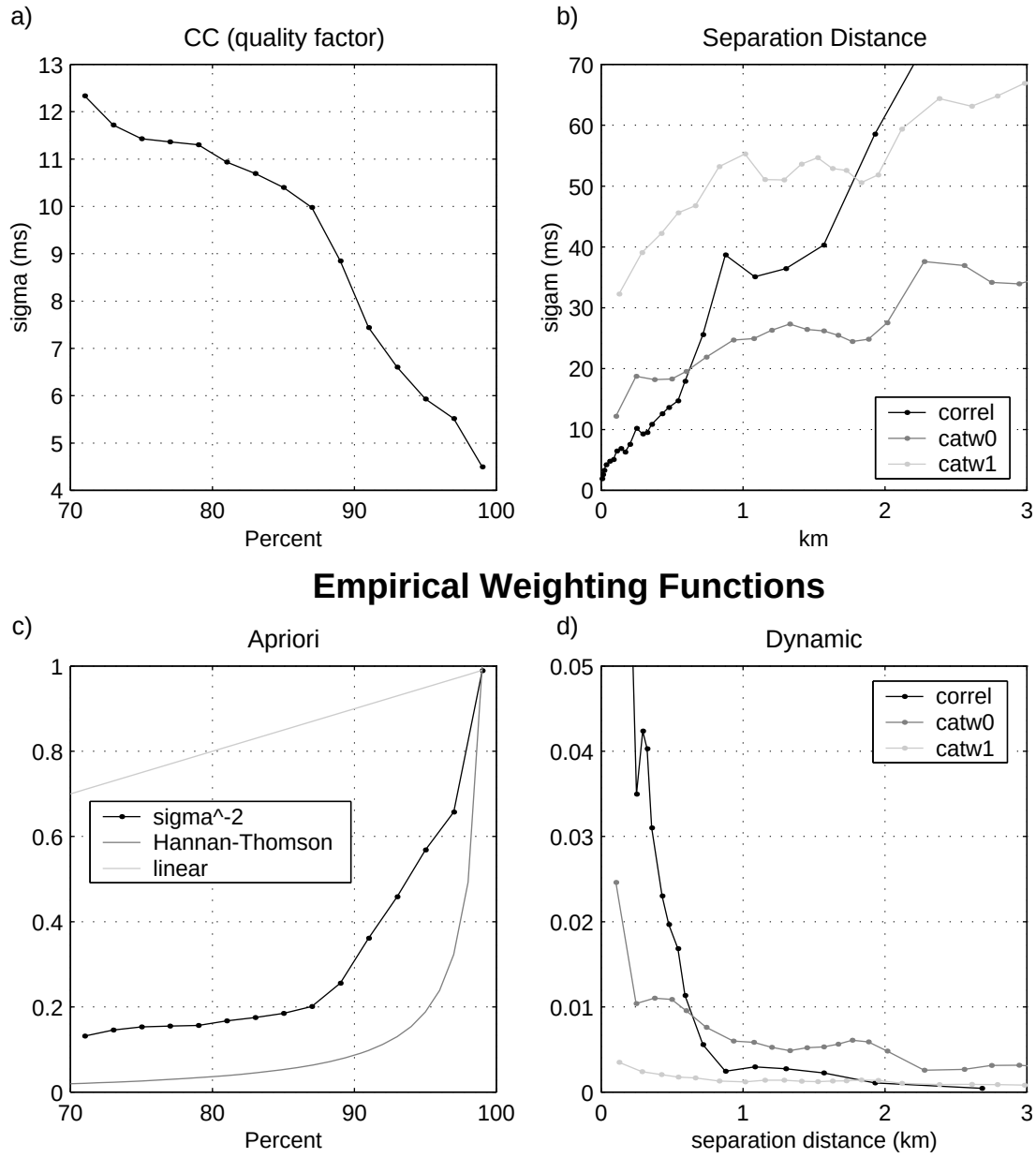

Figure 5.17: a) Standard deviation of residuals as a function of CC. b) Standard deviation of residuals as function of interevent distance for different data types. c) Example weighting functions based on data quality. d) Empirical weighting functions taken as the inverse variance normalized from 0 to 1.

sparse and has substantially more error than weight 1 data from the catalog, so perhaps those observations should be removed.

This also brings up the issue of thresholds vs. weighting functions. In some sense, they accomplish similar purposes for the location but each has certain advantages. The benefit of weighting functions is that no hard cutoff needs to be determined and so concerns of not having enough connectivity or observations are reduced. Thresholds are also intimately related to the difficulty of clustering. Weighting functions assign a unique value to each data point from a continuous spectrum according to its importance. They also eliminate the need to define a cut-off parameter. The value of thresholds is that they reduce the size of problems that would otherwise be too large so that only the best data is retained. They also sift out really bad data that might otherwise seriously degrade the solution.

5.10 Conclusions

The results described above are, to some extent, particular to to a certain set of seismicity recorded by the Northern California Seismic Network. As of yet only theoretical weighting functions are applied in the location algorithm and are tailored by trial and error for the current region. Deriving empirical weighting functions once better locations are obtained may help make this procedure more automatic and optimised for each area. For example, analysis of the streak in Figure 5.4 showed correlation data could be used out to 2 km horizontal distance. This same streak, however, is contained in the residual analysis for Figure 5.17 and so the fact that the correlation data breaks down earlier may indicate that a different distance weighting function should be applied for depth or for the other events not belonging to the streak. The weighting functions will most likely vary strongly with the strength of heterogeneity in the medium. In this study we have dealt with unmodeled velocity structure both by differencing arrival time measurements and by downweighting such measurements when the source offset is larger. An alternative approach would be to perform the combined location/velocity structure inverse problem.

We have presented a general methodology to quantify uncertainties in our measurements and modeling using post-fit residuals. This allowed us to set data thresholds, weighting functions and assess quantitatively the benefits and limitations of correlation measurements as compared to catalog data. The same approach can easily be applied to other areas. We believe that the combined correlation-double difference scheme will have similar one to two order of magnitude improvement for any given region of interest, regardless of station geometry, 3D velocity structure, seismicity type, or data quality. These issues are common to all earthquake location programs. Fundamentally, the relative relocation technique using differential travel times is able to remove the most model error as compared to all absolute travel time formulations. It is also able to take advantage of the correlation data in its natural format and fully utilize the most observations. Correlation data often achieves subsample precision, something catalog data can never match. If the input measurements to the location algorithm are improved, the output relocations are sure to be better. It remains to be seen how useful correlation data will be worldwide. Since the waveforms must be similar, it will most likely work best where earthquake density is high relative to the length scale of the problem, be it mining seismicity or teleseisms. As the evidence seems to suggest, if both model and measurement error can be substantially reduced, our projections are not that audacious. Since earthquake locations are so foundational to seismology, this may represent a significant advance for the field of earth science.

Acknowledgments. We are grateful to Doug Dodge for helpful discussions and development of the codes. We also benefited from conversions with Allan Rubin, Charlotte Rowe, and Cliff Thurber. DPS and GCB were supported by NSF Grant No. EAR-9725238. EZ was supported by USGS grant 00HQGR0062.

5.11 References

Aster, R.C., and C.A. Rowe, Automatic phase pick refinement and similar event association in large seismic data sets, in *Advances in seismic event location*, edited by C. Thurber and N. Rabinowitz, in prep.

Aster, R.C., and J. Scott, Comprehensive characterization of waveform similarity in microearthquake data sets, *Bull. Seismol. Soc. Am., 83*, 1307-1314, 1993.

Baisch, S., and G.H.R. Bokelmann, Seismic waveform attributes before and after the Loma Prieta earthquake: scattering change near the earthquake and temporal recovery, *J. Geophys. Res.,* , submitted 2001.

Bokelmann, G.H.R., Upper and Lower Mantle Small-Scale Heterogeneity Studied by Systematic Analysis of Portable Broadband Waveforms and Travel Times, Princeton University thesis, 187 pages, 1992.

Deichmann, N., and M. Garcia-Fernandez, Rupture geometry from high-precision relative hypocentre locations of microearthquake ruptures, *Geophys. J. Int., 110*, 501-5517, 1992.

Dodge, D.A., G.C. Beroza, and W.L. Ellsworth, Foreshock sequence of the 1992 Landers, California earthquake and its implications for earthquake nucleation, *J. Geophys. Res., 100*, 9,865-9,880, 1995.

Dodge, D.A., G.C. Beroza, and W.L. Ellsworth, Detailed observations of California foreshock sequences: implications for the earthquake initiation process, *J. Geophys. Res., 101*, 22,371-22,392, 1996.

Dodge, D.A., and G.C. Beroza, Source array analysis of coda waves near the 1989 Loma Prieta, California, mainshock: implications for the mechanism of coseismic velocity changes, *J. Geophys. Res., 102*, 24,437-24,458, 1997.

Ellsworth, W.L., Errors in measured and predicted travel times and their implications for the earthquake location problem,

Fréchet, J. Sismogenè et doublets sismiques, *Thèse d'Etat*, Université Scientifique et Médicale de Grenoble, 206 pp., 1985.

Frémont, M.-J., and S.D. Malone, High precision relative locations of earthquakes at Mount St. Helens, Washington, *J. Geophys. Res., 92*, 10,233-10,236, 1987.

Geller, R.J., and C.S. Mueller, Four similar earthquakes in Central California, *Geophys. Res. Let., 7*, 821-824, 1980.

Geiger, L., Herdbestimming bei Erdbeben aus den Ankunftszeiten, *K. Gessell. Wiss. Goett.*, *4* 331-349, 1910.

Got, J.-L., J. Fréchet, and F.W. Klein, Deep fault plane geometry inferred from multiplet relative relocation beneath the south flank of Kilauea, *J. Geophys. Res.*, *99*, 15,375-15,386, 1994.

Ito, A. High resolution relative hypocenters of similar earthquakes by cross-spectral analysis method, *J. Phys. Earth*, *33*, 279-294, 1995.

Jenkins, G.M. and D.G. Watts, *Spectral Analysis and its applications*, 525 pp., Holden-Day, San Francisco, California, 1968.

Menke, W., *Geophysical Data Analysis: Discrete Inverse Theory*, 289 pp., Academic Press, San Diego, California, 1989.

Neuhauser, D.S., B. Bogaert, and B. Romanowitz, Data access of Northern California seismic data from the Northern California Earthquake Data Center, *EOS, Trans. AGU*, *75*, 429, 1994.

Poupinet, G., W.L. Ellsworth, and J. Fréchet, Monitoring velocity variations in the crust using earthquake doublets: an application to the Calaveras Fault, California, *J. Geophys. Res.*, *89*, 5719-5731, 1984.

Pujol, J. Comments on the joint determination of hypocenters and station corrections, /bssa *78*, 1179-1189, 1988.

Richards-Dinger, K.B., and P.M. Shearer, Earthquake locations in southern California obtained using source-specific station terms, *J. Geophys. Res.*, *105*, 10,939-10,960, 2000.

Rubin, A.M., D. Gillard, and J.-L. Got, Streaks of microearthquakes along creeping faults, *Nature*, *400*, 635-641, 1999.

Schaff, D.P., G.C. Beroza, and B.E. Shaw, Postseismic response of repeating aftershocks, *Geophys. Res. Let.*, *25*, 4,549-4,552, 1998.

Schaff, D.P., G.H.R. Bokelmann, G.C. Beroza, F. Waldhauser, and W.L. Ellsworth, High resolution image of Calaveras Fault seismicity, submitted to *J. Geophys. Res.*, 2001.

Schaff, D.P., and G.C. Beroza, Coseismic and postseismic velocity changes measured by repeating earthquakes, submitted to *J. Geophys. Res.*, 2001.

Shearer, P.M., Improving local earthquake locations using the L1 norm and waveform cross correlation: application to the Whittier Narrows, California, aftershock sequence, *J. Geophys. Res.*, *102*, 8,269-8,283, 1997.

VanDecar, J.C., and R.S. Crosson, Determination of teleseismic relative phase arrival time using mulit-channel cross-correlation and least squares, *Bull. Seismol. Soc. Am., 80*,, 150-169, 1990.

Waldhauser, F., W.L. Ellsworth, and A. Cole, Slip-parallel seismic lineartions along the northern Hayward fault, California, *Geophys. Res. Let., 26*, 3,525-3,528, 1999.

Waldhauser, F., and W.L. Ellsworth, A double-difference earthquake location algorithm: method and application to the northern Hayward Fault, California, *Bull. Seismol. Soc. Am., 90*, 1,353-1,368, 2000.